

# Computational Acoustic Methods for the Design of Woodwind Instruments

Antoine Lefebvre



Computational Acoustic Modeling Laboratory  
McGill University  
Montreal, Quebec, Canada

December 2010

A thesis submitted to McGill University in partial fulfilment of the requirements for the  
degree of Doctor of Philosophy.

© Copyright 2010 by Antoine Lefebvre  
All Rights Reserved

## **Abstract**

This thesis presents a number of methods for the computational analysis of woodwind instruments. The Transmission-Matrix Method (TMM) for the calculation of the input impedance of an instrument is described. An approach based on the Finite Element Method (FEM) is applied to the determination of the transmission-matrix parameters of woodwind instrument toneholes, from which new formulas are developed that extend the range of validity of current theories. The effect of a hanging keypad is investigated and discrepancies with current theories are found for short toneholes. This approach was applied as well to toneholes on a conical bore, and we conclude that the tonehole transmission matrix parameters developed on a cylindrical bore are equally valid for use on a conical bore.

A boundary condition for the approximation of the boundary layer losses for use with the FEM was developed, and it enables the simulation of complete woodwind instruments. The comparison of the simulations of instruments with many open or closed toneholes with calculations using the TMM reveal discrepancies that are most likely attributable to internal or external tonehole interactions. This is not taken into account in the TMM and poses a limit to its accuracy. The maximal error is found to be smaller than 10 cents. The effect of the curvature of the main bore is investigated using the FEM. The radiation impedance of a wind instrument bell is calculated using the FEM and compared to TMM calculations; we conclude that the TMM is not appropriate for the simulation of flaring bells.

Finally, a method is presented for the calculation of the tonehole positions and dimensions under various constraints using an optimization algorithm, which is based on the estimation of the playing frequencies using the Transmission-Matrix Method. A number of simple woodwind instruments are designed using this algorithm and prototypes evaluated.

## Sommaire

Cette thèse présente des méthodes pour la conception d'instruments de musique à vent à l'aide de calculs scientifiques. La méthode des matrices de transfert pour le calcul de l'impédance d'entrée est décrite. Une méthode basée sur le calcul par Éléments Finis est appliquée à la détermination des paramètres des matrices de transfert des trous latéraux des instruments à vent, à partir desquels de nouvelles équations sont développées pour étendre la validité des équations de la littérature. Des simulations par Éléments Finis de l'effet d'une clé suspendue au-dessus des trous latéraux donnent des résultats différents de la théorie pour les trous courts. La méthode est aussi appliquée à des trous sur un corps conique et nous concluons que les paramètres des matrices de transmission développées pour les tuyaux cylindriques sont également valides pour les tuyaux coniques.

Une condition frontière pour l'approximation des pertes viscothermiques dans les calculs par Éléments Finis est développée et permet la simulation d'instruments complets. La comparaison des résultats de simulations d'instruments avec plusieurs trous ouverts ou fermés montre que la méthode des matrices de transfert présente des erreurs probablement attribuables aux interactions internes et externes entre les trous. Cet effet n'est pas pris en compte dans la méthode des matrices de transfert et pose une limite à la précision de cette méthode. L'erreur maximale est de l'ordre de 10 cents. L'effet de la courbure du corps de l'instrument est étudié avec la méthode des Éléments Finis. L'impédance de rayonnement du pavillon d'un instrument est calculée avec la méthode des matrices de transfert et comparée aux résultats de la méthode des Éléments Finis; nous concluons que la méthode des matrices de transfert n'est pas appropriée à la simulation des pavillons.

Finalement, une méthode d'optimisation est présentée pour le calcul de la position et des dimensions des trous latéraux avec plusieurs contraintes, qui est basé sur l'estimation des fréquences de jeu avec la méthode des matrices de transfert. Plusieurs instruments simples sont conçus et des prototypes fabriqués et évalués.

# Contents

<b>List of Tables</b>	<b>vi</b>
<b>List of Figures</b>	<b>viii</b>
<b>Preface</b>	<b>xiii</b>
<b>Acknowledgements</b>	<b>xiv</b>
<b>Introduction</b>	<b>1</b>
<b>1 Fundamentals of Woodwind Instrument Acoustics</b>	<b>6</b>
1.1 Tuning, Timbre and Ease of Play . . . . .	8
1.2 The Excitation Mechanism . . . . .	12
1.3 The Air Column . . . . .	14
1.3.1 Modelling Methods . . . . .	14
1.3.2 Cylindrical and Conical Waveguides . . . . .	17
1.3.3 Radiation at Open Ends . . . . .	23
1.3.4 Toneholes . . . . .	25
<b>2 Finite Element Simulations of Single Woodwind Toneholes</b>	<b>35</b>
2.1 Validation of the FEM . . . . .	37
2.2 From FEM Results to Transmission Matrices . . . . .	43
2.2.1 Transmission Matrix Parameters of a Tonehole . . . . .	44
2.2.2 Tonehole Model Validation . . . . .	45
2.3 Characterization of Woodwind Toneholes . . . . .	52

---

2.3.1	Estimation of the Required Accuracy of the Equivalent Lengths . . .	52
2.3.2	Data-fit Formulae Procedure . . . . .	53
2.3.3	The Single Unflanged Tonehole . . . . .	54
2.3.4	The Single Tonehole on a Thick Pipe . . . . .	65
2.3.5	Influence of the Keypad . . . . .	72
2.3.6	Impact of Conicity . . . . .	73
2.4	Summary . . . . .	75
<b>3</b>	<b>Finite Element Simulations of Woodwind Instrument Air Columns</b>	<b>78</b>
3.1	Validation . . . . .	81
3.2	Waveguides with a Single Tonehole . . . . .	83
3.3	A Cone with Three Toneholes . . . . .	86
3.4	A Cylinder with Twelve Toneholes . . . . .	90
3.5	A Cone with Twelve Toneholes . . . . .	94
3.6	Curvature of the Bore . . . . .	98
3.7	Radiation from the Bell . . . . .	101
3.8	Summary . . . . .	104
<b>4</b>	<b>An Approach to the Computer-Aided Design of Woodwind Instruments</b>	<b>106</b>
4.1	Selecting the Instrument's Bore Shape . . . . .	111
4.2	Calculating the Tonehole Positions and Dimensions . . . . .	113
4.3	Examples . . . . .	116
4.3.1	Keefe's Flute . . . . .	116
4.3.2	PVC Flute . . . . .	117
4.3.3	Chalumeau . . . . .	120
4.3.4	A Six-Tonehole Saxophone . . . . .	123
4.4	Summary . . . . .	125
	<b>Conclusion</b>	<b>127</b>
<b>A</b>	<b>The Single-Reed Excitation Mechanism</b>	<b>130</b>
A.1	Description . . . . .	131
A.2	Reed Admittance . . . . .	133

A.3 Generator Admittance . . . . .	135
A.4 The Reed's Effective Area . . . . .	137
A.5 Estimation of the Playing Frequencies . . . . .	139
<b>References</b>	<b>144</b>

# List of Tables

1.1	Comparison of the expressions for the open tonehole inner length correction $t_i^{(o)}$	30
1.2	Comparison of the expressions for the open tonehole series length corrections $t_a^{(o)}$	30
2.1	Series equivalent length $t_a^{(o)}$ in mm. Comparison between simulation, theories, and experimental data for the toneholes studied by <a href="#">Dalmont et al. (2002)</a> .	48
2.2	Series equivalent length $t_a^{(o)}$ in mm. Comparison between simulation, and theories and experimental data for the toneholes studied by <a href="#">Keefe (1982a)</a> .	48
2.3	Shunt length correction increment due to the presence of a hanging keypad	72
3.1	Comparison of the resonance frequencies for the cylindrical and conical waveguides with one open or one closed tonehole.	85
3.2	Comparison of the simulated and calculated resonance frequencies of a conical waveguide with three open or closed toneholes.	86
3.3	Comparison of the simulated and calculated resonance frequencies of a simple clarinet-like system with twelve open or closed toneholes.	90
3.4	Comparison of the simulated and calculated resonance frequencies of a conical waveguide with twelve open or closed toneholes.	94
3.5	Comparison of the simulated and calculated resonance frequencies for a straight and two curved alto saxophone necks.	98
4.1	Comparison of the tonehole layout of an optimized flute with Keefe's flute	117
4.2	Comparison of the tonehole layout for a flute	120
4.3	Comparison of the tonehole layout for two chalumeaux (equally tempered vs. just)	122

4.4	Comparison of the tonehole layout for two conical waveguides with six toneholes	124
A.1	Estimation of the playing frequencies for the successive harmonics of a conical bore with mouthpiece. . . . .	141
A.2	Estimation of the playing frequencies for the successive harmonics of a conical bore with cylindrical mouthpiece models. . . . .	143

# List of Figures

1.1	Input impedance of a cylindrical waveguide (top) and a conical waveguide (bottom): measured (filled circles) and calculated (solid line). . . . .	22
1.2	Diagram representing a tonehole on a pipe. . . . .	25
1.3	Block diagram of a symmetric tonehole . . . . .	26
2.1	Diagrams of the FEM models for the radiation of an unflanged pipe (top) and a flanged pipe (bottom). . . . .	39
2.2	Visualisation of the FEM mesh for the unflanged pipe test case. The pipe (top) and the radiation domain (bottom) are separated to help visualize the details. . . . .	40
2.3	Visualisation of the FEM mesh for the flanged pipe test case. . . . .	41
2.4	Real part (bottom graph) and imaginary part (top graph) of the radiation impedance of the pipes: FEM results for the unflanged pipe (squares) and for the flanged pipe (circles) compared with theory (dashed). . . . .	42
2.5	Visualisation of the FEM mesh for the flanged tonehole . . . . .	46
2.6	Visualisation of the FEM mesh for the unflanged tonehole . . . . .	49
2.7	Shunt equivalent length $t_s^{(o)}$ as a function of $ka$ for the two toneholes studied by <a href="#">Dalmont et al. (2002)</a> . . . . .	50
2.8	Shunt equivalent length $t_s^{(o)}$ as a function of $ka$ for the two toneholes studied by <a href="#">Keefe (1982a)</a> . . . . .	51
2.9	Difference between the shunt length correction $t_s^{(o)}$ and the tonehole height $t$ divided by the tonehole radius $b$ as a function of $\delta$ for a single unflanged tonehole. . . . .	56
2.10	Comparison of the expressions for the inner length correction $t_i^{(o)}/b$ . . . . .	57

2.11	Difference between the shunt length correction $t_s^{(o)}$ and the tonehole height $t$ divided by the tonehole radius $b$ as a function of $kb$ for a single unflanged tonehole. . . . .	58
2.12	Series length correction $t_a^{(o)}/b\delta^4$ as a function of $\delta$ for a single unflanged tonehole. . . . .	59
2.13	Series length correction $t_a^{(o)}/b\delta^4$ as a function of $t/b$ for $\delta = 1.0$ for a single unflanged tonehole. . . . .	60
2.14	Shunt length correction $t_s^{(c)}$ as a function of $\delta$ with $t/b = 0.1$ (bottom) and $t/b = 2.0$ (top) for a single closed tonehole. . . . .	61
2.15	Inner length correction $t_i^{(c)}/b$ for closed toneholes as a function of $kb$ for $\delta = 0.2, 0.5, 0.8, 1.0$ . . . . .	62
2.16	Series length correction $t_a^{(c)}/b\delta^4$ as a function of $\delta$ for a closed tonehole. . . . .	63
2.17	Series length correction $t_a^{(c)}/b\delta^4$ as a function of $t/b$ for $\delta = 1.0$ for a closed tonehole. . . . .	64
2.18	Diagram representing a tonehole on a pipe. . . . .	65
2.19	Difference between the shunt length correction $t_s^{(o)}$ and the tonehole height $t$ divided by the tonehole radius $b$ as a function of $\delta$ for a tonehole on a thick pipe. . . . .	67
2.20	Difference between the shunt length correction $t_s^{(o)}$ and the tonehole height $t$ divided by the tonehole radius $b$ as a function of $kb$ for a tonehole on a thick pipe. . . . .	68
2.21	Series length correction $t_a^{(o)}/b\delta^4$ as a function of $\delta$ for an open tonehole on a thick pipe. . . . .	69
2.22	Shunt length correction $t_s^{(c)}$ as a function of $\delta$ for a closed tonehole on a thick pipe. . . . .	70
2.23	Series length correction $t_a^{(c)}/b\delta^4$ as a function of $\delta$ for a closed tonehole on a thick pipe. . . . .	71
2.24	Block diagram of an unsymmetric tonehole . . . . .	73
2.25	Series length correction $t_a^{(o)}$ in mm for a tonehole on a conical bore with taper angle of 3 degrees. . . . .	75
3.1	Normalized input impedance of a closed cylinder of diameter 15 mm and length 300 mm. . . . .	82
3.2	Input impedance of a conical waveguide with three toneholes. . . . .	88

3.3	Magnitude of the reflection coefficient and open cylinder equivalent length for a conical waveguide with three open toneholes. . . . .	89
3.4	Input impedance of a cylindrical waveguide with 12 toneholes. . . . .	92
3.5	Magnitude of the reflection coefficient for a cylindrical waveguide with twelve open toneholes. . . . .	93
3.6	Input impedance of a conical waveguide with twelve toneholes. . . . .	96
3.7	Magnitude of the reflection coefficient for a conical waveguide with twelve open toneholes. . . . .	97
3.8	Diagram of the three instrument bores simulated for the study of curvature. . .	100
3.9	Impedance of an alto saxophone bell. . . . .	102
3.10	Open cylinder equivalent length $l_o$ of an alto saxophone bell. . . . .	103
4.1	Radius as a function of $x$ for the two saxophone-like conical instruments, differing in the geometry closer to the mouthpiece. . . . .	112
4.2	Diagram of Keefe's flute. . . . .	118
4.3	Diagram of a large-diameter and a small-diameter tonehole flute. . . . .	119
4.4	Input admittance of the large-toneholes flute for two fingerings. . . . .	121
A.1	Diagram of the excitation mechanism of a single reed instrument. . . . .	130
A.2	Block diagram of the single reed excitation mechanism system. . . . .	132
A.3	Equivalent volume $V_e$ due to reed admittance $Y_r$ . . . . .	135
A.4	Equivalent volume $V_e$ due to the generator admittance $Y_g$ as a function of frequency for three reeds. . . . .	138
A.5	Diagram of the mouthpiece geometry. . . . .	140
A.6	Total equivalent volume $V_e$ as a function of frequency. . . . .	142

# Nomenclature

$a$	main air column radius
$b$	tonehole radius
$\delta = b/a$	ratio of the tonehole radius to the main bore radius
$t$	tonehole height
$t_i$	tonehole inner length correction
$t_s$	tonehole shunt equivalent length
$t_a$	tonehole series equivalent length
$t_r$	tonehole radiation length correction
$t_m$	tonehole matching volume length correction
$t_e$	low frequency value of the tonehole shunt equivalent length
$s$	half the spacing between two toneholes
$h$	distance between a keypad and the tonehole
$v_\phi$	phase velocity
$f$	frequency
$\omega = 2\pi f$	angular frequency
$k = \omega/c$	wavenumber
$c$	speed of sound in a free field
$Z_0 = \rho c/S$	characteristic impedance
$\rho$	fluid density
$\mu$	fluid viscosity
$\gamma$	ratio of specific heats
$Pr$	Prandtl number
$S$	cross-sectional area
$p$	pressure

---

$U$	volume flow
$\bar{Z} = Z/Z_0$	normalized impedance
$\Gamma$	complex-valued propagation wavenumber
$\bar{Z}_c$	complex-valued characteristic impedance
$k_v = \sqrt{-jk/l_v}$	viscous diffusion wavenumber
$l_v = \mu/\rho c$	vortical characteristic length
$k_t = \sqrt{-jk/l_t}$	thermal diffusion wavenumber
$l_t = l_v/Pr$	thermal characteristic length
$J_0$	Bessel function of order 0
$J_1$	Bessel function of order 1
$L$	length
$\xi_s$	shunt resistance
$A, B, C, D$	coefficients of a transmission matrix
$j = \sqrt{-1}$	imaginary number

## Preface

The subject of this thesis is the acoustical design of woodwind instruments. The shape of an instrument's bore, including the position and dimensions of the toneholes, controls the playing behaviour of the instrument. In this thesis, acoustical methods for the design of this geometry are proposed. Mechanical aspects such as the key system or technical aspects such as fabrication methods are not discussed.

The impetus for this research was the desire to develop a method for the design and optimization of woodwind instruments with the objective of fabricating high quality instruments for the benefit of professional musicians. This project started many years ago and led to work on the development of an apparatus for the measurement of the acoustic impedance of the alto saxophone (Lefebvre, 2006). The first task I worked on when starting my doctoral studies was to redesign this measurement apparatus to incorporate many improvements and to experiment with another measurement technique (Lefebvre, Scavone, Abel, & Buckiewicz-Smith, 2007) as well as to verify the accuracy of the conical waveguide input impedance model with measurements (Lefebvre & Scavone, 2008). During this research project, I worked on a software package called *The Woodwind Instrument Acoustics Toolkit*<sup>1</sup> (WIAT), written in the Python language, which contains code for the Transmission-Matrix Method, the Multimodal-Decomposition Method, the processing of measurement and simulation data and the calculation of the positions and dimensions of the toneholes on woodwind instruments. For purposes of calculating the input impedance of woodwind instruments, I started working with the Boundary Element Method and the Finite Element Method and on the development of solutions to incorporate boundary layer losses. At the same time, I collaborated with my director, Gary Scavone, on research on the vocal tract influence in saxophone performance (Scavone, Lefebvre, & Silva, 2008) and with Andrey da Silva on a Lattice Boltzman Modelling of wave propagation in a duct with a mean flow (A. da Silva, Scavone, & Lefebvre, 2009). I also worked on an unpublished research project which consisted in using a strain gauge to measure the vibration of a saxophone reed under playing conditions. The signal acquired from this strain gauge may be used for scientific investigations on the reed motion or simply as a feedbackproof microphone. This is work to be continued in the future.

---

<sup>1</sup><http://www.music.mcgill.ca/caml/doku.php?id=wiat:wiat>

## Acknowledgements

I gratefully acknowledge the **Fonds Québécois de la Recherche sur la Nature et les Technologies** (FQRNT) for a doctoral research scholarship, without which this research would have been impossible, as well as the **Centre for Interdisciplinary Research in Music Media and Technology** (CIRMMT) for its support.

Many thanks to my director, Professor Gary P. Scavone, for his constant support, advice, encouragement and recommendations as well as to my colleague, Dr. Andrey Da Silva, for many enlightening discussions. Special thanks to Professor Jean-Pierre Dalmont for his work as an external reviewer for my thesis; the valuable comments and suggestions were helpful in enhancing the quality of the manuscript. I also wish to thank the Music Technology professors and students with whom I had many opportunities to discuss my research topic, and Géraud Boudou for help on the development of the optimization code.

I am grateful to Professor Larry Lessard for collaboration on the fabrication of composite material prototypes and to Professor Luc Mongeau for discussions about acoustic topics. I also wish to thank Guy Lecours, who supported my research through the opportunity to work in his metal workshop, and to Richard Cooper for invaluable help on English writing.

Finally, many thanks to my wife Maribel and my two daughters, Aurélie and Nicole, for patience and support all along the way of this endeavour.

# Introduction

Unlike electronic instruments and computer sound synthesis, which have undergone extensive development through research and experimentation in the last 100 years, traditional acoustical music instruments, such as violins, trumpets, clarinets, flutes and even the more recent saxophone, have remained mostly unchanged. These acoustical instruments were traditionally developed slowly through trial and error, requiring the innovations of many generations of makers to attain their modern shapes. Even though many of them have attained a high degree of perfection, possible innovations remain to be explored, such as exploiting new materials, modifying the shape of the instruments or seeking new compromises to improve their tuning. The standard practice for the design and fabrication of woodwind instruments consists in repeating existing designs and incorporating small changes possibly aided by simple desk calculations. This implies that new makers have to start by copying existing instruments. As a new instrument maker and an engineer, I wish to develop a software system that would enable the design of such instruments from scratch. I want to better exploit the scientific knowledge of woodwind instruments to develop methods for the design of these instruments that do not rely on a previous design.

The objective of this research is to propose methods for the computer aided design of woodwind instruments. The design of these instruments is a challenging problem because of the high accuracy that is required to meet the highly exacting standards professional musicians demand. The smallest frequency difference of successive tones that can be detected by a listener is approximately 8 cents (0.5%) at a frequency of 200 Hz and diminishes to 3 cents

(0.2%) at 1 kHz (Hartmann, 1996). The cent is a measure of the frequency interval between two frequencies  $f_1$  and  $f_2$ . The interval  $c$  is calculated as  $c = 1200 \log_2(f_2/f_1)$ . There are 100 cents in one equally tempered semitone. An interval in cents may also be expressed in percent with  $\% = 100(f_2 - f_1)/f_1 = 100(2^{c/1200} - 1)$ . In a musical context, the instrumentalists are constantly adjusting the playing frequencies of their instruments through embouchure manipulations in order to produce the desired frequencies, which are changing as a function of the musical context. As an example, the instrumentalist playing the major third ( $5/4$ ) of a major chord should play 14 cents lower than the frequency of an equally tempered major third ( $2^{1/3}$ ). Even though the instrumentalists can adjust their pitch by more than this interval, 14 cents remain a relatively significant change and a mistuning of the instrument could possibly increase the required frequency variation. For example, if the note used to play a major third was itself 10 cents sharp, then the player would be required to lower the frequency by 24 cents. We assume in this thesis that the playing frequencies of modern instruments will likely be tuned with an equal temperament (division of the octave in 12 equal semitones), but that may not be the ideal tuning. This thesis does not try to answer this question. Rather, it is concerned with the development of methods to calculate the positions and dimensions of the toneholes on an instrument to achieve the desired tuning, whatever that is. Based on this discussion, we believe that the tuning of an instrument should have *a general accuracy of  $\pm 5$  cents*.

There exists no simple way to calculate the position and dimension of each tonehole one by one, as a consequence of the physics of wave propagation. This implies that the playing frequency of each fingering depends on each part of the instrument; modifying the geometry of one part of the instrument, such as a tonehole, results in playing frequency changes for every note of the instrument. The solution involves using a global optimization algorithm that can calculate the solution to the problem (that is, the locations and dimensions of the toneholes), making use of an underlying method for the estimation of the playing frequencies of a hypothetical instrument. Apart from being accurate, this method must also be fast because

the playing frequencies of the instrument under design will be recalculated a large number of times for each of its fingering during the optimization process. Today, large computer clusters such as those used by [CLUMEQ](http://www.clumeq.ca/)<sup>2</sup> (960 computers, each with 8 cores running at 2.8 GHz and 24 Gbytes of memory), located in Quebec city at Laval University, would enable the optimization of woodwind instruments based on computationally expensive methods, such as the Finite Element Method (FEM). However, we instead aim to develop a software system that can run in a reasonable amount of time on a personal computer (a single computer with 2 cores running at 2 GHz and 2 Gbytes of memory). One method that executes rapidly and does not require much memory is the Transmission Matrix Method (TMM). As an example, the TMM calculation of the input impedance of a conical instrument with 12 toneholes for 1400 frequency points takes less than 1 second. The same problem, calculated using the FEM, cannot be solved on a personal computer due to insufficient memory. This problem was solved on a high performance “personal” computer in the *Computational Acoustic Modeling Laboratory*<sup>3</sup> (CAML), located in the Music Technology Area of the Schulich School of Music at McGill University, Montreal, Canada, which has 8 cores and 8 Gbytes of memory. The time for calculating the input impedance for 140 frequency points is approximately 2.5 hours. There is a substantial gain of more than  $7 \times 10^5$  in terms of calculation time for this example case. Even though it would be possible to fine-tune the finite element mesh in order to obtain the required accuracy with a smaller number of elements and reduce the calculation time, it is unlikely that we can achieve a similar performance as with the TMM. This is why we chose the TMM method for the optimization algorithm presented in Chap. 4 and the FEM for the development of TMM models in Chap. 2.

In Chapter 1, the current state of scientific knowledge regarding the excitation mechanism and air columns of woodwind instruments is summarized. The Transmission-Matrix Method (TMM) is presented for the calculation of the input impedance of acoustic systems, with an

---

<sup>2</sup><http://www.clumeq.ca/>

<sup>3</sup><http://www.music.mcgill.ca/caml/>

extensive review of the literature concerning the modelling of cylindrical and conical waveguides with boundary layer losses, of open and closed toneholes and of the radiation from open ends and bells.

The accuracy of the input impedance calculated using the FEM depends on the accuracy of the transmission matrix models of each segment of the instrument, the most important being the model of an open or closed tonehole. In Chapter 2, the Finite Element Method (FEM) is used to validate the accuracy and extend the validity of the TMM model of a tonehole. A method is proposed to obtain the transmission matrix parameters of an object from the results of simulations using the FEM. This method is applied to the cases of a single unflanged tonehole and a single tonehole on a thick pipe. Revised one-dimensional transmission-matrix models of open and closed toneholes are presented to extend the validity of the current models. Simulation results for the case of a tonehole on a conical waveguide and for the case of a hanging keypad above such a tonehole are analysed.

One other source of inaccuracy in the TMM comes from a fundamental hypothesis of the method: that the evanescent modes excited near a discontinuity does not interact with the evanescent modes from an adjacent discontinuity, i.e. that they are uncoupled. In the case of woodwind instruments, the toneholes are located sufficiently close from each other for a coupling to exist. The errors introduced by this neglected coupling may be estimated by comparing the FEM simulations of complete instruments with TMM calculations. This is the object of Chapter 3; the input impedance of simple woodwind-like instruments is evaluated using the FEM and compared to theoretical calculations based on the TMM. Thermoviscous losses are accounted for with an impedance boundary condition based on acoustic boundary layer theory. The systems are surrounded by a spherical radiation domain with a second-order non-reflecting spherical wave boundary condition on its outer surface. This method is also useful for the calculation of the transmission-matrix parameters of curved bores with varying cross-section, for which no theoretical solution exists. Furthermore, simulation results of a bell are compared with theoretical calculations.

Finally, in Chapter 4, an approach to the design of woodwind instruments is presented. This includes a discussion of the selection of the instrument's bore shape and a presentation of the method for the calculation of the tonehole positions and dimensions. This is followed by the application of the method to simple six-tonehole instruments, which were built and tested.

# Chapter 1

## Fundamentals of Woodwind Instrument Acoustics

Musical acoustics, the branch of acoustics concerned with studying and describing the physics of musical sound production and transmission, has undergone greatly increased understanding in the last several decades. In particular, the mechanics of musical instruments has emerged as a specialized field of research. The state of knowledge at the beginning of the 21st century has attained the necessary accuracy for the use of scientific methods in the design of instruments satisfying the highly exacting standards professional musicians demand. Furthermore, computers can now process huge numbers of calculations more quickly and effectively than ever before, allowing for the simulation of hypothetical changes to an instrument and the determination of parameters that optimize tuning, timbre and response throughout the instrument's entire range.

Although musical instruments rely on a number of mechanisms to produce sound, we are focusing on instruments that utilize the vibration of a column of air, the length of which can be effectively varied with closed or open side holes, usually called *toneholes*. Such instruments may vibrate under the action of different excitation mechanisms, such as an air jet directed across an open hole (flutes), a single reed mounted on a mouthpiece (clarinets and saxophones)

or a double reed (oboes and bassoons). The role of this mechanism is to convert a static pressure or flow from the instrumentalist into a tone, the frequency of which is controlled mainly by the properties of the instrument's body, a linear resonator also called the *air column* (Rayleigh, 1896/1945; Backus, 1963; Nederveen, 1969/1998a). The quality of the sound that radiates from such instruments depends on the coupling between the excitation mechanism and the instrument's body. The excitation mechanism works as an oscillating valve modulating the quantity of air that enters the instrument as a function of its opening. Because it is a non-linear system, the valve generates a complex wave shape composed of many frequency components harmonically related to the fundamental rate of vibration. Acoustic waves travel back and forth from the tip to the first opening in the instrument's bore and the fundamental period of vibration is related to the time it takes for acoustic waves to complete this travel, which depends on the boundary conditions at the ends and the shape of the bore. Any perturbation in the shape of the bore – enlargements, contractions, discontinuities, roughness, bends, etc. – affects the wave shape (thus, the frequency content that determines the timbre) and the travel time. Subtle variations in the body's geometry, on an order of magnitude smaller than a millimetre, can have a noticeable effect on the resulting sound and the instrumentalist's feel. Great care must be taken in the design of toneholes; their positions and dimensions affect both the pitch and the timbre of the notes.

This quick overview suggests the level of refinement mathematical models should have. However, the difficulty in accurately quantifying the mechanical properties of the player's embouchure poses a limit to the accuracy of the calculations. Nevertheless, with reasonable assumptions based on experimentation, mathematical models coming from musical acoustic science can be solved to predict an instrument's behaviour with surprising accuracy and thereby broaden the field of musical instrument engineering.

In the following sections, current theories describing the mechanics of the excitation mechanisms (Sec. 1.2) and the modelling of the air column (Sec. 1.3) are presented. This is preceded by a review of general considerations important for the design of woodwind instruments.

## 1.1 Tuning, Timbre and Ease of Play

There are many influential factors in obtaining a good, well-tuned sound from an instrument, such as the skill of the player, the quality of the instrument, and the mouthpiece assembly. The correct tuning of an instrument depends on the use of a properly sized mouthpiece for clarinets and saxophones, a properly adjusted double reed for oboes and bassoons and the properties of the embouchure hole and head for the concert flute. The design of an excitation mechanism is in itself a complicated and subtle problem that is not within the scope of this study. The method proposed here for the design of an instrument body presupposes that the characteristics of an existing excitation mechanism are known. This is discussed in Sec. 1.2.

The instrument body itself is a complex assemblage of many parts; and although manufacturers generally sell their instruments in working condition, it is necessary to regularly readjust the mechanics to ensure a tight sealing of the toneholes in their closed state, to adjust the spring force, and to adjust the key system timing and the pad' heights. The procedure to adjust the instrument consists of gluing on bits of felt or cork of an appropriate thickness and in bending the metallic parts. A correct adjustment of the instrument is critical; otherwise, it may become unplayable. Furthermore, the problem of adjustment raises an important point: the instrumentalist who is faced with the task of evaluating an instrument cannot evaluate its intrinsic value; he evaluates the quality of the adjustment as much as the instrument itself. A fair comparison between any two instruments demands that they both be adjusted with the same care.

Although many researchers believe that the material from which an instrument is made has no influence at all (Coltman, 1971; Nief, Gautier, Dalmont, & Gilbert, 2008), there is some evidence that the impact of wall vibration is not negligible in the case of instruments made of thin metallic sheets, such as brasses and saxophones (Blaikley, 1879; Pyle, 1997; Nederveen, 1969/1998a; Kausel & Mayer, 2008), but that this influence would be limited to subtle timbre variations noticeable possibly only by experienced musicians. For purposes of the present

study, we will not consider the material further.

The acoustic properties of woodwind instruments are mainly a consequence of their geometry. The diameter of the bore as a function of the distance along the instrument's spine is the most important factor in determining the instrument's response. Contrasting examples are the cylindrical and the conical bore. Slight variations of the basic instrument shape produce a displacement of the resonances that influence the tuning, the timbre and the playability of the instrument. The curvature of the bore has a secondary influence.

The sounding pitch of the instrument is controlled by the action of closing or opening toneholes located along the instrument's body. The position and geometry of these toneholes, as well as the height of the pad above them when in the open state, are of primary importance for the tuning and response of the instrument. Small details, such as the radius of curvature at the junction of the tonehole with the bore, undercutting<sup>1</sup>, the thickness of the wall of the chimney and the type of pad and resonator<sup>2</sup>, may also have an influence. For an open tonehole, the resulting playing frequency will be higher if the tonehole is located closer to the excitation point, if it has a larger diameter and if it has a shorter height. Furthermore, increasing the distance between a pad and the tonehole has the following result: the pitch is raised, the note becomes easier to play and the timbre is brighter. Conversely, when the pad is closer to the tonehole, the pitch is lowered, the note becomes more difficult to play and the timbre is darker. Because closer pads allow for faster playing action, the optimal location may be the closest one that still allows the note to be played freely. The playing frequency of the instrument not only depends on the geometry of the first open tonehole but also on the presence of closed toneholes above (closer to the mouthpiece) and/or on the presence of one or more open or closed toneholes below it. In general, closed side holes placed above an open tonehole lower the playing frequencies.

---

<sup>1</sup>A fabrication technique that consists in removing material on the internal side of a tonehole on wooden instruments. This reduces the sharpness of the corner.

<sup>2</sup>Some pads are provided with a central disk of various sizes, shapes and materials misleadingly called a "resonator" in the musical community.

The first open tonehole is generally followed by a series of more open toneholes; for some notes, the first open tonehole is followed by one or more closed toneholes and then one or more open toneholes, a situation called cross-fingering, whereby the playing frequency is lowered and the timbre darkened compared to the standard row of open holes. The importance of this effect depends on the geometry of the first open tonehole; when it is smaller in diameter and taller, the effect of the following tonehole is more important than if the first open tonehole has a larger diameter and a shorter height. This phenomenon is important for the proper functioning of cross-fingering, which is a common way to play semitones on a simple instrument without a key system, such as the recorder. When designing an instrument, there is some latitude in choosing the diameter, height and position of the holes because the same playing frequencies can be obtained from different geometries. If the first open tonehole for a specific fingering is moved slightly upward (closer to the mouthpiece), the resonance frequency of the fingering could be preserved if the diameter is reduced and/or the height increased by the proper amount. Similarly, if this tonehole is moved downward, the diameter must be increased and/or the height reduced to maintain the same resonance frequency. Even though the playing frequencies would be the same in each case, the resulting timbre would vary. Furthermore, if one tonehole is displaced and its geometry adjusted, the resonance frequencies of the other fingerings would likely be modified, requiring modifications to the other tonehole geometries. This interdependence of the toneholes complicates the design or modification of woodwind instruments.

The location and dimension of the register holes also affects the relative tuning of the registers because their locations are chosen to minimize the negative impact (detuning) they have when located away from their ideal locations (there is a different optimal location of the register hole for each note of the first register of an instrument).

The description of wind instrument behaviour is generally based on linear acoustic theories in which the acoustic wave is supposed to be of sufficiently low amplitude for the second-order

terms in the Navier-Stokes equation to be negligible (Keefe, 1983). The presence of non-linear effects (such as vortices, turbulence and acoustic streaming) causes undesirable results for instrumentalists and must be avoided.

In order to predict the timbre of the resulting sound, one method consists of determining the Fourier components of the pressure in the mouthpiece by coupling a non-linear reed model with the linear resonator using the harmonic-balance method (Gilbert, 1991; Fritz, Farner, & Kergomard, 2004), and eventually, the radiated sound field may be evaluated from the pressure at each opening of the instrument. Another approach is to calculate the cut-off frequency  $f_c$  of the tonehole lattice, which behaves like a high-pass filter. Idealized geometries that consist of a series of equally spaced identical toneholes were studied by Benade (1960) and Keefe (1990). This cut-off frequency is expressed as:

$$f_c = \frac{v_\phi (b/a)}{2\pi \sqrt{2st}}, \quad (1.1.1)$$

where  $v_\phi$  is the phase velocity of the sound in the instrument,  $b$  is the tonehole radius,  $a$  is the instrument radius,  $s$  is half the spacing between the holes and  $t$  is the tonehole height. An increase of the cut-off frequency correlates with a brighter tone (Benade, 1990) and may be obtained with wider, shorter height and more closely spaced holes. In the case of instruments with non-uniformly sized holes, which is always the case with real instruments, the cut-off frequency may be evaluated from the reflection coefficient; at the cut-off frequency, the magnitude of this coefficient presents a minimum. Evaluating the cut-off frequency is important for the design of an instrument, particularly because of cross-fingerings, where the inter-hole distance is much larger than for normal fingerings. In such a case, the darkening of the sound, due to the greater spacing of the holes needs to be compensated by a larger diameter and/or a shorter height. For the lowest notes of the instrument, the shape of the bell must be adjusted to present a cut-off frequency similar to that of the rest of the instrument.

Ease of play depends upon many factors, including the magnitude of the impedance resonances, the harmonicity (or alignment) of the resonances (Worman, 1971) and the occurrence of non-linear effects. Gazengel (1994) reports that the importance of the harmonicity of the higher resonances was recognized by early researchers such as Bouasse in 1929. A more recent publication discussing the question is that of Fletcher (1978). The magnitude of the impedance resonances, particularly the one corresponding to the fundamental frequency, determines the ease of play for soft sounds, for which fewer higher harmonics are present. The occurrence of non-linear effects, at a relatively loud playing level, may destroy the sound quality and impose a limit on the available dynamic range. As reported by Keefe (1983), short and small holes, as well as holes with sharp edges at the junction with the bore, are likely to pose problems at high dynamic levels.

## 1.2 The Excitation Mechanism

There are two main types of excitation mechanisms used in woodwind instruments, those operating at impedance minima, based on an air jet directed across an open hole (flutes) and those operating at impedance maxima, based on a source of pressure activating a non-linear valve (single and double reed instruments). Even though they are as simple as blowing air across a hole on a pipe or setting in vibration a piece of cane mounted on a mouthpiece, they happen to be quite difficult to analyse mathematically. They are very sensitive to small changes to their geometry and depend heavily on the instrumentalist, which is inherently difficult to characterize. Many researchers have attempted to characterize mathematically and experimentally these mechanisms; see Chaigne and Kergomard (2008) for a review. The design of the body of an instrument depends very much on the properties of this mechanism, and any attempt to calculate the position of the toneholes with an incorrect excitation mechanism model will inevitably give incorrect results.

The mathematical study of the “air reed” mechanism of flute-like instruments requires a

complex aeroacoustic analysis and is not fully understood today. Fortunately, for purposes of designing an instrument, most of these complexities may be ignored, as it has been shown that the playing frequencies of these instruments are equal to their resonance frequency, including the effect of the presence of the player's mouth (Nederveen, 1969/1998a).

For single-reed instruments, the mouthpiece assembly, which consists of the mouthpiece itself, a cane or synthetic reed and a ligature, has an important role in determining the playing characteristics of the instrument. The scientific literature on the subject is sparse and mainly discusses the impact of the mouthpiece volume on the tuning of an instrument. Nederveen (1969/1998a) showed that the equivalent mouthpiece volume of saxophone mouthpieces (including the effect of the reed's motion) should be approximately the same as the missing part of the truncated cone. There is some evidence that this requirement is not sufficient; a short and wide mouthpiece does not behave in the same way as a long and slim mouthpiece of the same volume. The literature also discusses the coupling of simple reed models (generally one-dimensional, mass-spring-damper systems) with the linear resonator (Nederveen, 1969/1998a; Gilbert, 1991; Barjau & Gibiat, 1997). The situation for double-reeds is slightly more complex (Vergez, Almeida, Caussé, & Rodet, 2003). Recently, numerical simulations of the mouthpiece assembly have been performed using the Finite Element Method (Facchinetti, Boutillon, & Constantinescu, 2003) and the Lattice Boltzmann Method (A. da Silva, Scavone, & Walstijn, 2007), and these suggest that the usual approximation of an equivalent mouthpiece volume may be inadequate, that the interaction of the reed with the mouthpiece lay as well as the modal vibration of the reed participate in the quality of the resulting sound and that the fluid-structure interaction in the mouthpiece plays an important role. A mathematical analysis of the single-reed excitation mechanism is provided in Appendix A, along with experimental results for the playing frequencies of a simple conical waveguide played with an alto saxophone mouthpiece.

For the design of a woodwind instrument, the best approach still consists of an experimental characterization. That is, the excitation mechanism for which the instrument is to be

designed is played on a simplified instrument (such as a cylinder or a cone with no toneholes, bell or any other kind of discontinuity) of various sizes. Because the acoustic properties of these types of simple instruments are accurately known, an empirical characterization of the excitation mechanism is possible. This is the approach that was advocated by Benade and Keefe ([Keefe, 1989](#)) for the design of woodwind instruments, and this is also what we shall use. To ensure best results, this characterization must be done with professional musicians.

## 1.3 The Air Column

The analysis of wind instrument air columns is a challenging scientific problem that has captured the attention of mathematicians and philosophers since the early development of acoustics ([Lindsay, 1966](#)). The musical acoustician wishing to predict the properties of wind instruments with the level of accuracy that a musician's remarkably sensitive ear can detect, needs to take into account very fine details of the physical phenomena involved in the production of sound. The present state of scientific knowledge in this field is advanced, although some refinements are necessary if one wants to improve current instruments by scientific calculation.

The air columns of most instruments have quite a complicated geometry. Based on either a cylindrical or a conical bore, they deviate from these ideal geometries in some of their parts ([Nederveen, 1969/1998a](#)): pipes may be bent for practical reasons, some instruments terminate in a flaring bell, instruments sometimes present slight contractions or enlargements in some of their parts and, finally, instruments may be provided with toneholes or valves.

### 1.3.1 Modelling Methods

Numerical methods such as the Boundary Element Method (BEM), Finite Difference Method (FDM), Finite Element Method (FEM) and Lattice Boltzmann Method (LBM) have been used for the analysis of wind instruments ([Nederveen, Jansen, & Hassel, 1998](#); [A. R. da Silva, 2008](#); [Kantartzis, Katsibas, Antonopoulos, & Tsiboukis, 2004](#); [Noreland, 2002](#); [Dubos et al.,](#)

1999a). Such methods, based on the discretization of the geometry in small elements for which fundamental equations can be solved, have the advantage that complex geometries can be handled easily. On the other hand, they pose serious problems for their use as part of an automatic optimization design algorithm because of the huge computation time necessary to solve a complete model of an instrument for all of its fingerings.

Another approach to the modelling of wind instruments is the Transmission-Matrix Method (TMM) (Plitnik & Strong, 1979; Caussé, Kergomard, & Lurton, 1984; Keefe, 1990; Mapes-Riordan, 1993; Walstijn & Campbell, 2003). The TMM approximates the geometry of a structure as a sequence of concatenated segments, each being mathematically represented as a 4x4 matrix, in which the terms are complex-valued and frequency-dependent. Calculating the acoustic properties of the system at each frequency of interest requires multiplying together the matrix of each segment. The four terms of these matrices are calculated using mathematical models that were developed from theoretical calculations, semi-empirical methods or from the results of numerical simulations.

For purposes of designing wind instruments with the aid of an optimization algorithm, an efficient method is required in order to obtain results in a reasonable amount of time. The TMM fulfils this requirement but, even though its accuracy is said to be “good enough”, we propose to compare the results of the TMM with the FEM for verification purposes and for the development of transmission-matrix models. This is the subject of Chapters 2 and 3.

The TMM method for calculating the input impedance of woodwind instruments is described below, followed by a number of sections presenting results from the literature on modelling each part of an instrument using the TMM. The input impedance function fully characterizes the one-dimensional response of a wind instrument when non-linear effects are negligible. Using the TMM, this impedance can be efficiently and accurately calculated for frequencies sufficiently low that no higher-order modes are propagated, that is, for cylinders, when  $2\pi f < 1.841c/a$ , where  $c$  is the speed of sound and  $a$  its radius; see Scavone (1997, p. 18)

for cones. This maximal frequency is above 10 kHz for the concert flute and the clarinet; it becomes lower for larger instruments but, because these larger instruments play lower frequency notes, the higher frequency of interest is also lower. Even though, to our knowledge, there is no study that determines a sufficient number of resonances to characterize the behavior of an instrument, we estimate that from 5 to 10 resonances are enough. A low pitch instrument such as the barytone saxophone plays its lowest note at a frequency of approximately 70 Hz, which require to calculate the impedance up to a maximal frequency of a little more than 700 Hz whereas no higher-order modes are propagated below around 1500 Hz. Therefore, it seems that these higher-order modes always occurs at frequencies sufficiently high that they do not perturb the acoustics of the instrument.

Another of the hypotheses on which the TMM is based – that the evanescent modes excited near each discontinuity decay sufficiently within each segment of the model to be independent of one another – is only partially fulfilled but generally introduces negligible errors, as reported by [Keefe \(1983\)](#). The worst case would happen for instruments with closely spaced large holes, an issue that is investigated further in [Chapter 3](#) to determine the possible consequences of this effect.

Each section of an instrument is represented by a matrix  $\mathbf{T}$  relating the pressure and volume flow from the output to the input plane and is expressed as:

$$\begin{bmatrix} p_{in} \\ Z_0 U_{in} \end{bmatrix} = \begin{bmatrix} T_{11} & T_{12} \\ T_{21} & T_{22} \end{bmatrix} \begin{bmatrix} p_{out} \\ Z_0 U_{out} \end{bmatrix}, \quad (1.3.1)$$

where  $Z_0 = \rho c / S$  is approximately equal to the characteristic impedance  $Z_c$  of the waveguide at the location of the plane,  $\rho$  is the fluid density,  $c$  is the speed of sound in free field and  $S$  is the cross-sectional area of the pipe. The properties of the complete instrument are then calculated from each transmission matrix  $\mathbf{T}_n$  and the normalized radiation impedance  $\bar{Z}_{rad} = p_{out} / Z_0 U_{out}$

as:

$$\begin{bmatrix} p_{in} \\ Z_0 U_{in} \end{bmatrix} = \left( \prod_{i=1}^n \mathbf{T}_i \right) \begin{bmatrix} \bar{Z}_{rad} \\ 1 \end{bmatrix}. \quad (1.3.2)$$

The normalized input impedance is then calculated simply as  $\bar{Z}_{in} = p_{in}/Z_0 U_{in}$ .

### 1.3.2 Cylindrical and Conical Waveguides

The air columns of woodwind instruments are waveguides comprising cylindrical or conical sections with open or closed toneholes. The theoretical expression of the transmission matrix of a lossy cylinder of length  $L$  is:

$$\mathbf{T}_{cyl} = \begin{bmatrix} \cosh(\Gamma L) & \bar{Z}_c \sinh(\Gamma L) \\ \sinh(\Gamma L)/\bar{Z}_c & \cosh(\Gamma L) \end{bmatrix}, \quad (1.3.3)$$

where  $\Gamma$  is a complex-valued propagation wavenumber and  $\bar{Z}_c = Z_c/Z_0$  is a normalized complex-valued characteristic impedance. Various sources discuss the theory of wave propagation in a waveguide with boundary layer losses (Kirchhoff, 1868; Tijdeman, 1975; Keefe, 1984; Pierce, 1989; Chaigne & Kergomard, 2008). These parameters can be calculated exactly with  $\Gamma = \sqrt{\bar{Z}_v \bar{Y}_t}$  and  $\bar{Z}_c = \sqrt{\bar{Z}_v / \bar{Y}_t}$ , where

$$\bar{Z}_v = jk \left( 1 - \frac{2}{k_v a} \frac{J_1(k_v a)}{J_0(k_v a)} \right)^{-1}, \quad (1.3.4)$$

$$\bar{Y}_t = jk \left( 1 + (\gamma - 1) \frac{2}{k_t a} \frac{J_1(k_t a)}{J_0(k_t a)} \right). \quad (1.3.5)$$

The meaning of the symbols is:

$k = \omega/c$	wavenumber,
$\omega = 2\pi f$	angular frequency,
$c$	speed of sound in free field,
$\mu$	fluid viscosity,
$\rho$	fluid density,
$a$	radius of the waveguide,
$\gamma$	ratio of specific heats,
$Pr = c_p\mu/\kappa$	Prandtl number,
$k_v = \sqrt{-jk/l_v}$	viscous diffusion wavenumber,
$l_v = \mu/\rho c$	vortical characteristic length,
$k_t = \sqrt{-jk/l_t}$	thermal diffusion wavenumber,
$l_t = l_v/Pr$	thermal characteristic length,
$J_0$	Bessel function of the first kind and order 0,
$J_1$	Bessel function of the first kind and order 1.

The values of the fluid properties of air vary with the temperature  $T$  in Celcius degrees and

may be calculated with (Keefe, 1984):

$$\begin{aligned}\Delta T &= T - 26.85, \\ \mu &= 1.8460 \times 10^{-5}(1 + 0.00250\Delta T) && [\text{kg}/(\text{ms})], \\ \rho &= 1.1769(1 - 0.00335\Delta T) && [\text{kg}/\text{m}^3], \\ c &= 3.4723 \times 10^2(1 + 0.00166\Delta T) && [\text{m}/\text{s}], \\ \gamma &= 1.4017(1 - 0.00002\Delta T), \\ Pr &= 0.71,\end{aligned}$$

If losses are not considered in the cylindrical waveguide, Eq. (1.3.3) simplifies to:

$$\mathbf{T}_{cyl} = \begin{bmatrix} \cos kL & j \sin kL \\ j \sin kL & \cos kL \end{bmatrix}. \quad (1.3.6)$$

For a conical waveguide, the transmission matrix is (Kulik, 2007):

$$\mathbf{T}_{cone} = r \begin{bmatrix} -t_{out} \sin(\bar{k}L - \theta_{out}) & j \sin(\bar{k}L) \\ jt_{in}t_{out} \sin(\bar{k}L + \theta_{in} - \theta_{out}) & t_{in} \sin(\bar{k}L + \theta_{in}) \end{bmatrix}, \quad (1.3.7)$$

where  $x_{in}$  and  $x_{out}$  are, respectively, the distance from the apex of the cone to the input and output planes of the cone;  $r = x_{out}/x_{in}$ ,  $L = x_{out} - x_{in}$  is the length of the cone;  $\theta_{in} = \arctan(kx_{in})$ ,  $\theta_{out} = \arctan(kx_{out})$ ,  $t_{in} = 1/\sin\theta_{in}$ ,  $t_{out} = 1/\sin\theta_{out}$  and  $\bar{k} = (1/L) \int_{x_{in}}^{x_{out}} k(x)dx$ , where  $k(x)$  is the propagation constant ( $k = i\Gamma$  in our notation) which depends on the radius at position  $x$ . The calculated input impedance of an unflanged open conical waveguide is compared to impedance measurement data in Fig. 1.1. The length of the cone is 965.2 mm with an input diameter of 12.5 mm and an output diameter of 63.1 mm. The measurement was made by the author using a two-microphone transfer function (TMTF) technique reported in Lefebvre and Scavone (2008).

When losses are not taken into account, the transmission matrix of a lossless expanding conical frustum is (Fletcher & Rossing, 1998):

$$\mathbf{T}_{cone} = r \begin{bmatrix} -t_{out} \sin(kL - \theta_{out}) & j \sin kL \\ jt_{in}t_{out} \sin(kL - \theta_{out} + \theta_{in}) & t_{in} \sin(kL + \theta_{in}) \end{bmatrix}, \quad (1.3.8)$$

where the symbols have the same definitions as in the previous equation.

To obtain the transmission matrix of a converging conical frustum, one can reverse the results obtained in the previous expression. The pressure and acoustic flow at the output of the diverging cone become those at the input of the converging cone, and vice versa. Because of the reversal in the direction, both acoustic flows need to be multiplied by negative one. We obtain:

$$\mathbf{T}_{reversed} = \frac{1}{AD - BC} \begin{bmatrix} D & B \\ C & A \end{bmatrix}, \quad (1.3.9)$$

where  $A$ ,  $B$ ,  $C$  and  $D$  are the coefficients of the diverging cone. This method may be used to obtain the transmission matrix of any reversed waveguide, that is, when the output plane becomes the input plane. This is not the same as inverting the transmission matrices; the inversion would lead to a negative sign before the  $A$  and  $D$  terms in Eq. (1.3.9).

Because many wind instruments are bent for practical reasons, the question of the effect of the curvature on the acoustic properties of waveguides has captured the attention of many researchers. Rayleigh (1896/1945) presupposes that the velocity potential is constant on any section perpendicular to the main axis to conclude that a curved pipe is equivalent to a straight pipe of the same length, as measured along the centre line. Nederveen (1969/1998a, p. 60), considering that the pressure is constant over the same cross-sections, concludes that the bent pipe appears slightly shorter and wider, which leads to the apparent phase velocity  $c\sqrt{\rho/\rho_B}$ , where  $\rho/\rho_B = (R^2 - R\sqrt{R^2 - a^2})/(\frac{1}{2}a^2)$  and  $R$  is the radius of curvature of the centre line of the pipe. As reported by Brindley (1973), neither of these two assumptions can be true. Furthermore, such expressions do not consider boundary layer losses.

---

Other attempts at estimating the effect of curvature have been reported by [Keefe and Benade \(1983\)](#); [Nederveen \(1998b\)](#); [Kim and Ih \(1999\)](#); [Kantartzis et al. \(2004\)](#); [Félix, Nederveen, Dalmont, and Gilbert \(2008\)](#). The influence of curvature is shown to be frequency dependent and much more complex than predicted by the simplified theories. Notably, in the case of the saxophone, the influence of the neck on the overall properties of the instrument depends on the curvature. That is, the neck curvature will have different influences depending on a given fingering. Furthermore, the boundary layer losses also play a significant role. Therefore, any attempt at calculating the acoustic properties of a curved bore must take into account both the curvature and the boundary layer losses. This problem can be tackled with the FEM and a special impedance boundary condition approximating the losses, as is demonstrated in [Sec. 3.6](#).

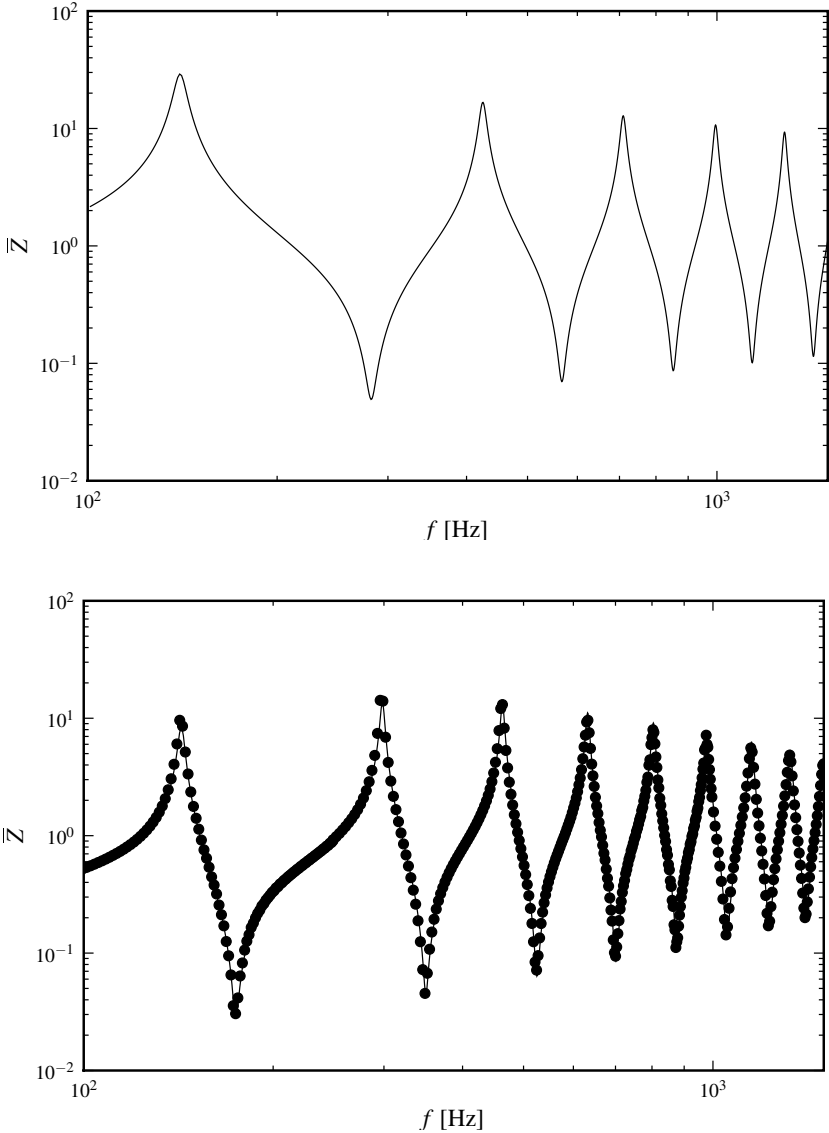


Figure 1.1: Input impedance of a cylindrical waveguide (top) and a conical waveguide (bottom): measured (filled circles) and calculated (solid line).

### 1.3.3 Radiation at Open Ends

Acoustic waves propagating in a waveguide are partly reflected and partly transmitted when they encounter any discontinuity. The portion of the incident wave reflected from the open end of a wind instrument helps maintain the self-sustained oscillations. At the open end of a pipe, the phase relation between the reflected and incident waves is non-zero. Thus, it always behaves as if the pipe was slightly longer than its actual size. This phenomenon occurs because the air vibrating at the open end accelerates the air surrounding this opening, which produces mass loading and effectively causes a phase shift between the reflected and the incident waves. The portion of the incident wave which is transmitted through the open end radiates into the space surrounding the instrument.

Many wind instruments terminate in a flaring waveguide called the “bell”, which allows the instrument designer to control the amount of reflected and transmitted energy as well as the phase shift of the reflected wave in a frequency-dependent way.

In the low-frequency limit, the radiation behaviour can be taken into account by an “end-correction”, which is the length of pipe that presents the same inertance as the radiation loading. In the case of a flanged termination (pipe opening in an infinite wall), the length correction is  $\delta_\infty = 0.8216a$ , whereas it is  $\delta_0 = 0.6133a$  for an unflanged termination (semi-infinite pipe of zero thickness), where  $a$  is the radius of the pipe. For a semi-infinite pipe of non-zero wall thickness, [Dalmont and Nederveen \(2001\)](#) give:

$$\delta/a = \delta_\infty + \frac{a}{b}(\delta_0 - \delta_\infty) + 0.057\frac{a}{b} \left[ 1 - \left(\frac{a}{b}\right)^5 \right], \quad (1.3.10)$$

where  $b$  is the external radius of the pipe.

The radiation impedance is frequency dependent. For an unflanged pipe it was calculated by [Levine and Schwinger \(1948\)](#). The evaluation of the exact solution demands performing a number of numerical integrals. An approximate formula for this impedance was given by

Caussé et al. (1984):

$$\begin{aligned} \bar{Z}_r = & 0.6113jka - j(ka)^3[0.036 - 0.034 \log ka + 0.0187(ka)^2] + \\ & (ka)^2/4 + (ka)^4[0.0127 + 0.082 \log ka - 0.023(ka)^2] \end{aligned} \quad (1.3.11)$$

The analysis of a flaring waveguide, which is often called a “horn” in the literature, involves a non-separable Laplacian operator (Noreland, 2002). The consequence is that higher-order evanescent modes couple with the plane wave mode. Any one-dimensional plane wave solution, such as Webster’s equation (Webster, 1919; Eisner, 1967), is an approximation and has only limited application to low-frequency and minimal flare contexts. The approach that consists of calculating the input impedance of horns from the multiplication of the transmission matrix of many truncated cones approximating the geometry is also a plane wave approximation and suffers from the same limitations as the Webster equation. Furthermore, there is no model available for the radiation impedance, because the form of the wave front at the opening is unknown. Nederveen and Dalmont (2008) propose a correction term to the one-dimensional approximation to account for the additional inertance in rapidly flaring horns.

In order to take into account the complexities of the sound field of horns, as well as the radiation behaviour from the open end, Noreland (2002) proposes a two-dimensional, finite-difference, time-domain (FDTD) method. The impedance at the throat of the horn can be coupled to a standard one-dimensional, transmission-line model for the non-flaring part of the instrument. Noreland (2002) found that the discrepancies between the TMM and the FDTD began to be noticeable at around 500 Hz. This numerical method does not include viscothermal losses.

Another approach to the calculation of the input impedance of horns is the multimodal decomposition method, originally presented by Pagneux, Amir, and Kergomard (1996). This method has the advantage that no discretization of the geometry is necessary. It involves solving a system of ordinary differential equations, the size of which depends on the number of modes that are to be taken into account. Increased precision of the results demands to change

only one parameter: the number of modes. This method can also accommodate the boundary layer losses for each mode, as presented by [Bruneau, Bruneau, Herzog, and Kergomard \(1987\)](#). The boundary condition at the open end needs to be specified as a multimodal radiation impedance matrix. Such an impedance matrix can be calculated in the case of a flanged opening, using the theory presented by [Zorumski \(1973\)](#). Unfortunately, no theories exist to calculate the multimodal impedance radiation matrix for an unflanged opening, which depends upon the external shape of the horn. Our solution to this problem consists in using the FEM as will be shown in [Sec. 3.7](#).

### 1.3.4 Toneholes

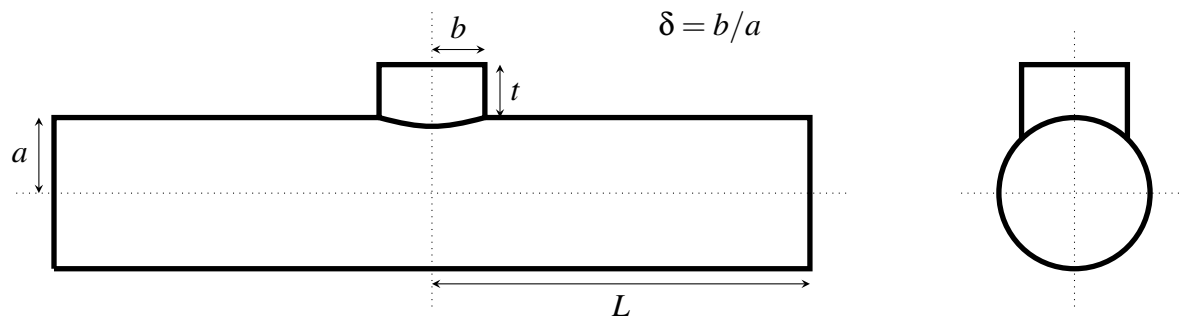


Figure 1.2: Diagram representing a tonehole on a pipe.

The presence of toneholes perturbs the sound field inside the air column. Varying their locations and geometric proportions provides a way to control the playing frequency and timbre of the instrument. Modelling woodwind instrument toneholes accurately is critical to the prediction of the playing characteristics of an instrument. In contrast to the bell, which influences the instrument's behaviour primarily when all the toneholes are closed, the toneholes are used for all the other notes and are, therefore, the most important elements of a woodwind

instrument's air column. The transmission matrix representing a tonehole is defined as:

$$\mathbf{T}_{hole} = \begin{bmatrix} A & B \\ C & D \end{bmatrix}, \quad (1.3.12)$$

which, when inserted between two segments of cylindrical duct, relates the input and output quantities:

$$\begin{bmatrix} p_{in} \\ Z_0 U_{in} \end{bmatrix} = \mathbf{T}_{cyl} \mathbf{T}_{hole} \mathbf{T}_{cyl} \begin{bmatrix} p_{out} \\ Z_0 U_{out} \end{bmatrix}, \quad (1.3.13)$$

where  $Z_0 = \rho c/S$  is approximately equal to the characteristic impedance of the waveguide of cross-sectional area  $S = \pi a^2$  and where the transmission matrix of a cylindrical duct of length  $L$  was defined in Eq. (1.3.6).

### Tonehole Transmission Matrices

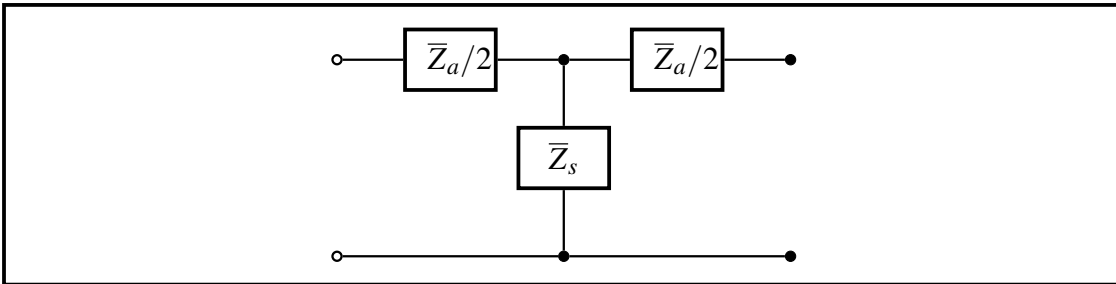


Figure 1.3: Block diagram of a symmetric tonehole

The transmission matrix of a tonehole may be approximated as a symmetric  $T$  section depending on two parameters, the shunt impedance  $\bar{Z}_s = Z_s/Z_0$  and the series impedance  $\bar{Z}_a =$

$Z_a/Z_0$  (Keefe, 1981), resulting in:

$$\begin{aligned} \mathbf{T}_{hole} &= \begin{bmatrix} 1 & \bar{Z}_a/2 \\ 0 & 1 \end{bmatrix} \begin{bmatrix} 1 & 0 \\ 1/\bar{Z}_s & 1 \end{bmatrix} \begin{bmatrix} 1 & \bar{Z}_a/2 \\ 0 & 1 \end{bmatrix} \\ &= \begin{bmatrix} 1 + \frac{\bar{Z}_a}{2\bar{Z}_s} & \bar{Z}_a(1 + \frac{\bar{Z}_a}{4\bar{Z}_s}) \\ 1/\bar{Z}_s & 1 + \frac{\bar{Z}_a}{2\bar{Z}_s} \end{bmatrix}. \end{aligned} \quad (1.3.14)$$

This equation was further simplified by Keefe (1981), who replaces all occurrences of  $\bar{Z}_a/\bar{Z}_s$  by zero on the assumption that  $|\bar{Z}_a/\bar{Z}_s| \ll 1$ , an approximation that introduces small but non-negligible errors in the calculation of the resonance frequencies.

The impedances  $\bar{Z}_s$  and  $\bar{Z}_a$  must be evaluated for the open ( $o$ ) and closed ( $c$ ) states of the tonehole as a function of geometry and frequency. Mathematical expressions for these impedances are available in the literature and are reviewed below.

### Open Tonehole — Shunt Impedance

The open tonehole shunt impedance may be expressed as (Keefe, 1982b)<sup>3</sup>:

$$\bar{Z}_s^{(o)} = \frac{1}{\delta^2} [jkt_s^{(o)} + \xi_s], \quad (1.3.15)$$

where  $\xi_s$  is the open tonehole shunt resistance,  $t_s^{(o)}$  the tonehole's equivalent length and  $\delta = b/a$  is the ratio of the radius of the tonehole to the radius of the air column. The shunt resistance does not influence the calculated playing frequencies of a woodwind instrument; thus, most research efforts concentrate on the determination of the correction of the shunt length. However, it is potentially important to take this resistance into account if aspects other than the tuning, such as the “ease of play” or the “response” of the instrument, are to be assessed from

<sup>3</sup> $\bar{Z}_s^{(o)} = Z_s/Z_0 = (Z_{0h}/Z_0)[jkt_s^{(o)} + \xi_s]$ , where  $Z_{0h} = \rho c/\pi b^2$  and  $Z_0 = \rho c/\pi a^2$ , which leads to  $Z_{0h}/Z_0 = (a/b)^2 = 1/\delta^2$

TMM calculations. In the most recent literature (Dalmont et al., 2002),  $t_s^{(o)}$  is written:

$$kt_s^{(o)} = kt_i + \tan k(t + t_m + t_r) \quad (1.3.16)$$

where  $t$  is the height of the tonehole as defined in Fig. 1.2,  $t_m$  is the matching volume equivalent length,  $t_r$  is the radiation length correction and  $t_i$  the inner length correction. Nederveen et al. (1998) obtained an accurate approximation for  $t_m$ :

$$t_m = \frac{b\delta}{8} (1 + 0.207\delta^3), \quad (1.3.17)$$

where  $\delta = b/a$  is the ratio of the radius of the tonehole to the radius of the main bore.

The terms  $t_i$  and  $t_r$  are generally difficult to calculate analytically; and, in the case where  $t$  is short, the coupling between the inner and outer length corrections prevents their separate analysis (Dalmont et al., 2002, sec. 2.7). The radiation length correction  $t_r$  depends on the external geometry. In the low-frequency approximation, it may be that of a flanged pipe ( $0.8216b$ ), an unflanged pipe ( $0.6133b$ ) or another intermediary value for more complicated situations. The expressions provided in the literature for the inner length correction  $t_i$  are summarized in Table 1.1. These expressions are only valid for toneholes of large height ( $t > b$ ). Note that the term  $\delta^2$  in Eq. (5) of Dalmont et al. (2002), which refers to Eq. (55b) of Dubos et al. (1999b), was removed to make this equation consistent with the convention of the series length correction used in this thesis, the modified equation is reported here as Eq. 1.3.25.

In the limiting case where  $t \rightarrow 0$  and  $b \rightarrow 0$  (very small radius and chimney), the low-frequency characteristics of the tonehole are those of a hole in an infinitely thin wall (Pierce, 1989, Eq. 7-5.10) and the total equivalent length of the hole becomes:

$$t_e = t + (\pi/2)b = t + 1.5708b. \quad (1.3.18)$$

If the tonehole is tall but the radius  $b \rightarrow 0$ , the tonehole's equivalent length becomes:

$$t_e = t + 0.6133b + 0.8216b = t + 1.4349b, \quad (1.3.19)$$

that is, the length of the tonehole with an unflanged length correction at the tonehole's radiating end and a flanged radiation length correction inside the instrument.

### Open Tonehole — Series Impedance

The series impedance of the open tonehole is a small negative inertance (acoustic mass):

$$\bar{Z}_a^{(o)} = jkt_a^{(o)}/\delta^2, \quad (1.3.20)$$

which reduces slightly the effective length of the instrument (raises the resonance frequencies). No significant resistive term was detected experimentally (Dalmont et al., 2002). This equation, with the division by  $\delta^2$ , is based on a series impedance defined as  $Z_a = jkZ_{0h}t_a$ , where  $Z_{0h} = \rho c/\pi b^2$ . This definition was used by Keefe (1982b). If, instead, the series impedance is defined as  $Z_a = jkZ_0t_a$  such as in (Dalmont et al., 2002), the term  $\delta^2$  doesn't appear. Depending on the convention used, the equations for the series length corrections will differ by a factor  $\delta^2$ . Table 1.2 summarizes the equations found in the literature, converted to the form used in this thesis.

### Closed Tonehole — Shunt Impedance

The shunt impedance of a closed tonehole behaves mainly as an acoustic compliance (capacitance in the electric-circuit analog) (Nederveen, 1969/1998a). This can be written:

$$\bar{Z}_s^{(c)} = -j\frac{1}{\delta^2kt_s^{(c)}}. \quad (1.3.21)$$

Nederveen (1969/1998a), Eq. (38.3)	$t_i^{(o)} = (1.3 - 0.9\delta)b$	(1.3.22)
Keefe (1982b), Eq. (67a)	$t_i^{(o)} = (0.79 - 0.58\delta^2)b$	(1.3.23)
Nederveen et al. (1998), Eq. (40)	$t_i^{(o)} = (0.82 - 1.4\delta^2 + 0.75\delta^{2.7})b$	(1.3.24)
Dubos et al. (1999b), Eq. (55b) and (73)	$t_i^{(o)} = t_s^{(o)} - t_a^{(o)}/4,$ $t_s^{(o)} = (0.82 - 0.193\delta - 1.09\delta^2 + 1.27\delta^3 - 0.71\delta^4)b$	(1.3.25)

Table 1.1: Comparison of the expressions for the open tonehole inner length correction  $t_i^{(o)}$ 

Keefe (1982b), Eq. (68b)	$t_a^{(o)} = -\frac{0.47b\delta^4}{\tanh(1.84t/b)+0.62\delta^2+0.64\delta}$	(1.3.26)
Nederveen et al. (1998), Fig. 11	$t_a^{(o)} = -0.28b\delta^4$	(1.3.27)
Dubos et al. (1999b), Eq. (74)	$t_a^{(o)} = -\frac{b\delta^4}{1.78\tanh(1.84t/b)+0.940+0.540\delta+0.285\delta^2}$	(1.3.28)
Dubos et al. (1999b), not numbered	$t_a^{(o)} = -(0.37 - 0.087\delta)b\delta^4$	(1.3.29)

Table 1.2: Comparison of the expressions for the open tonehole series length corrections  $t_a^{(o)}$ 

The simplest expression for the shunt length correction is that of a closed cylinder of equivalent volume:

$$kt_s^{(c)} = \tan k(t + t_m). \quad (1.3.30)$$

An inner length correction may be considered as well for the closed tonehole, but its influence is small relative to the cotangent term and becomes significant only in the high frequencies (Keefe, 1990). A recent expression including the inner length correction is (Nederveen et al., 1998, Eq. 7):

$$\bar{Z}_s^{(c)} = \frac{j}{\delta^2} \left[ kt_i - \cot k(t + t_m) \right], \quad (1.3.31)$$

where  $t_i$  is the same as for the open tonehole as defined in Eq. (1.3.24).

### Closed Tonehole — Series Impedance

The closed tonehole series impedance behaves as a small negative inertance, as in the case of the open tonehole. This can be expressed as:

$$\bar{Z}_a^{(c)} = jkt_a^{(c)}/\delta^2, \quad (1.3.32)$$

where  $t_a^{(c)}$  is the series length correction. [Keefe \(1981, Eq. 54\)](#) proposed:

$$t_a^{(c)} = -\frac{0.47b\delta^4}{\coth(1.84t/b) + 0.62\delta^2 + 0.64\delta}, \quad (1.3.33)$$

whereas [Dubos et al. \(1999a, Eq. 74\)](#) calculated the length correction in the same situation as:

$$t_a^{(c)} = -\frac{b\delta^4}{1.78 \coth(1.84t/b) + 0.940 + 0.540\delta + 0.285\delta^2}. \quad (1.3.34)$$

### The Effect of a Hanging Pad

If a key is hanging above the hole, the length correction  $t_r$  increases by ([Dalmont & Nederveen, 2001, Eq. \(48\)](#)):

$$\Delta t_r = \frac{b}{3.5(h/b)^{0.8}(h/b + 3w/b)^{-0.4} + 30(h/r)^{2.6}}, \quad (1.3.35)$$

where  $r$  is the radius of the key,  $h$  its distance to the hole,  $b$  the radius of the tonehole and  $w$  the thickness of the tonehole wall. This expression was obtained from the analysis of an unflanged pipe with a circular disk using the Finite Difference Method. This expression is thus likely to be valid for a tonehole of taller height but needs to be verified for shorter toneholes.

### Mutual Interaction between Toneholes

Modelling woodwind instruments as a transmission line composed of independent parts, such as toneholes and segments of waveguides, implicitly assumes there are no higher-order internal interactions or external couplings between the different parts of an instrument. This

assumption may break down when the evanescent modes occurring near a discontinuity interact with another part of the instrument or if the radiated sound from one part of the instrument interacts with another part. This is likely to occur for instruments with large toneholes such as the saxophone and the concert flute.

This problem has been considered by [Keefe \(1983\)](#). At low frequencies, the evanescent modes caused by a discontinuity diminish rapidly in amplitude away from the discontinuity. It is generally assumed that their amplitude is not negligible within a distance of one main bore diameter on either side of the discontinuity. Thus, [Keefe](#) defined an internal interaction parameter  $\delta$ :

$$\delta = a/(s - b), \quad (1.3.36)$$

where  $a$  is the radius of the main bore,  $b$  is the radius of the tonehole and  $s$  is half the distance between the two holes (centre to centre). Higher values of this parameter indicate a higher likelihood of internal interaction. He also defined an external interaction parameter:

$$\varepsilon = \frac{1}{4} \frac{b^2}{2st_e}, \quad (1.3.37)$$

where  $t_e$  is the effective length of the tonehole. This parameter indicates the importance of the change in tonehole's length correction due to the external interaction.

[Keefe \(1983\)](#) measured the pressure on a planar surface in an experimental air column featuring two holes at a distance typical of an alto saxophone and demonstrated that the evanescent modes are still present and not negligible (around 8 to 10 dB differences in SPL at different points on this surface). Another experiment was designed to measure the effective length of a tonehole in the presence of a second identical hole at a different distance  $s$ . When the toneholes are far from each other, the effective length of each hole is equal to the single tonehole value as described previously. When the toneholes are closer to each other, the effective length is longer than the single tonehole value. This effect becomes even more important when a key is located above the hole. This problem will be considered using the FEM in Chapter 3 in order

to quantify the error introduced in the TMM if this effect is neglected.

### Non-linear Effects in Toneholes

[Keefe \(1983\)](#) studied the non-linear phenomena in short, wide diameter toneholes. He concluded that the ratio  $2b/t$  of tonehole radius to tonehole height is an important parameter in the design of an instrument. When a tonehole is short, the acoustic flow in the tonehole may be subject to a greater convective acceleration (the term  $\vec{v} \cdot \nabla \vec{v}$  in the Navier-Stokes equations), a term that is dropped in the development of linear acoustic equations. Any theory based on linear acoustics will underestimate the losses when this non-linear effect occurs. It is important to remember that the fabrication of prototypes based on the Transmission-Matrix Theory can lead to dysfunctional instruments because there is no consideration of these losses. These losses increase with the sound pressure level in the instrument and may pose a limit to the dynamic range available to instrumentalists. Woodwind instruments are often constructed with a radius of curvature at the junction between the bore and the hole, which reduces this convective acceleration. Instrument makers empirically try to minimize these non-linear losses by smoothing discontinuities at the bore / hole junction. The toneholes of good instruments made of wood, such as clarinets, oboes, renaissance flutes, and other similar instruments, are known to be undercut, that is, material was removed from under the tonehole, effectively reducing the sharpness of the edges. On metal instruments, the corners are rounded. The presence of non-linearity in toneholes has been investigated experimentally by [Dalmont et al. \(2002\)](#), who found that non-linear losses add a real part to the series impedance:

$$\Re\{Z_a\} = K_a M_h Z_c, \quad (1.3.38)$$

where  $K_a = 0.4 \pm 0.05/\delta^2$  and  $M_h = v_h/c$ . There is also a real part to the shunt impedance:

$$\Re\{Z_h\} = K_h M_h Z_c, \quad (1.3.39)$$

where  $K_h = 0.5 \pm 0.1$  and depends on the radius of curvature at the junction between the tonehole and the air column.

## Chapter 2

# Finite Element Simulations of Single Woodwind Toneholes

The design of a woodwind instrument using computer models requires accurate calculations of the resonance frequencies of an air column with open and closed toneholes. Although there have been many theoretical, numerical, and experimental research studies on the single woodwind tonehole (Keefe, 1982b, 1982a; Nederveen et al., 1998; Dubos et al., 1999b; Dalmont et al., 2002), it is known that current Transmission Matrix theories are not valid if the tonehole height  $t$  is shorter than the radius  $b$  (see Fig. 1.2) because “in that case the radiation field and the inner field are coupled” (Dalmont et al., 2002). It is expected that the shunt and series length corrections of the toneholes vary with the height of the tonehole. Furthermore, the magnitude of a potential influence of the conicity of the main bore on the tonehole parameters is unknown and current theories of the effect of a hanging keypad may not be valid for short toneholes.

The goals of the research presented in this chapter are to apply Finite Element Methods (FEM) for the calculation of the Transmission Matrix parameters of woodwind instrument toneholes and to develop new formulas that extend the validity of current tonehole theories. The FEM allows for a three-dimensional representation of a structure with coupled internal

and external domains; it solves the Helmholtz equation  $\nabla^2 p + k^2 p = 0$ , taking into account any complexities of the geometry under study with no further assumptions. For all the simulation results in this thesis, curved third-order Lagrange elements are used. All open simulated geometries include a surrounding spherical radiation domain that uses a second-order non-reflecting spherical-wave boundary condition on its surface, as described by Bayliss, Gunzburger, and Turkel (1982). Further discussion of this topic can be found in Tsynkov (1998) and Givoli and Neta (2003). It should be noted that no boundary layer losses are accounted for in the FEM simulations in this chapter. The inclusion of these losses greatly complicates the development of fit formulas because the results no longer scale linearly with the physical dimensions of the system. This is because the losses depend on the boundary layer thickness. Nevertheless, the inclusion of boundary layer losses in simulations using the FEM is discussed in Chapter 3. Our FEM simulations were computed using the “pressure acoustic” module of the software package COMSOL (version 3.5a) with the Matlab interface. The COMSOL/Matlab scripts for the simulations in this chapter are available from the CAML<sup>1</sup> website, by contacting the author<sup>2</sup> or, for pdf viewers supporting file attachment, directly in this document (see the margin icons). Only a few PDF readers, such as Adobe Reader, support file attachments.

The first section of this chapter presents the results of a validation of the FEM by calculating the radiation impedance of a flanged and an unflanged pipe. The second section describes the methodology with which the Transmission Matrix parameters of an object are obtained from FEM simulations. Next, the main section of this chapter presents the results of the characterization of a single unflanged tonehole and a single tonehole on a thick pipe, including an estimation of the required accuracy of the equivalent lengths, a description of our data-fit procedure, an investigation of the influence of the keypad and a study of the impact of the conicity of the main bore. Finally, a summary section reiterates the various findings and contributions

---

<sup>1</sup><http://www.music.mcgill.ca/caml/doku.php?id=projects:fem>

<sup>2</sup>[antoine.lefebvre2@mail.mcgill.ca](mailto:antoine.lefebvre2@mail.mcgill.ca)

to the field presented in this chapter.

## 2.1 Validation of the FEM

In this section, we verify the validity of the acoustic FEM and of the non-reflecting boundary condition with two simple simulation cases in 3D. We calculated, from the results of simulations, the radiation impedance of a flanged cylindrical pipe and an unflanged cylindrical pipe as a function of frequency and compared the results with theoretical expressions.

A schema of the models for both cases is depicted in Fig. 2.1, where  $a = 10$  mm. Only one quarter of the model was solved, taking advantage of the symmetries. On the symmetry planes, a null normal acceleration boundary condition (BC) is imposed. In order to obtain accurate results, the mesh along the circular edge at the opening of the pipe was refined to 64 points on the circumference. The mesh, for the unflanged pipe case, is displayed in Fig. 2.2 and, for the flanged pipe case, in Fig. 2.3. The maximal frequency simulated corresponds to  $ka = 1$  (approximately 5.5 kHz), which has a wavelength of about 63 mm. The number of degrees of freedom (DOF) in a model is recommended to be at least 1728 per wavelength cubed (12 DOF/wavelength in each direction). At our maximal frequency, this is approximately  $7 \times 10^6$  DOF/m<sup>3</sup>.

In the case of the unflanged pipe, our model has 41259 DOF (1825 mesh points and 8362 elements), which results in a density 45 times higher than the requirement. Many DOF are concentrated near the open end of the pipe. The density of the DOF is much smaller near the spherical surface but is still within the requirement.

In the case of the flanged pipe, our model has 25319 DOF (1144 mesh points and 5062 elements), which results in a density more than 200 times higher than the requirement. Once again, many DOF are concentrated near the open end of the pipe.

The COMSOL/Matlab simulation scripts used for these simulations are `unflangedpipe.m` and `flangedpipe.m`.



The radiation impedance is obtained from the input impedance  $Z_{in} = p_{in}/Z_c U_{in}$  with this equation:

$$\bar{Z}_r = \frac{\bar{Z}_{in} \cos(kL) - j \sin(kL)}{\cos(kL) - j \bar{Z}_{in} \sin(kL)}. \quad (2.1.1)$$

The results are compared with theory in Fig. 2.4. The unflanged pipe theoretical curve was evaluated from a numerical integration of the [Levine and Schwinger \(1948\)](#) solution. The match is very good in this case. The flanged pipe theoretical curve was calculated from an approximate formula from [Norris and Sheng \(1989, Eq. \(29\)\)](#). The differences between our simulations and theory grow with frequency but comparison with [Norris and Sheng \(1989, Fig. 7\)](#) reveal similar discrepancies with their numerical calculations, suggesting that the approximate formula is the cause.

These results confirm the validity of the FEM used in this thesis and suggest refining the mesh along edges where the flow displays strong acceleration. Our procedure consisted in solving the same problem with a gradually finer mesh until the results stabilize. The same procedure was applied for the simulation of toneholes in the next sections.

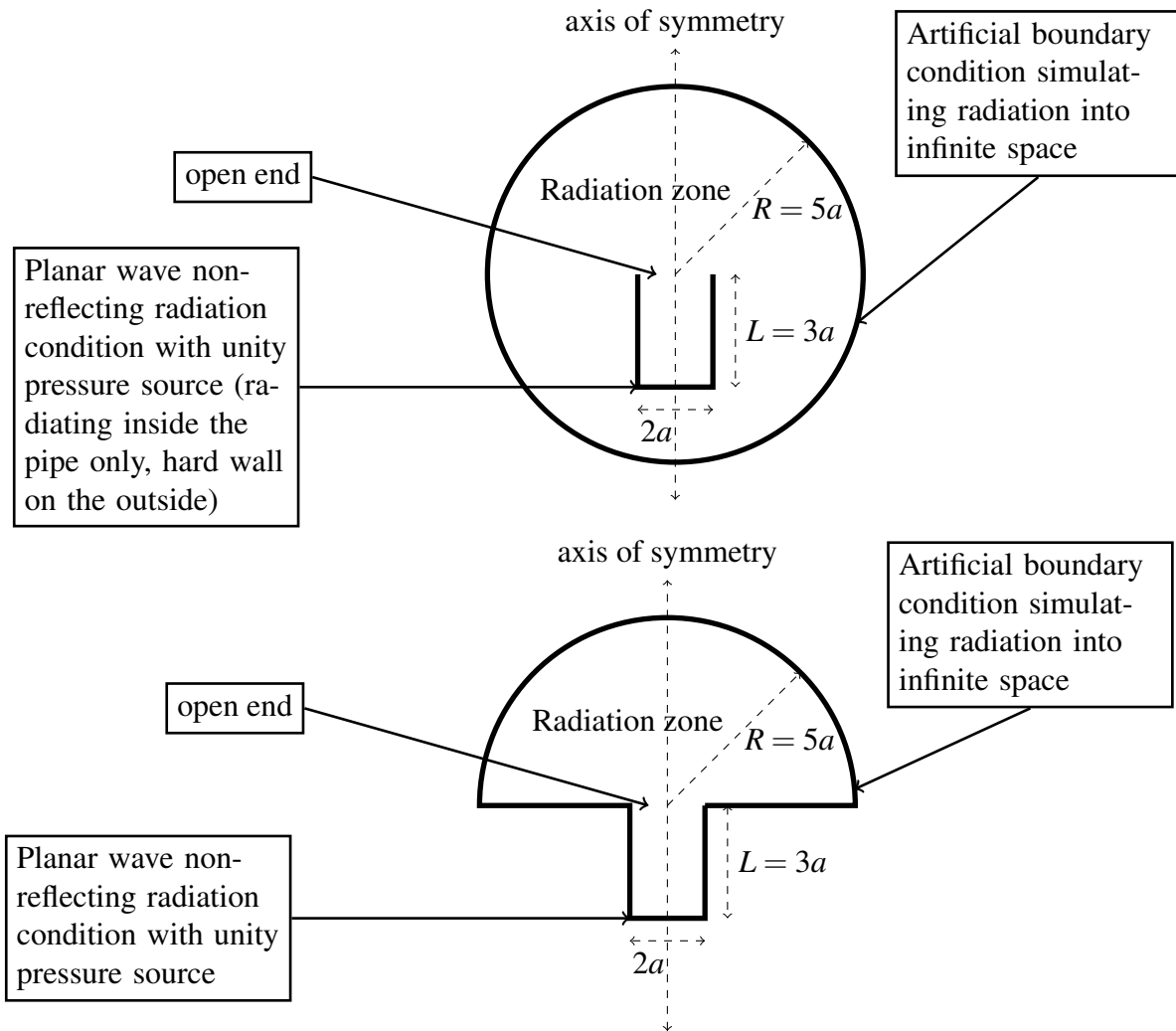


Figure 2.1: Diagrams of the FEM models for the radiation of an unflanged pipe (top) and a flanged pipe (bottom).

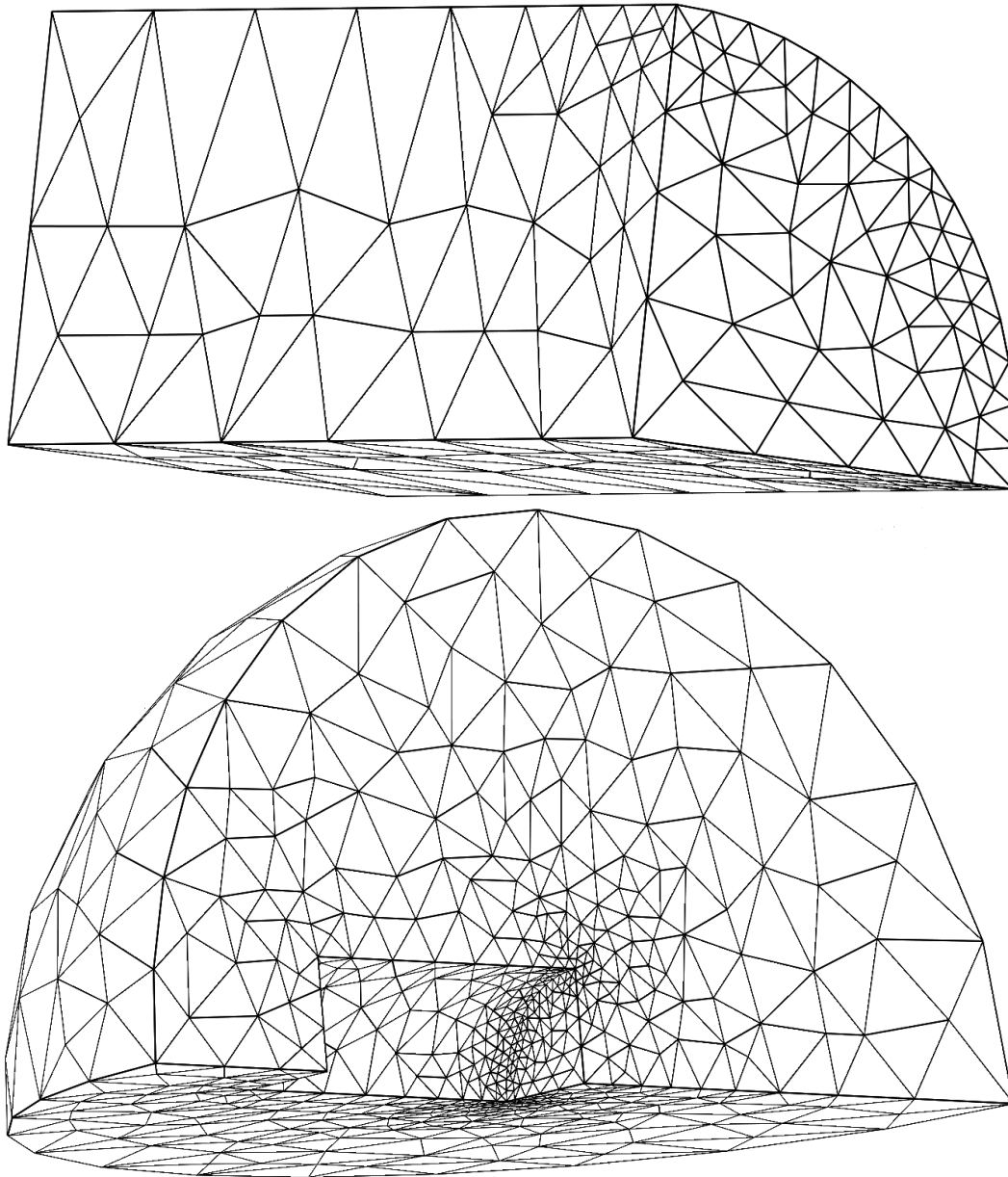


Figure 2.2: Visualisation of the FEM mesh for the unflanged pipe test case. The pipe (top) and the radiation domain (bottom) are separated to help visualize the details.

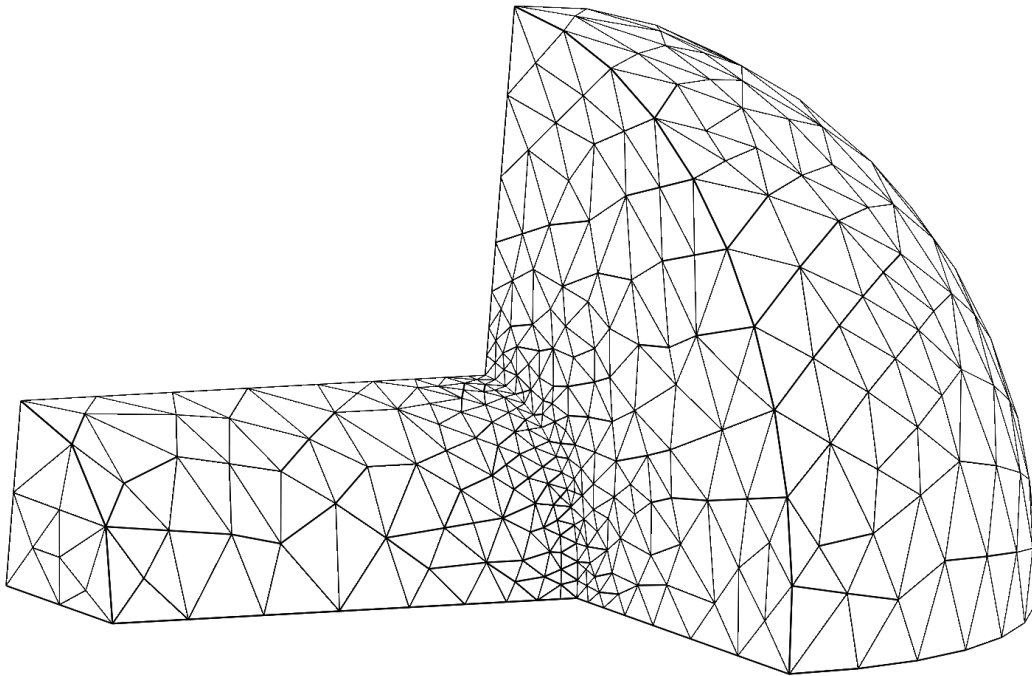


Figure 2.3: Visualisation of the FEM mesh for the flanged pipe test case.

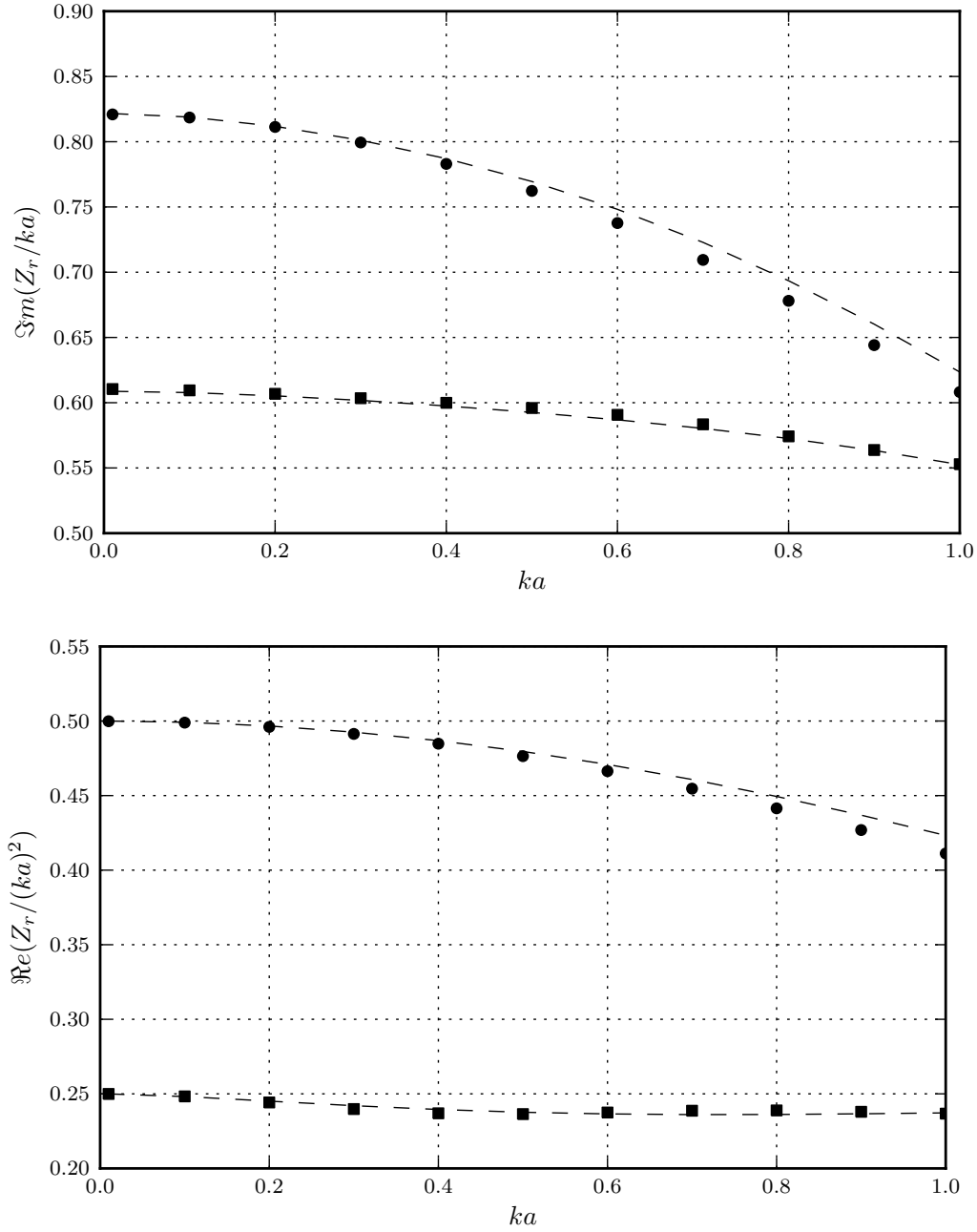


Figure 2.4: Real part (bottom graph) and imaginary part (top graph) of the radiation impedance of the pipes: FEM results for the unflanged pipe (squares) and for the flanged pipe (circles) compared with theory (dashed).

## 2.2 From FEM Results to Transmission Matrices

In this section, we present a method to calculate the transmission matrix  $\mathbf{T}_{obj}$  of an object from the FEM. This method is useful to characterize an object that is part of a waveguide, i.e. which has an input and an output plane. It can be used to obtain the Transmission Matrix of any type of discontinuity in a waveguide. One requirement is that the evanescent modes occurring near the discontinuity must be sufficiently damped at the input and output planes of the simulated model. In general, cylindrical segments are thus required before and after the discontinuity. These modes decay exponentially with distance and a length of five times the radius will ensure that they have decayed by a factor of more than  $1 \times 10^{-3}$  following calculations based on the theory of guided waves presented in [Pierce \(1989, Chapter 7\)](#). The transmission matrix obtained from the simulations is given by  $\mathbf{T} = \mathbf{T}_{cyl_1} \mathbf{T}_{obj} \mathbf{T}_{cyl_2}$  where the Transmission Matrix of a cylindrical duct was defined in Eq. (1.3.6). The effect of the cylinders is removed by calculation using the inverse of the cylinder's transmission matrix:

$$\mathbf{T}_{obj} = \mathbf{T}_{cyl_1}^{-1} \mathbf{T} \mathbf{T}_{cyl_2}^{-1}. \quad (2.2.1)$$

A transmission matrix  $\mathbf{T}$  contains four frequency-dependent, complex-valued parameters relating input quantities to output quantities, as previously defined in Eq. (1.3.1). In order to obtain these four parameters from finite element simulation results, we need to simulate the problem two times with different boundary conditions. By combining the results for the two simulation cases (subscripts 1 and 2), we can write a system of linear equations to solve for the four parameters of the transmission matrix:

$$\begin{bmatrix} p_{out_1} & Z_0 U_{out_1} & 0 & 0 \\ 0 & 0 & p_{out_1} & Z_0 U_{out_1} \\ p_{out_2} & Z_0 U_{out_2} & 0 & 0 \\ 0 & 0 & p_{out_2} & Z_0 U_{out_2} \end{bmatrix} \begin{bmatrix} T_{11} \\ T_{12} \\ T_{21} \\ T_{22} \end{bmatrix} = \begin{bmatrix} p_{in_1} \\ Z_0 U_{in_1} \\ p_{in_2} \\ Z_0 U_{in_2} \end{bmatrix}. \quad (2.2.2)$$

If the object under investigation is symmetric (reversing the input and output conditions leads to exactly the same system), we can take advantage of this feature to solve only one-half of the geometry. On the symmetry plane, we define alternatively a null normal acceleration for the symmetric case (case 1) and a null pressure for the anti-symmetric case (case 2). From the values of the pressure and normal velocity on the input plane of the model, we can deduce the values on the output plane for both simulation cases:

$$p_{out_1} = p_{in_1}, \quad (2.2.3)$$

$$Z_0 U_{out_1} = -Z_0 U_{in_1}, \quad (2.2.4)$$

$$p_{out_2} = -p_{in_2}, \quad (2.2.5)$$

$$Z_0 U_{out_2} = Z_0 U_{in_2}. \quad (2.2.6)$$

### 2.2.1 Transmission Matrix Parameters of a Tonehole

The transmission matrix representing a tonehole is defined as the matrix  $\mathbf{T}_{hole}$  which, when inserted between two segments of cylindrical duct, relates the input and output quantities as presented in Sec. 1.3.4. The matrix  $\mathbf{T} = \mathbf{T}_{cyl} \mathbf{T}_{hole} \mathbf{T}_{cyl}$  is obtained with the procedure described above. The transmission matrix for the tonehole is then retrieved by removing the effect of the cylindrical pipes:

$$\mathbf{T}_{hole} = \begin{bmatrix} A & B \\ C & D \end{bmatrix} = \mathbf{T}_{cyl}^{-1} \mathbf{T} \mathbf{T}_{cyl}^{-1}. \quad (2.2.7)$$

The tonehole transmission matrix is approximated as a symmetric  $T$  section depending on two parameters, the shunt impedance  $\bar{Z}_s$  and the series impedance  $\bar{Z}_a$ , which becomes:

$$\mathbf{T}_{hole} = \begin{bmatrix} 1 & \bar{Z}_a/2 \\ 0 & 1 \end{bmatrix} \begin{bmatrix} 1 & 0 \\ 1/\bar{Z}_s & 1 \end{bmatrix} \begin{bmatrix} 1 & \bar{Z}_a/2 \\ 0 & 1 \end{bmatrix} = \begin{bmatrix} 1 + \frac{\bar{Z}_a}{2\bar{Z}_s} & \bar{Z}_a(1 + \frac{\bar{Z}_a}{4\bar{Z}_s}) \\ 1/\bar{Z}_s & 1 + \frac{\bar{Z}_a}{2\bar{Z}_s} \end{bmatrix}. \quad (2.2.8)$$

Thus, we may extract the two impedances from the finite element simulation results with:

$$\bar{Z}_s = 1/C, \quad (2.2.9)$$

$$\bar{Z}_a = 2(A - 1)/C, \quad (2.2.10)$$

and the shunt and series equivalent lengths with:

$$t_s = \Re e \left( \frac{\delta^2 \bar{Z}_s}{jk} \right), \quad (2.2.11)$$

$$t_a = \Re e \left( \frac{\delta^2 \bar{Z}_a}{jk} \right). \quad (2.2.12)$$

### 2.2.2 Tonehole Model Validation

The results of our FEM simulations are compared with the experimental data obtained by [Dalmont et al. \(2002\)](#) and [Keefe \(1982a\)](#). [Dalmont et al. \(2002\)](#) measured the shunt and series equivalent lengths of a single flanged tonehole on a pipe of radius  $a = 10$  mm as a function of frequency for two different tonehole geometries: (1)  $\delta = 0.7$ ,  $t/b = 1.3$  and (2)  $\delta = 1.0$ ,  $t/b = 1.01$ . Both tonehole geometries were flanged at their open end. We have also compared our simulation results with data obtained by [Keefe \(1982a\)](#), who measured the shunt and series equivalent lengths of a single unflanged tonehole on a cylinder of radius  $a = 20$  mm for two tonehole geometries: (1)  $\delta = 0.66$ ,  $t/b = 0.48$  and (2)  $\delta = 0.32$ ,  $t/b = 3.15$ . The geometry of a tonehole is shown in [Fig. 1.2](#) for an unflanged opening. In the case of the flanged tonehole, the same parameters are used and the only difference is that the tonehole terminates in an infinite wall.

The mesh of the FEM model for the tonehole with  $\delta = 0.7$  studied by [Dalmont et al. \(2002\)](#) is shown in [Fig. 2.5](#). It consists of 56015 DOF (2512 mesh points and 11236 elements). The refinement of the mesh along the edge at the opening of the tonehole is such that there are approximately 100 elements on the circumference (25 elements for one quarter). The mesh is

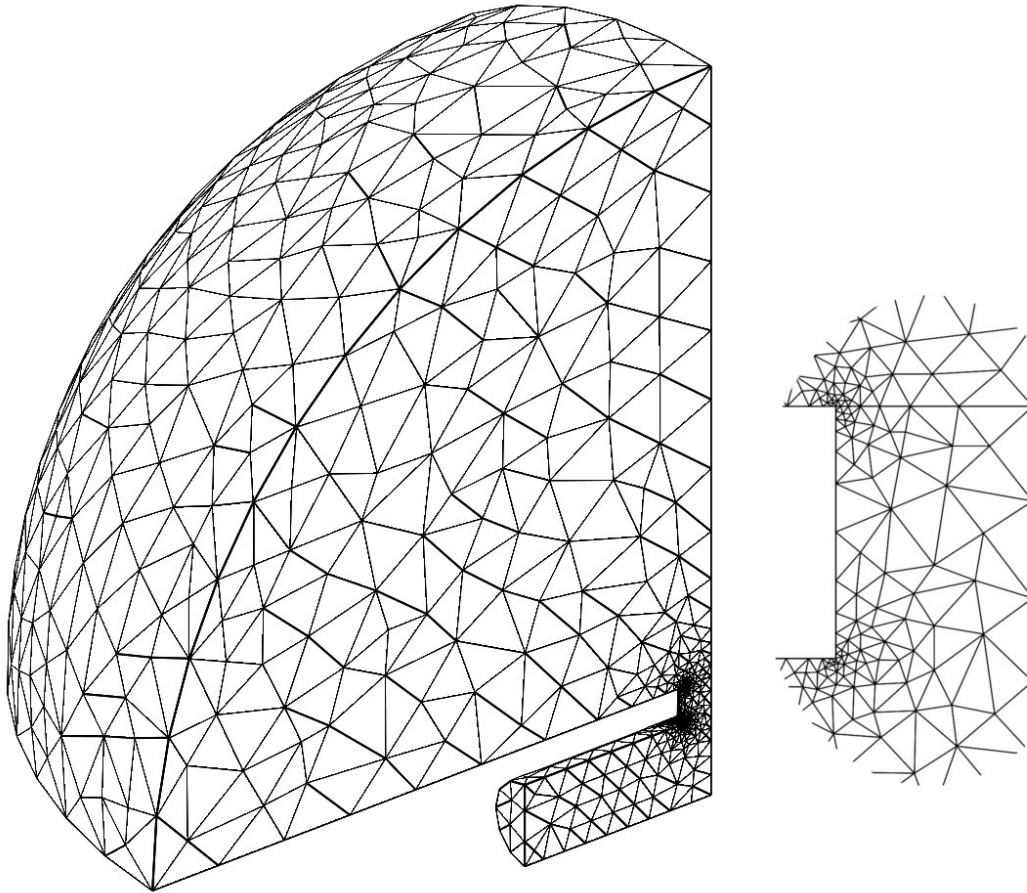


Figure 2.5: Visualisation of the FEM mesh for the flanged tonehole

similar for the second tonehole. The COMSOL/Matlab simulation script for the simulation of both toneholes is `toneholeflangeddalmont.m`. 

The mesh of the FEM model for the tonehole with  $\delta = 0.66$  studied by Keefe (1982a) is shown in Fig. 2.6. It consists of 176210 DOF (7382 mesh points and 36750 elements). The refinement of the mesh along the edge at the opening of the tonehole is such that there are approximately 100 elements on the circumference (25 elements for one quarter). The mesh is similar for the second tonehole. The COMSOL/Matlab simulation script for the simulation of both toneholes is `toneholeunflangedkeefe.m`. 

The shunt equivalent length  $t_s^{(o)}$  obtained from our FEM simulations is displayed in Figs. 2.7

and 2.8 in comparison to the experimental results found in the literature. Our FEM simulation results are in good general agreement with the experimental results of [Dalmont et al. \(2002\)](#), but a few interesting observations are worth mentioning: (1) the experimental data reveals a larger shunt equivalent length  $t_s^{(o)}$  at low frequencies for both tonehole geometries compared to both the theoretical formula and our simulation results, which match; (2) the equivalent length  $t_s^{(o)}$  predicted by our FEM simulation results matches the experimental data for the larger diameter tonehole in the higher frequency range, predicting a larger length correction than the current theory.

In the case of the unflanged toneholes studied by [Keefe \(1982a\)](#), we found good agreement between the theoretical values, our simulations and his experimental data for the tonehole of tall height. For the unflanged tonehole of short height, there are discrepancies: the experimental data and our simulation results give larger shunt equivalent lengths for the higher frequencies compared to the theory.

The shunt losses  $\xi_s$  in the FEM results are  $0.25(kb)^2$  for all values of  $\delta$  and  $t/b$  in the low-frequency limit, in agreement with the theory.

Tables 2.1 and 2.2 compare the values of the series equivalent lengths  $t_a^{(o)}$  found in the FEM with published experimental values and predictions of the theoretical equations. For the results in Table 2.1, our FEM simulations for the smaller tonehole ( $\delta = 0.7$ ) agree with the values predicted by the theoretical formulas and with the experimental values obtained by [Dalmont et al. \(2002\)](#). For the larger tonehole ( $\delta = 1.0$ ), our simulations agree with the experimental data provided by [Dalmont et al. \(2002\)](#) and with all of the theoretical formulas except that from [Keefe](#), Eq. (1.3.26). The agreement with the results in Table 2.2 is satisfactory.

Tonehole			
$\delta$	$t/b$	Description	$t_a^{(o)}/\delta^2$ [mm]
0.7	1.3	FEM	1.02
		Dalmont et al.	$0.95 \pm 0.3$
		Eq. (1.3.26)	0.94
		Eq. (1.3.27)	0.96
		Eq. (1.3.28)	1.06
		Eq. (1.3.29)	1.06
1.0	1.01	FEM	2.90
		Dalmont et al.	$2.8 \pm 0.3$
		Eq. (1.3.26)	2.12
		Eq. (1.3.27)	2.80
		Eq. (1.3.28)	2.89
		Eq. (1.3.29)	2.83

Table 2.1: Series equivalent length  $t_a^{(o)}$  in mm. Comparison between simulation, theories, and experimental data for the toneholes studied by Dalmont et al. (2002).

Tonehole			
$\delta$	$t/b$	Description	$t_a^{(o)}$ [mm]
0.66	0.48	FEM	0.78
		Keefe	$0.8 \pm 0.2$
		Eq. (1.3.26)	0.84
		Eq. (1.3.27)	0.70
		Eq. (1.3.28)	0.93
		Eq. (1.3.29)	0.78
0.32	3.15	FEM	0.000019
		Keefe	not measurable
		Eq. (1.3.26)	0.000024
		Eq. (1.3.27)	0.000018
		Eq. (1.3.28)	0.000021
		Eq. (1.3.29)	0.000021

Table 2.2: Series equivalent length  $t_a^{(o)}$  in mm. Comparison between simulation, and theories and experimental data for the toneholes studied by Keefe (1982a).

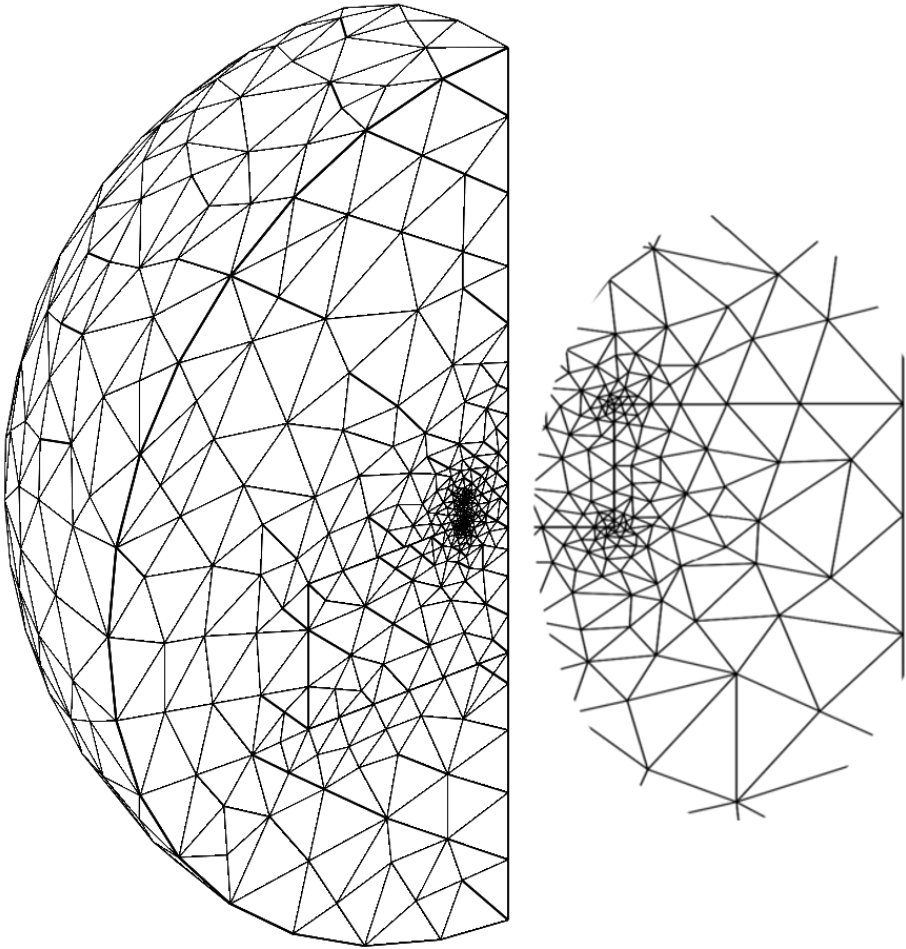


Figure 2.6: Visualisation of the FEM mesh for the unflanged tonehole

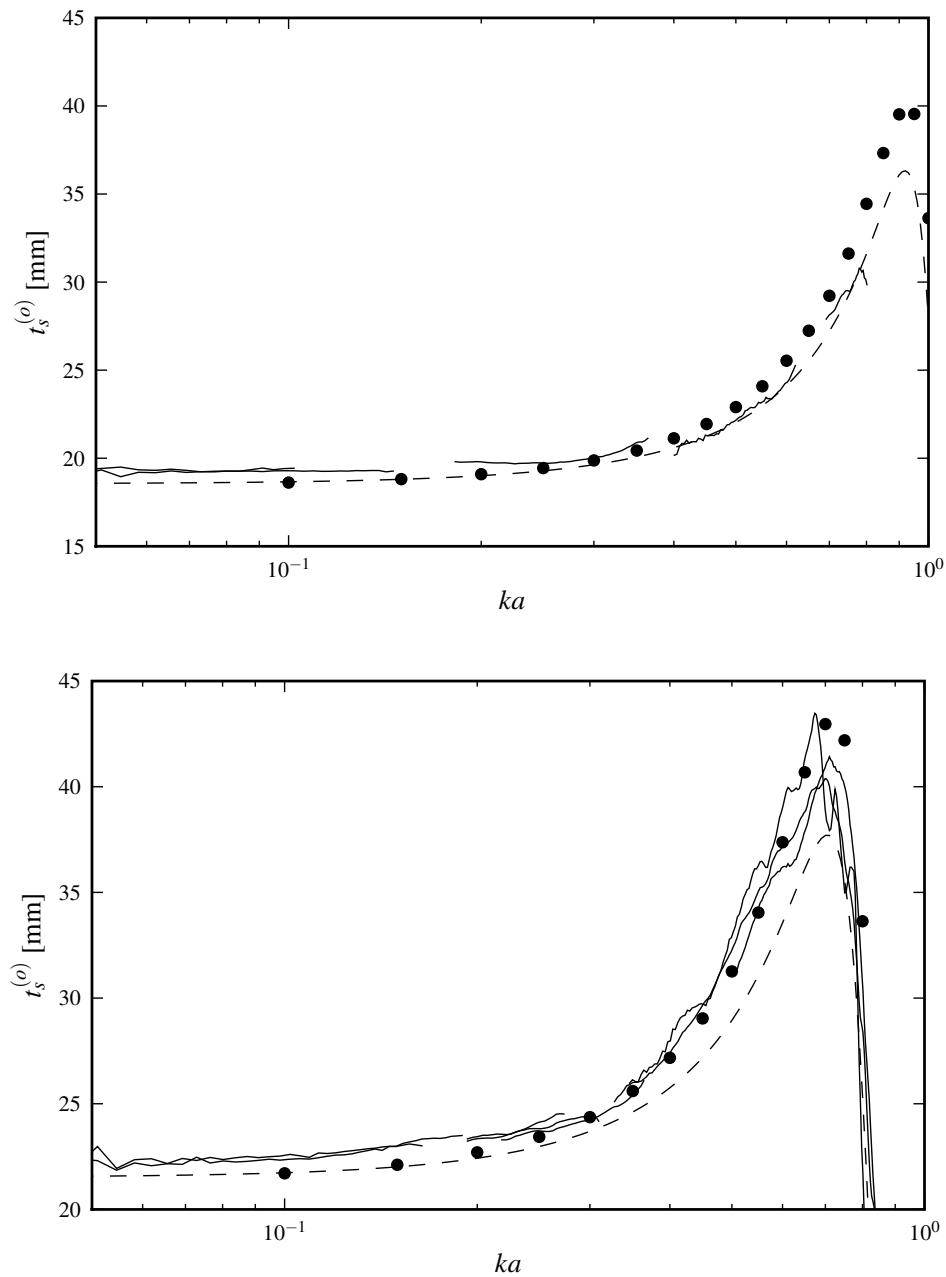


Figure 2.7: Shunt length correction  $t_s^{(o)}$  as a function of  $ka$  for the two toneholes studied by [Dalmont et al. \(2002\)](#):  $\delta = 0.7$  and  $t/b = 1.3$  (top graph),  $\delta = 1.0$ ,  $t/b = 1.01$  (bottom graph). FEM results (filled circles), experimental data from [Dalmont et al. \(2002\)](#) (solid lines) and theoretical results with Eq. (1.3.16) (dashed).

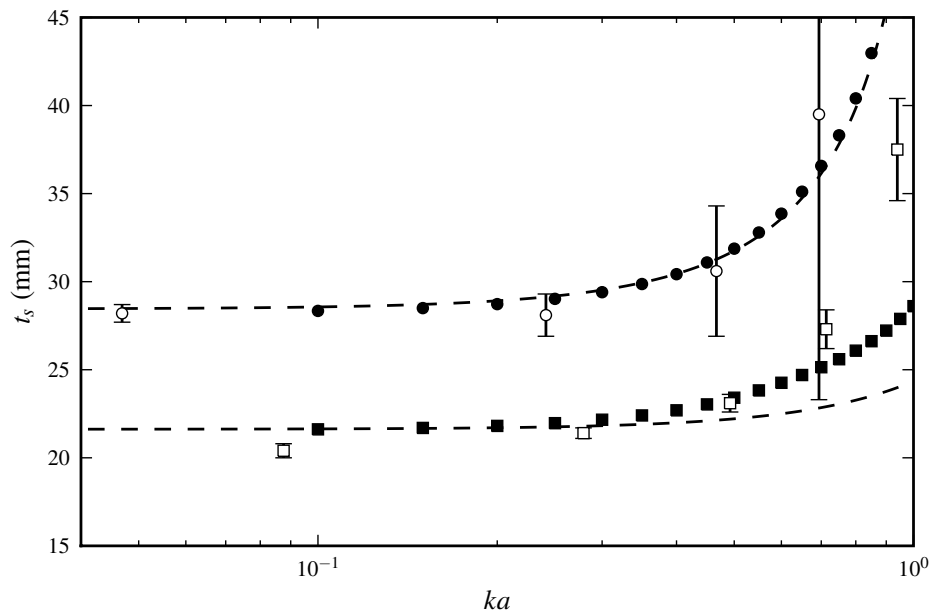


Figure 2.8: Shunt equivalent length  $t_s^{(o)}$  as a function of  $ka$  for the two toneholes studied by Keefe (1982a):  $\delta = 0.66$  and  $t/b = 0.48$  (bottom curves),  $\delta = 0.32$  and  $t/b = 3.15$  (top curves). FEM results: for  $\delta = 0.66$  (filled circles) and for  $\delta = 0.32$  (filled squares). Experimental data from Keefe (1982a) (markers with error bar) and theoretical results with Eq. (1.3.16) (dashed).

## 2.3 Characterization of Woodwind Toneholes

In this section, we present the characterization of two types of woodwind instrument toneholes using the FEM and the procedure described in the previous section. This is preceded by an estimation of the required accuracy of the equivalent lengths and a description of the data-fit procedure used for developing formulae. The influence of the keypad and the angle of conicity of the main bore are also studied.

### 2.3.1 Estimation of the Required Accuracy of the Equivalent Lengths

We previously estimated that an accuracy of  $\pm 5$  cents of the calculated frequency of the resonances of an instrument is sufficient (see Introduction). We investigated the minimum error range necessary to achieve this accuracy for the shunt and series equivalent lengths of open and closed toneholes. To estimate this error, we calculated the frequency displacement of the resonances of various woodwind instruments for each of their fingerings with an increment artificially added to the equivalent lengths.

In total, 18 instruments were analyzed. One half of the instruments were based on a conical bore, the other half, on a cylindrical bore. Each instrument was equipped with 12 toneholes of identical values of  $\delta$  and  $t/b$ . The instruments we configured with 9 different combinations of tonehole parameters. The ratio  $\delta = b/a$  of the toneholes were alternately 0.5, 0.7 and 0.9 and, for each of these values, three heights were studied:  $t/b = 0.2, 0.5$  and  $1.0$ . In order for the results to be representative of real instruments, the positions of the toneholes were calculated using the optimization algorithm that is presented in Chap. 4 for the instruments to play a chromatic scale by opening the toneholes one by one, starting from a  $D_3$  (146.83 Hz).

We found that an increment of  $0.1b$  to the shunt equivalent length of open side holes resulted in a frequency shift varying between 2 to 4 cents for every fingering. This value was smaller for tall toneholes on a cylindrical bore and larger for the conical bore (for all heights). The value was also larger for notes of higher fundamental frequency. As a safe error tolerance,

we selected  $\pm 0.1b$ . An increment of  $0.1b\delta^4$  to the series equivalent length for open side holes causes a frequency shift smaller than 2 cents.

For closed toneholes, the error on the series equivalent length has a cumulative effect. The maximal error always occurs when all the toneholes are closed. The value estimated here is based on an instrument with 12 toneholes. The error would be larger for an instrument with more toneholes. The impact on the resonance frequencies is much more important for larger diameter toneholes. For the conical instrument, with  $\delta = 0.9$  and for all heights, we found that an increment of  $0.1b\delta^4$  causes a frequency shift of 25 cents. It becomes 4 cents when  $\delta = 0.5$ . This error is smaller on the cylindrical instrument, for  $\delta = 0.9$ , the frequency shift is 16 cents for the same increment in the series equivalent length. We found an expression as a function of  $\delta$  for the error on the series length correction that cause a frequency shift of approximately  $\pm 5$  cents:  $0.015/\delta^3$ .

In the following sections, these estimated values are used to display the range of validity of the various length corrections in the figures using gray regions.

### 2.3.2 Data-fit Formulae Procedure

In the following sections, equations are developed from the FEM simulation results using a data-fit procedure. We used the “leastsq” method from the SciPy.Optimize python module which is a wrapper around the Fortran Minpack “lmdr” function which implements a modified Levenberg-Marquardt algorithm to minimize the sum of the squares of  $M$  nonlinear functions in  $N$  variables. The output of the method includes an estimate of the parameters and the variance-covariance matrix from which a standard deviation estimate of the parameters can be calculated.

The data-fit procedure requires that an equation of a valid form is supplied to the algorithm. Many different equation forms were tried until the results displayed a small residual for all values of the independent variables. This required inspection of the simulation results visually

and to “intuitively” determine the form of the equations that are likely to be valid. The result is that a polynomial equation works for the dependance of the length corrections with  $\delta$  whereas a hyperbolic tangent works for the dependance with  $t/b$ .

### 2.3.3 The Single Unflanged Tonehole

In this section, we present the results of FEM simulations for the characterization of a single unflanged tonehole, as depicted in Fig. 1.2. This is the type of tonehole found on instruments made of thin sheet metal, such as the concert flute and the saxophone. The goal of the research presented here is to derive TMM tonehole parameters that are valid over a wider range of geometries than those previously available. The mesh is similar to that used for the validation test cases presented in Sec. 2.2.2. The COMSOL/Matlab simulation script for the simulations in this section is `toneholeunflanged.m`.

The single open tonehole was simulated using the FEM for a wide range of geometric parameters ( $\delta = b/a$  from 0.2 to 1.0 by step of 0.05,  $t/b$  from 0.1 to 0.3 by step of 0.05 and from 0.3 to 1.3 by step of 0.2 and  $ka$  from 0.1 to 1.0 by step of 0.05 with an additional low-frequency point at  $ka = 0.01$ ). The lowest frequency simulated was 55 Hz. For all parameters, the four terms of the transmission matrix were obtained and the shunt and series length corrections calculated using the procedure previously described in Sec. 2.2. The accuracy of the results from the FEM is estimated to be better than 1% on the shunt and series equivalent length, which is an order of magnitude better than the required accuracy.

For the low-frequency value of the shunt equivalent length  $t_e$ , we were able to obtain a data-fit formula that matches the complete set of results with a standard deviation on the parameters smaller than  $5 \times 10^{-7}$ . No data was obtained for toneholes with  $\delta < 0.2$  because, for such small-diameter toneholes, we were not able to obtain valid results. In order to ensure that the data-fit formula would be valid for all values of  $\delta$ , we added the two theoretical constraints



expressed in Eqs. (1.3.18) and (1.3.19). The equation that we obtained is:

$$t_e/b = \lim_{k \rightarrow 0} t_s^{(o)}/b = t/b + [1 + f(\delta)g(\delta, t/b)]h(\delta), \quad (2.3.1)$$

with

$$f(\delta) = 0.095 - 0.422\delta + 1.168\delta^2 - 1.808\delta^3 + 1.398\delta^4 - 0.416\delta^5,$$

$$g(\delta, t/b) = 1 - \tanh(0.778t/b),$$

and

$$h(\delta) = 1.435 + 0.030\delta - 1.566\delta^2 + 2.138\delta^3 - 1.614\delta^4 + 0.502\delta^5.$$

The open shunt impedance as a function of frequency is then evaluated as:

$$\bar{Z}_s^{(o)} = \frac{j}{\delta^2} \tan kt_e, \quad (2.3.2)$$

where  $t_e$  is evaluated with Eq. (2.3.1). This expression works well when  $ka < 0.2$ . Attempts were made to develop a formula that matches the simulation data for frequencies up to  $ka = 1$ . However, none of the forms of equations that were tried with the least mean square data fitting procedure allowed to reduce the residual sufficiently. The frequency dependence of the equivalent length vary too significantly as a function of the geometrical parameters of the toneholes.

In Fig. 2.9, the simulation results are shown for the two extreme cases of short (circles) and tall (squares) toneholes as well as the data-fit formula (dotted) and the theoretical Eq. (1.3.16). This figure shows the sum of the radiation length correction and the inner length correction. As expected, for the toneholes of short height, this length correction is larger than for the tall toneholes, because the unflanged tonehole ending becomes gradually “flanged” by the body of the instrument. Even for a tonehole of greater height, the new data-fit formula does not match exactly with the current theory, suggesting that the inner length correction found with

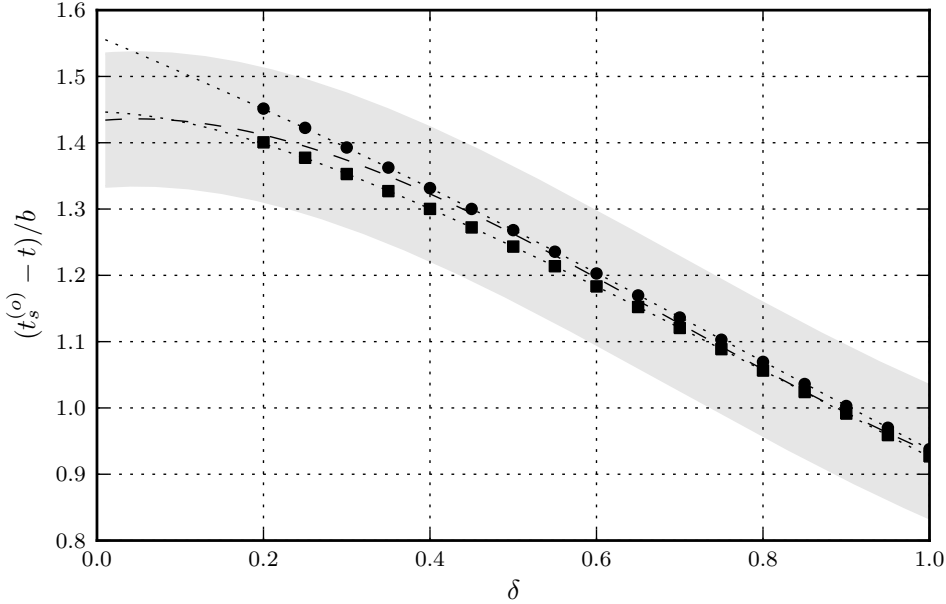


Figure 2.9: Difference between the shunt length correction  $t_s^{(o)}$  and the tonehole height  $t$  divided by the tonehole radius  $b$  as a function of  $\delta$  for a single unflanged tonehole: FEM results for tall (squares) and short (circle) toneholes. Data-fit formula (dotted) and the TMM results using Eq. (1.3.16) (dashed). Validity range in gray (see Sec. 2.3.1).

our FEM simulation is different. We can obtain the inner length correction  $t_i$  by subtracting the unflanged pipe radiation length correction  $t_r = 0.6133b$  and the matching volume length correction  $t_m$ , Eq. (1.3.17), from Eq. (2.3.1) with  $t \rightarrow \infty$ :

$$t_i/b = 0.822 - 0.095\delta - 1.566\delta^2 + 2.138\delta^3 - 1.640\delta^4 + 0.502\delta^5. \quad (2.3.3)$$

This formula is compared with the formulas from the literature in Fig. 2.10. The gray area in Fig. 2.9 shows the region of validity of the current theoretical expression. It appears that the details of this open shunt length correction are not important with respect to the required accuracy and that the dependence over the tonehole height may be neglected. A sufficiently accurate approximate formula to the low-frequency value of the equivalent length of the tonehole, including the matching volume, the inner correction and the radiation correction could

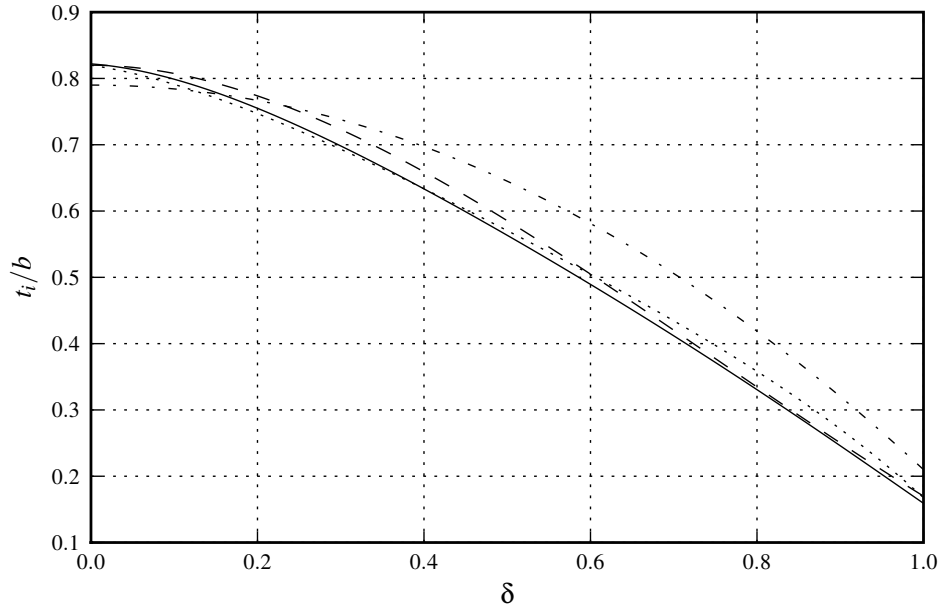


Figure 2.10: Comparison of the expressions for the inner length correction  $t_i^{(o)}/b$ : new formula Eq. (2.3.3) (solid curve) and equations from the literature Eq. (1.3.23) (dash-dot), Eq. (1.3.24) (dashed) and Eq. (1.3.25) (dotted).

be:

$$t_e = t + b(1.50 - 0.55\delta). \quad (2.3.4)$$

The most important discrepancy between current tonehole theories and our simulation results concerns the frequency dependence of the shunt length correction for toneholes of short height, which is displayed in Fig. 2.11 for three tonehole with  $t/b = 0.1$ : (1)  $\delta = 0.2$ , (2)  $\delta = 0.5$  and (3)  $\delta = 1.0$ . For each of these toneholes, the shunt length correction increases more than predicted with frequency. Eq. (2.3.2) in this chapter better predicts the frequency dependence compared to current theory, but discrepancies remain. Similar results were obtained by Keefe (1982a) (see Fig. 2.8). One consequence of this behaviour is that the higher resonances of an instrument with a short chimney height are lower in frequency than predicted by the current theory. This effect tends to shrink the ratio of higher resonances relative to the

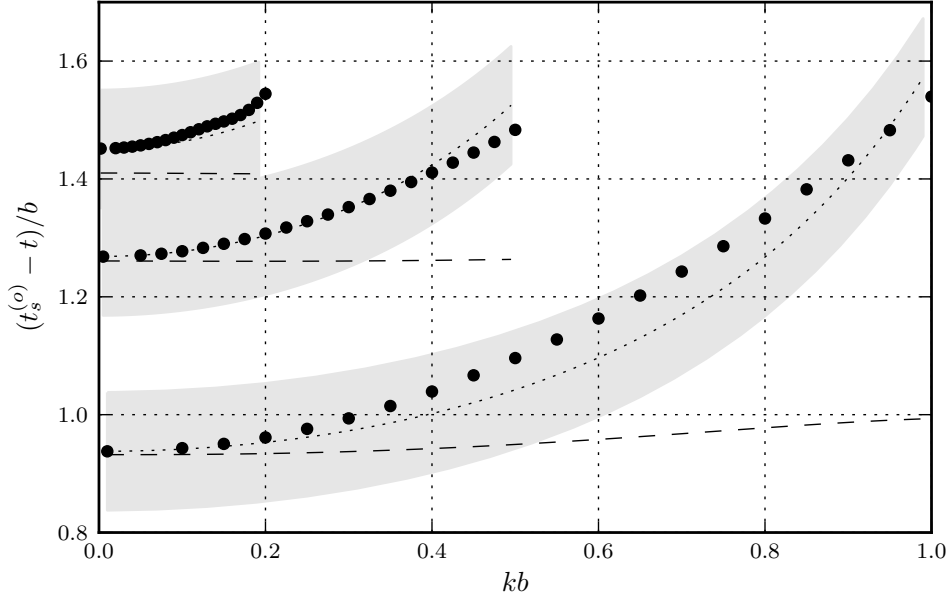


Figure 2.11: Difference between the shunt length correction  $t_s^{(o)}$  and the tonehole height  $t$  divided by the tonehole radius  $b$  as a function of  $kb$  for three values of  $\delta$  (0.2, 0.5 and 1.0, from top curve to bottom curve) and a value of  $t/b = 0.1$  for a single unflanged tonehole: results of FEM simulations (filled circles), current TMM theory with Eq. (1.3.16) (dashed) and new results with Eq. (2.3.2) (dotted). Validity range in gray (see Sec. 2.3.1).

fundamental. For conical instruments, this counteracts the natural spreading of the resonances that occurs in truncated cones.

For the low-frequency value of the series length correction, we obtained the following data-fit formula with a standard deviation on the parameters smaller than  $6 \times 10^{-5}$ :

$$t_a^{(o)}/b\delta^4 = -f(\delta, t/b)g(\delta), \quad (2.3.5)$$

where

$$f(t/b) = 1 + (0.333 - 0.138\delta) \left[ 1 - \tanh(2.666t/b) \right],$$

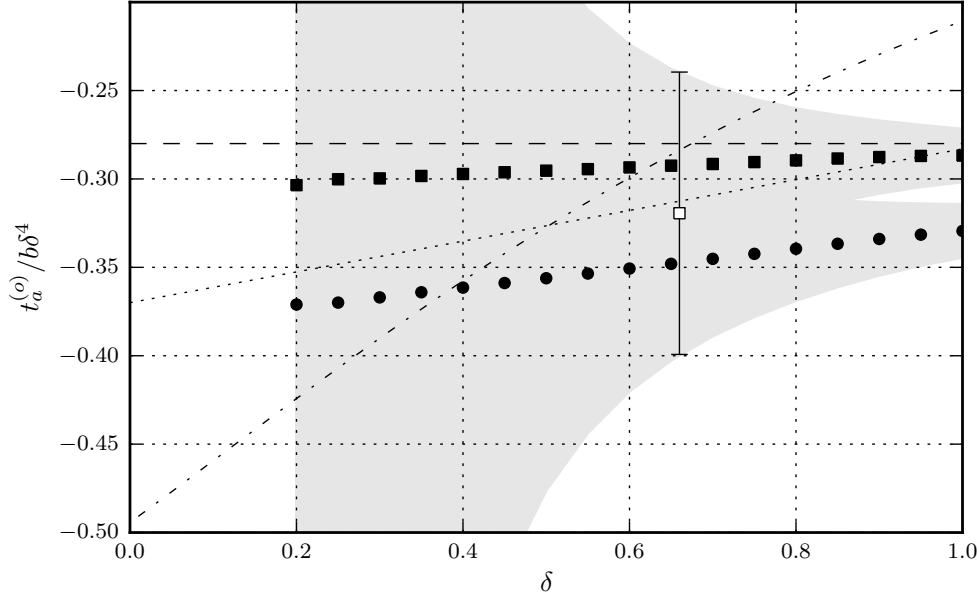


Figure 2.12: Series length correction  $t_a^{(o)}/b\delta^4$  as a function of  $\delta$  for a single unflanged tonehole. FEM results: limit for large  $t/b$  (filled squares), limit for small  $t/b$  (filled circles). Theoretical formulas: Eq. (1.3.26) (dash-dot), Eq. (1.3.27) (dashed) and Eq. (1.3.28) (dotted). Validity range in gray (see Sec. 2.3.1).

and

$$g(\delta) = 0.307 - 0.022\delta - 0.002\delta^2.$$

Fig. 2.12 displays the results of our simulations for two extreme cases: short chimney height (circles) and tall chimney height (squares), in comparison to theoretical formulas from the literature and an experimental data point from Keefe (1982a). In the case of tall chimney height, Eq. (1.3.27) provides a good approximation. The dependence of the series length correction on the tonehole height is displayed in Fig. 2.13 for a tonehole with  $\delta = 1.0$ , which reveals that neither Eq. (1.3.28) nor Eq. (1.3.26) matches our FEM results. The range of validity represented by the gray region shows that the discrepancies are mostly affecting short-height large-diameter toneholes.

The results of our simulations for closed toneholes confirm the validity of the low-frequency

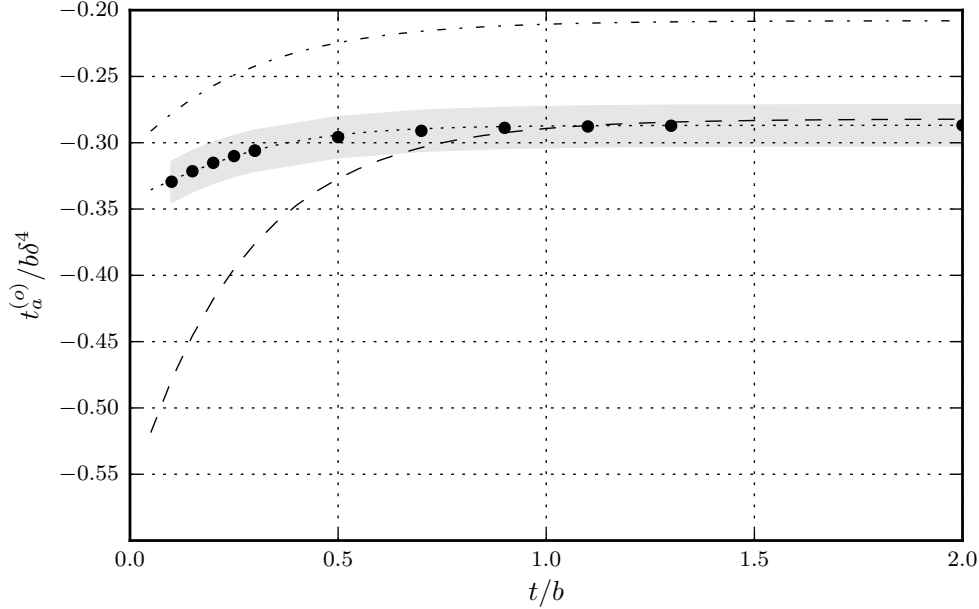


Figure 2.13: Series length correction  $t_a^{(o)}/b\delta^4$  as a function of  $t/b$  for  $\delta = 1.0$  for a single unflanged tonehole. FEM results (filled circles). Data fit formula Eq. (2.3.5) (dotted). Theory: Eq. (1.3.28) (dashed), Eq. (1.3.26) (dash-dot). Validity range in gray (see Sec. 2.3.1).

limit of the shunt length correction. Fig. 2.14 shows that the low-frequency value of the shunt length correction is very well represented by the length  $t + t_m$ , that is, by the volume of the tonehole. The cotangent term in Eq. (1.3.31) tends toward infinity when  $k(t + t_m) \rightarrow 0$ ; consequently, the influence of an inner length correction is expected to be maximal when  $k(t + t_m) \approx \pi/2$  and negligible when it goes toward zero. As an example, for a tonehole height of 5 mm, the maximal influence of the inner length correction occurs above 20 kHz; whereas for a tonehole of 50 mm chimney height, this occurs above 2 kHz. Therefore, this term has a negligible influence even in the higher frequency range of woodwind instruments, except possibly for instruments with very tall toneholes, such as the bassoon (for which  $t$  varies between 5 to 40 mm). Nevertheless, to study this term, it is useful to define the impedance of the closed side hole as:

$$\bar{Z}_s^{(c)} = -\frac{j}{\delta^2} \cot k(t + t_m + t_i^{(c)}), \quad (2.3.6)$$

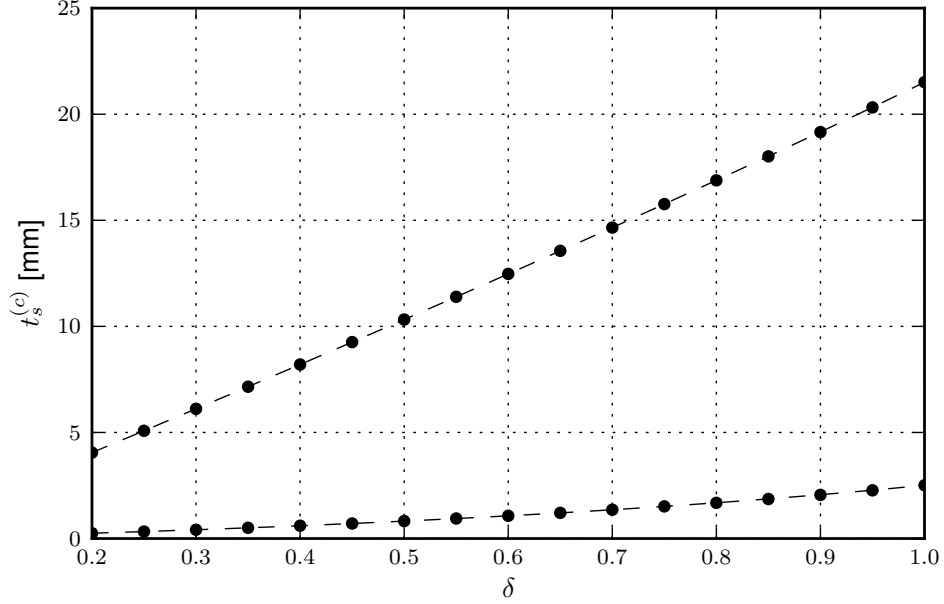


Figure 2.14: Shunt length correction  $t_s^{(c)}$  as a function of  $\delta$  with  $t/b = 0.1$  (bottom) and  $t/b = 2.0$  (top) for a single closed tonehole. FEM results (filled circles). Theoretical value ( $t + t_m$ ) where  $t_m$  is calculated using Eq. (1.3.17) (dashed).

where  $t_m$  is the matching volume length correction defined in Eq. (1.3.17) and  $t_i^{(c)}$  is the inner length correction (located inside the cotangent term rather than outside, thus it is not equivalent to the value from the literature). We can obtain the value of  $t_i^{(c)}$  from our simulation results with:

$$t_i^{(c)} = \frac{1}{k} \tan^{-1} \left( \frac{1}{j\delta^2 \bar{Z}_s^{(c)}} \right) - t - t_m. \quad (2.3.7)$$

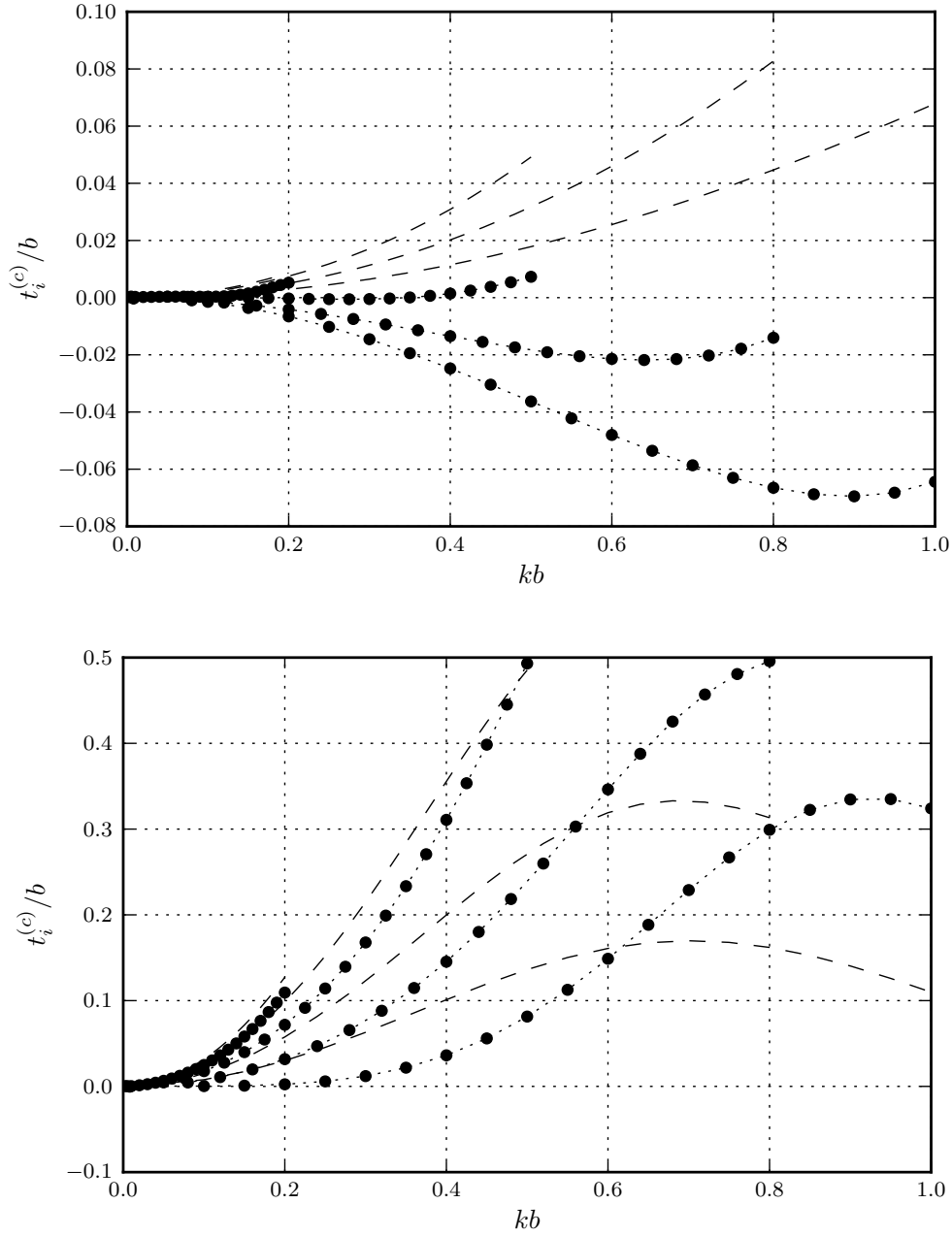


Figure 2.15: Inner length correction  $t_i^{(c)}/b$  for closed toneholes as a function of  $kb$  for  $\delta = 0.2, 0.5, 0.8, 1.0$ . Results of FEM simulations (filled circles) compared to theory (dashed). Top:  $t/b = 0.5$ , bottom:  $t/b = 2.0$ . The dotted line is a visual aid.

This value may be compared with the current theoretical values by applying the previous equation to the calculated impedance of the closed side hole using Eq. (1.3.31). This is shown in Fig. 2.15. Discrepancies between the simulation results and the theoretical values exist. In the case of the short-height tonehole (top graph), the magnitude of the inner length correction is very small, but it is noteworthy that its value is negative for the two larger-diameter toneholes ( $\delta$  values of 0.8 and 1.0). Discrepancies are also apparent for the tall tonehole (bottom graph). In this case, the discrepancies are also more important for the larger-diameter toneholes. Further research is required to characterize this effect fully. For instruments with normal-sized toneholes (flutes, clarinets, saxophones), this is likely negligible, as explained previously.

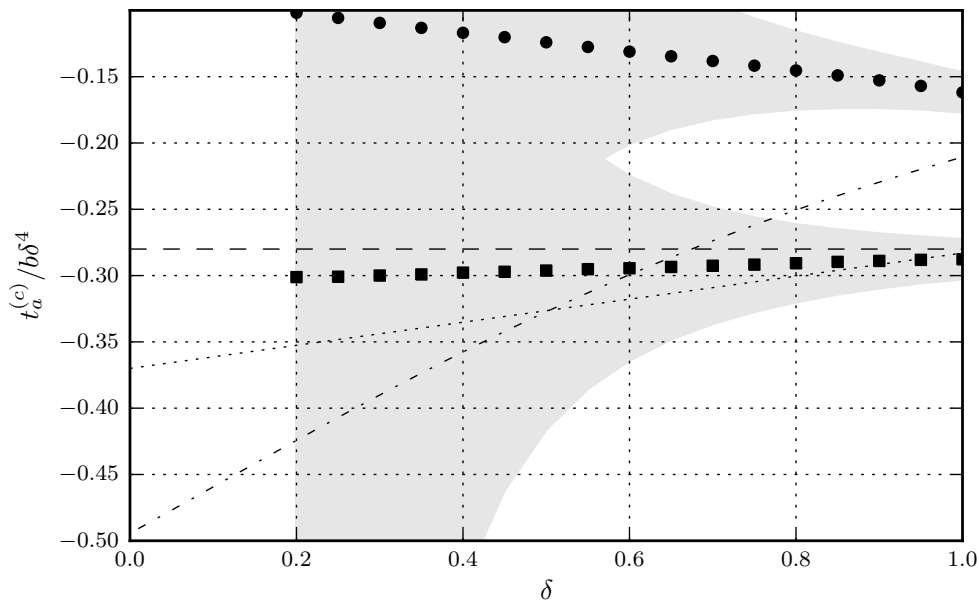


Figure 2.16: Series length correction  $t_a^{(c)}/b\delta^4$  as a function of  $\delta$  for a closed tonehole. FEM results: limit for large  $t/b$  (filled squares), limit for small  $t/b$  (filled circles). Theoretical formulas: Eq. (1.3.26) (dash-dot), Eq. (1.3.27) (dashed) and Eq. (1.3.28) (dotted). Validity range in gray (see Sec. 2.3.1).

In the case of the series length correction of closed toneholes, we obtained a new formula

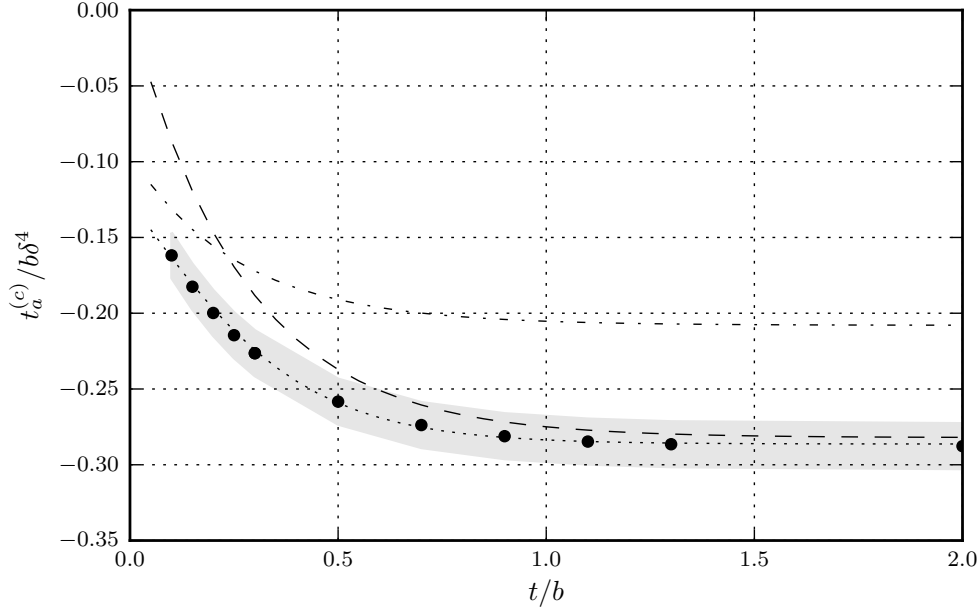


Figure 2.17: Series length correction  $t_a^{(c)}/b\delta^4$  as a function of  $t/b$  for  $\delta = 1.0$  for a closed tonehole. FEM results (filled circles). Data fit formula Eq. (2.3.5) (dotted). Theory: Eq. (1.3.28) (dash-dot), Eq. (1.3.26) (dashed). Validity range in gray (see Sec. 2.3.1).

that takes into account more precisely the height and radius of the toneholes:

$$\frac{t_a^{(c)}}{b\delta^4} = -f(\delta, t/b)g(\delta), \quad (2.3.8)$$

where

$$f(\delta, t/b) = 1 - [0.923 - 0.363\delta][1 - \tanh(2.385t/b)],$$

$$g(\delta) = 0.302 - 0.019\delta + 0.003\delta^2.$$

For every parameters, the standard deviation is smaller than  $2.5 \times 10^{-5}$ .

In Fig. 2.16, we consider the low-frequency limit of the series length correction  $t_a^{(c)}$  for short and tall tonehole heights compared to previous theories. The results for the tall tonehole are the same as for an open hole (see Fig. 2.12). When the toneholes are short in height, the

series length correction term diminishes in magnitude. Fig. 2.17 presents this length correction as a function of the ratio  $t/b$  for one tonehole ( $\delta = 1.0$ ) compared with current theories.

### 2.3.4 The Single Tonehole on a Thick Pipe

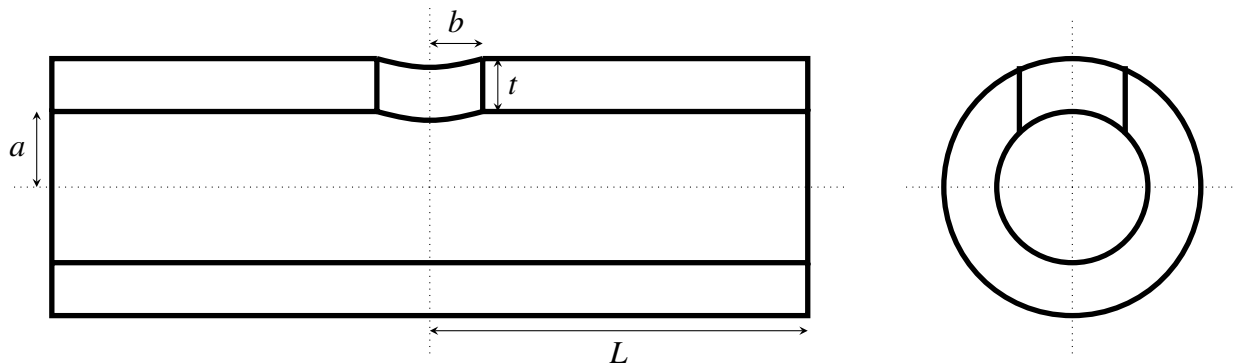


Figure 2.18: Diagram representing a tonehole on a pipe.

For many woodwind instruments, the toneholes are directly drilled in the wall of a thick pipe and no chimneys are used. This is the case for most of the simple keyless instruments made of wood, such as flutes, recorders, shepherd's pipes, chalumeaux, and many others. Some of the toneholes found on clarinets are also of this type. The previously developed model is not valid in this case because the radiation condition at the opening of the tonehole is not the same; instead of resembling that of an unflanged pipe, it becomes “flanged” by a cylindrical surface, that of the instrument's body. Furthermore, the volume of the tonehole is smaller. Such a tonehole is depicted in Fig. 2.18.

The FEM model and the mesh refinement is similar to that of the previous section. The COMSOL/Matlab simulation script for the simulations in this section is `toneholethickpipe.m`. 

Toneholes of this kind are often closed directly by the instrumentalist's fingers, thus reducing the internal volume of the tonehole in the closed state. If the instrument walls are thin, the volume of the instrument may even be reduced, compared to a situation without toneholes, which would raise the sounding pitch slightly.

The method to characterize the shunt and series impedance for this tonehole geometry is the same as for the unflanged tonehole presented previously; the details are not repeated here. For small-diameter toneholes ( $\delta \rightarrow 0$ ), the length correction for a short hole remains as in the previous model ( $t_e = t + (\pi/2)b$ ). For tall toneholes ( $t \rightarrow \infty$ ), however, the total length correction becomes  $t_e = t + 1.643b$ , that is,  $t$  plus two times a flanged end correction. Using these theoretical results combined with the FEM results, the following data-fit formula for the shunt length correction was obtained with a standard deviation on the parameters smaller than  $3 \times 10^{-5}$ :

$$t_e/b = \lim_{k \rightarrow 0} t_s^{(o)}/b = t/b + [1 + f(\delta)g(\delta, t/b)]h(\delta), \quad (2.3.9)$$

with

$$f(\delta) = -0.044 + 0.269\delta - 1.519\delta^2 + 2.332\delta^3 - 1.897\delta^4 + 0.560\delta^5,$$

$$g(\delta, t/b) = 1 - \tanh(0.788t/b),$$

and

$$h(\delta) = 1.643 - 0.684\delta + 0.182\delta^2 - 0.394\delta^3 + 0.295\delta^4 - 0.063\delta^5.$$

The FEM results for short and tall toneholes, as well as this data-fit formula, are displayed in Fig. 2.19 in comparison to a theoretical curve; no theoretical results were directly applicable to this type of hole, which explains the difference. The displayed theoretical curve corresponds to the previous type of tonehole with an infinite flange instead of an unflanged termination. One observation is that the dependency upon thickness is reversed: the tall toneholes have a larger shunt length correction; whereas for the unflanged tonehole, the short toneholes have a larger correction. The shunt impedance as a function of frequency is then obtained with:

$$\bar{Z}_s^{(o)} = \frac{j}{\delta^2} \tan kt_e, \quad (2.3.10)$$

which is only valid for the lower frequencies (see Fig. 2.20).

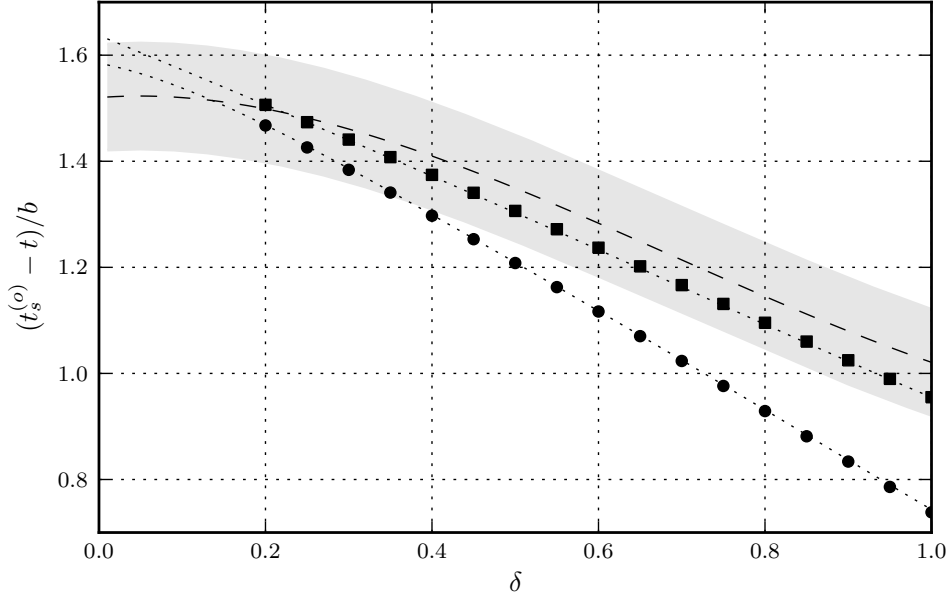


Figure 2.19: Difference between the shunt length correction  $t_s^{(o)}$  and the tonehole height  $t$  divided by the tonehole radius  $b$  as a function of  $\delta$  for a tonehole on a thick pipe: FEM results for tall (squares) and short (circle) toneholes. Data fit formula (dotted). Current theory with Eq. (1.3.16) (dashed). Validity range in gray (see Sec. 2.3.1).

For the low-frequency value of the open series length correction, we obtained, with a standard deviation of the parameters smaller than  $2.5 \times 10^{-5}$ :

$$t_a^{(o)}/b\delta^4 = -f(\delta, t/b)g(\delta), \quad (2.3.11)$$

where

$$f(t/b) = 1 + (0.261 - 0.022\delta) \left[ 1 - \tanh(2.364t/b) \right],$$

and

$$g(\delta) = 0.302 - 0.010\delta - 0.006\delta^2.$$

This is similar to the expression for the unflanged toneholes, and the differences are mainly for the short-height toneholes. This is displayed in Fig. 2.21

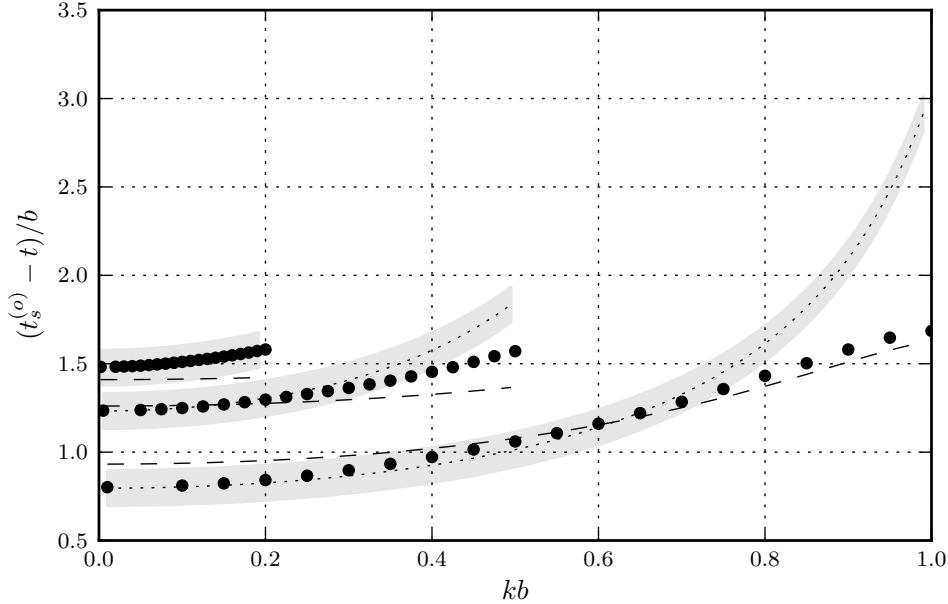


Figure 2.20: Difference between the shunt length correction  $t_s^{(o)}$  and the tonehole height  $t$  divided by the tonehole radius  $b$  as a function of  $kb$  for three values of  $\delta$  (0.2, 0.5 and 1.0, from top curve to bottom curve) and a value of  $t/b = 0.5$  for a tonehole on a thick pipe. Results of FEM simulations (filled circles), current theory with Eq. (1.3.16) (dashed) and new results with Eq. (2.3.10) (dotted). Validity range in gray (see Sec. 2.3.1).

The shunt losses  $\xi_s$  in the FEM results are  $0.25(kb)^2$  for all values of  $\delta$  and  $t/b$  in the low-frequency limit, in agreement with the theory.

For closed side holes, contrary to the unflanged toneholes previously shown, there are two matching volume length corrections: one that must be added as usual, but another that has to be removed from the top of the hole. The total equivalent length of the closed side holes becomes:

$$t_e = t + \frac{b\delta}{8} (1 + 0.207\delta^3) - \frac{b^2}{8(a+t)} \left( 1 + 0.207\left(\frac{b}{a+t}\right)^3 \right). \quad (2.3.12)$$

This equivalent length is further reduced by the finger of the instrumentalist, because these toneholes generally do not use a keypad. We may suppose that the finger is a sphere of a certain radius  $R$ , and that it occupies the volume of the spherical cap of radius  $b$  and height

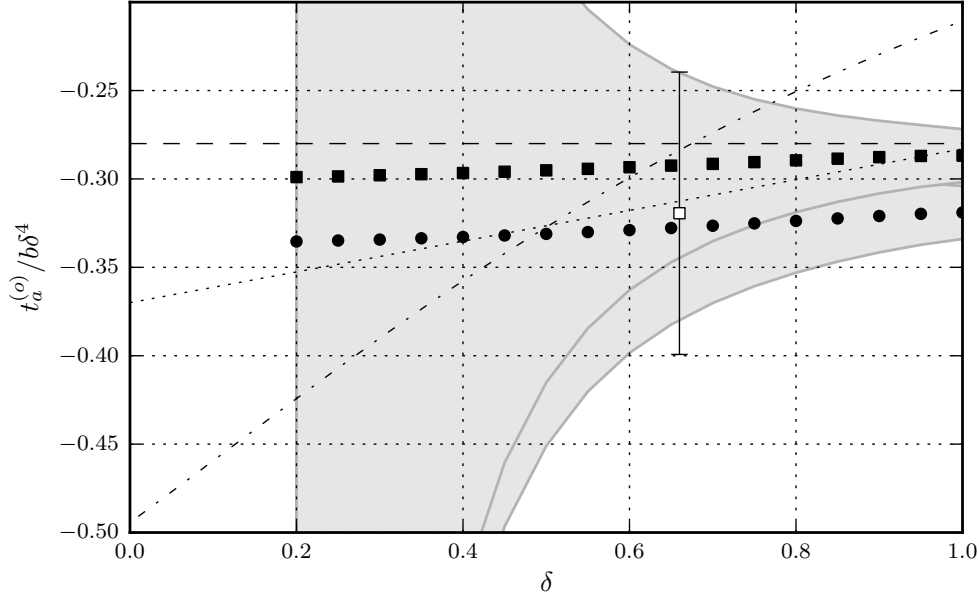


Figure 2.21: Series length correction  $t_a^{(o)}/b\delta^4$  as a function of  $\delta$  for an open tonehole on a thick pipe. FEM results: limit for large  $t/b$  (filled squares), limit for small  $t/b$  (filled circles). Theoretical formulas: Eq. (1.3.26) (dash-dot), Eq. (1.3.27) (dashed) and Eq. (1.3.28) (dotted). Validity range in gray (see Sec. 2.3.1).

$h = R - \sqrt{R^2 - b^2}$ , that is,  $V_{cap} = (1/6)\pi h(3b^2 + h^2)$ . The associated equivalent length is  $t_f = V_{cap}/S_h = (1/6)\pi h(3 + (h/b)^2)$ . This presence of the finger significantly reduces the volume of the closed side hole as  $\delta$  increases. For purposes of the FEM simulations, the closed tonehole did not take into account the presence of a finger; it is closed by a circular surface corresponding to the outside of the instrument.

From the simulation results, we found that the shunt length correction is well approximated by the volume of the tonehole, as can be seen in Fig. 2.22.

The low-frequency limit of the series length correction for the closed side hole (without fingers) was found to be, with a standard deviation smaller than  $3.5 \times 10^{-5}$ :

$$t_a^{(c)}/b\delta^4 = -f(\delta, t/b)g(\delta), \quad (2.3.13)$$

where

$$f(t/b) = 1 - (0.956 - 0.104\delta) \left[ 1 - \tanh(2.390t/b) \right],$$

and

$$g(\delta) = 0.299 - 0.018\delta + 0.006\delta^2.$$

This is displayed in Fig. 2.23.

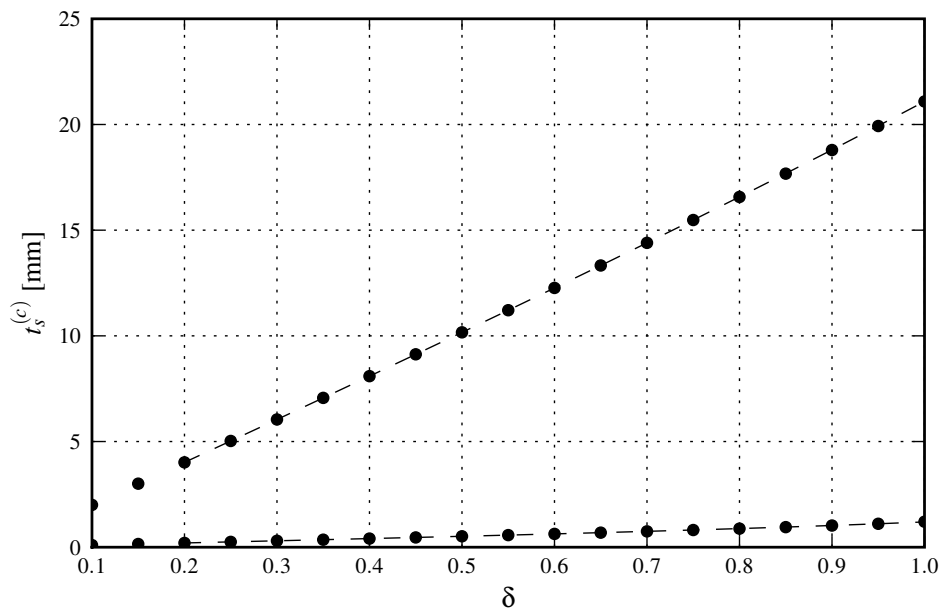


Figure 2.22: Shunt length correction  $t_s^{(c)}$  as a function of  $\delta$  for a closed tonehole on a thick pipe. FEM results:  $t/b = 2$  (top curve),  $t/b = 0.1$  (bottom curve). Theoretical Eq. (2.3.12) (dashed).

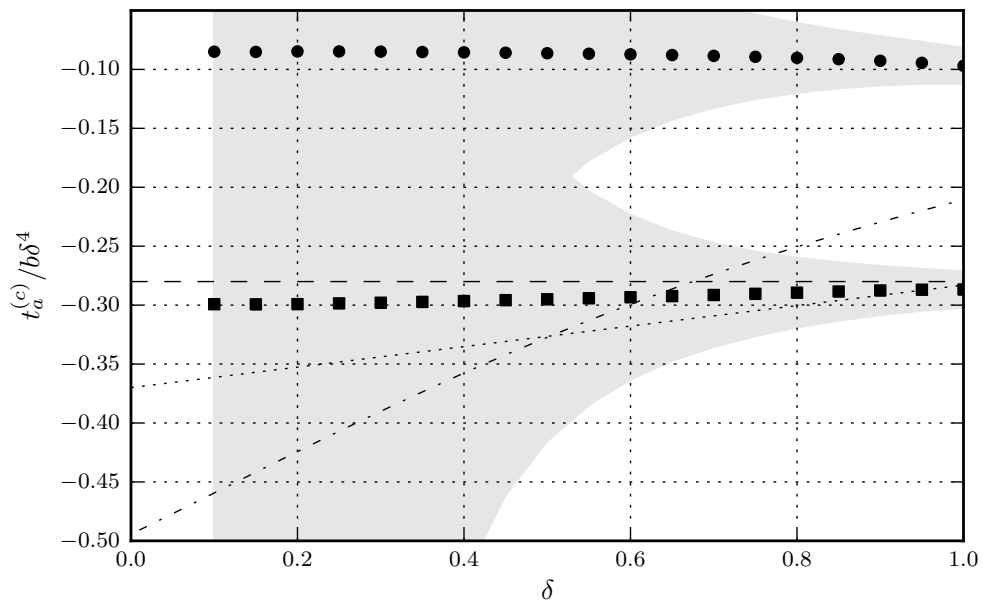


Figure 2.23: Series length correction  $t_a^{(c)}/b\delta^4$  as a function of  $\delta$  for a closed tonehole on a thick pipe. FEM results: limit for large  $t/b$  (filled squares), limit for small  $t/b$  (filled circles). Theoretical formulas: Eq. (1.3.26) (dash-dot), Eq. (1.3.27) (dashed) and Eq. (1.3.28) (dotted). Validity range in gray (see Sec. 2.3.1).

### 2.3.5 Influence of the Keypad

Geometry		length corrections $t_p/b$		
t/b	h/a	FEM	Eq. (1.3.35)	Error [%]
0.1	0.1	1.408	1.187	18.6
	0.3	0.505	0.455	11.0
	0.5	0.260	0.234	11.1
0.25	0.1	1.313	1.187	10.6
	0.3	0.482	0.455	5.9
	0.5	0.249	0.234	6.4
0.5	0.1	1.283	1.187	8.1
	0.3	0.469	0.455	3.1
	0.5	0.242	0.234	3.4
1.0	0.1	1.268	1.187	6.8
	0.3	0.460	0.455	1.1
	0.5	0.236	0.234	0.9
2.0	0.1	1.261	1.187	6.2
	0.3	0.455	0.455	0.0
	0.5	0.232	0.234	0.9

Table 2.3: Shunt length correction increment due to the presence of a hanging keypad

The presence of a hanging keypad above a tonehole adds a significant length correction to the radiation impedance of the tonehole. The most recent characterization of this effect was developed by [Dalmont and Nederveen \(2001\)](#), reported here in Eq. (1.3.35). This equation requires verification. The geometry simulated by [Dalmont and Nederveen \(2001\)](#) was a long open-ended unflanged pipe and not a tonehole on the side of a cylindrical pipe. It is likely that their results are valid for tall toneholes, where the inner acoustic field is uncoupled to the radiation condition. In the case of toneholes of shorter height, this equation may not be valid. Using the FEM, we calculated the shunt length correction for a tonehole with a hanging keypad (with a radius of  $1.4b$ ). We solved the model for a value of  $\delta = 0.7$  and different values of the chimney height  $t/b = 0.1, 0.25, 0.5, 1.0$  and  $2.0$ . For each of these tonehole geometries, we

used three keypad heights  $h/b = 0.1, 0.3$  and  $0.5$ . The radius  $a$  of the main bore was 10 mm, the thickness of the tonehole wall was 0.67 mm and the thickness of the keypad 2.5 mm. The COMSOL/Matlab simulation script is `toneholeunflangedthickwithpad.m`.

The length correction of the tonehole without keypad was subtracted from the length correction with keypad to obtain the value  $t_p/b$ , which was compared to the prediction of Eq. (1.3.35). From the data presented in Table 2.3, we can conclude that the equation obtained by Dalmont and Nederveen (2001) is valid for toneholes with taller chimney heights, but that the length correction is larger than predicted when the tonehole is shorter.

### 2.3.6 Impact of Conicity

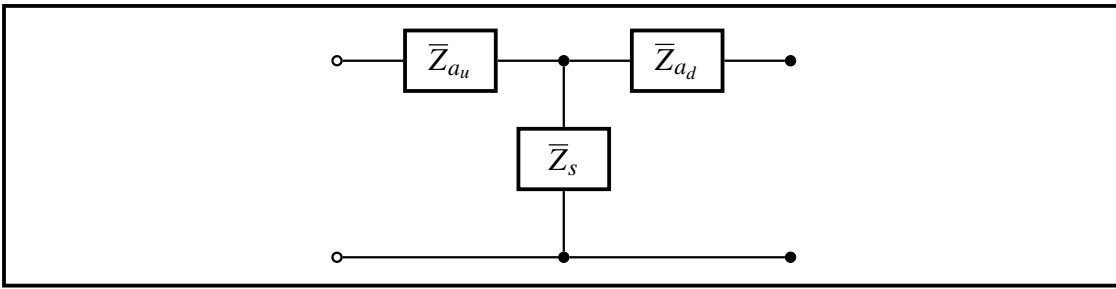


Figure 2.24: Block diagram of an unsymmetric tonehole

Previous studies of woodwind instrument toneholes have only considered holes in cylindrical waveguides. Although the influence of an air column taper on the transmission matrix parameters of the tonehole is likely small, because the taper angle of woodwind instruments is generally small, the magnitude of this potential effect is unknown.

A tonehole on a conical bore is no longer symmetric. In this situation, we propose to modify the model represented by Eq. (1.3.14) with:

$$\mathbf{T}_{hole} = \begin{bmatrix} 1 & \bar{Z}_{a_u} \\ 0 & 1 \end{bmatrix} \begin{bmatrix} 1 & 0 \\ 1/\bar{Z}_s & 1 \end{bmatrix} \begin{bmatrix} 1 & \bar{Z}_{a_d} \\ 0 & 1 \end{bmatrix} = \begin{bmatrix} 1 + \bar{Z}_{a_u}/\bar{Z}_s & \bar{Z}_{a_u} + \bar{Z}_{a_d} + \bar{Z}_{a_u}\bar{Z}_{a_d}/\bar{Z}_s \\ 1/\bar{Z}_s & 1 + \bar{Z}_{a_d}/\bar{Z}_s \end{bmatrix}, \quad (2.3.14)$$

where  $\bar{Z}_{a_u}$  is the series impedance for the upstream half of the tonehole and  $\bar{Z}_{a_d}$  for the downstream half.

In a manner similar to that for toneholes on cylindrical bores, we obtained the Transmission Matrix of the tonehole on a conical bore using Finite Element simulations. The transmission matrix  $\mathbf{T}_{hole}$  of the tonehole was obtained from the transmission matrix  $\mathbf{T}$  of the simulated system by multiplying this matrix by the inverse of the Transmission Matrix of the two segments of truncated cones,  $\mathbf{T}_{cone_u}$  and  $\mathbf{T}_{cone_d}$ :

$$\mathbf{T}_{hole} = \mathbf{T}_{cone_u}^{-1} \mathbf{T} \mathbf{T}_{cone_d}^{-1}, \quad (2.3.15)$$

where the Transmission Matrix of a conical waveguide is defined by Eq. (1.3.8)

We were interested in determining whether or not the shunt impedance  $\bar{Z}_s$  is different from that derived for a cylindrical bore and to determine the effect of the asymmetry on the values of  $\bar{Z}_{a_u}$  and  $\bar{Z}_{a_d}$ . The tonehole parameters were obtained for two conical waveguides with taper angles of 3 and 6 degrees. The COMSOL/Matlab simulation script for the simulation of the tonehole on a conical bore is `toneholeunflangedconical.m`. This script is for an angle of 3 degrees and must be edited to simulate the 6 degree case. 

As for toneholes on a cylindrical bore, we developed a data-fit formula for the shunt equivalent length of the open tonehole from the simulation data (with the same set of parameters). Then we calculated the differences between the two fit formulas and determined that the maximal difference is  $4 \times 10^{-5} b$  in both cases. This is a very small difference and we are confident in concluding that the shunt length corrections are unchanged relative to their values on a cylindrical bore.

A conclusion for the series length correction is more difficult to obtain. As can be seen in Fig. 2.25, the upstream and downstream values of the series length correction are very close to one another. Since the impact of the series length correction is relatively small and becomes increasingly less important as the toneholes grow smaller, this difference is likely to

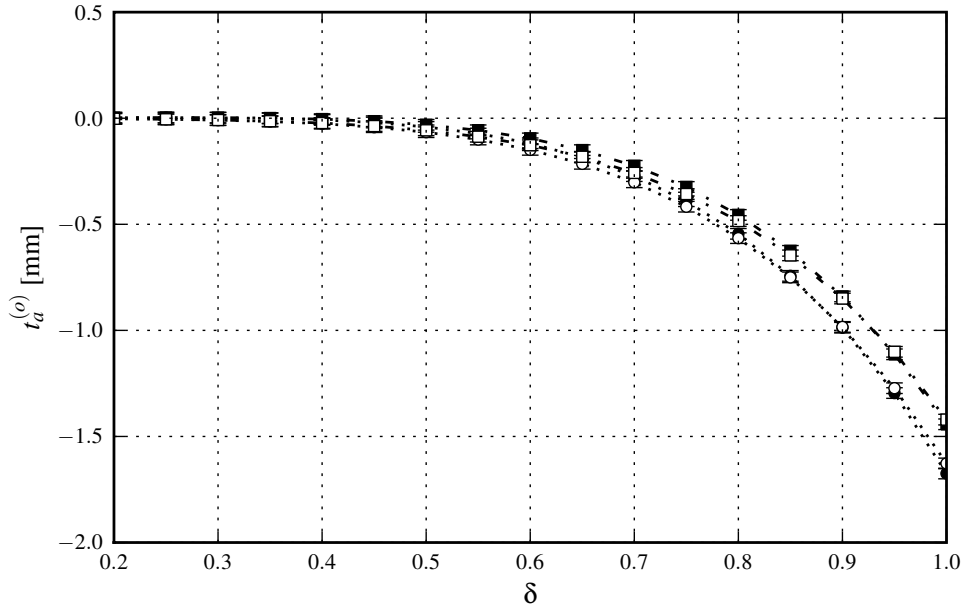


Figure 2.25: Series length correction  $t_a^{(o)}$  in mm for a tonehole on a conical bore with taper angle of 3 degrees: limit for tall (squares) and short (circles) toneholes – upstream part (filled), downstream part (unfilled).

be negligible.

From this analysis, we conclude that the use of Transmission-Matrix parameters developed for toneholes on cylindrical bores are valid for conical bores, at least up to an angle of 6 degrees and probably for wider angles as well.

## 2.4 Summary

In this chapter, we have developed a methodology to obtain the transmission-matrix parameters of an object from simulations using the FEM. Using this method, the transmission-matrix parameters of any type of waveguide geometry may be obtained. This method was validated against published experimental measurements of toneholes. Good general agreement is found,

but the low-frequency value of the shunt equivalent length  $t_s^{(o)}$  is slightly larger in the experimental measurement of [Dalmont et al. \(2002\)](#).

The methodology was applied to the case of open and closed toneholes for a wide range of geometrical parameters. Two types of toneholes were studied: (1) unflanged toneholes such as those found on saxophones and concert flutes, and (2) toneholes on a thick pipe such as those found on the clarinet, oboe, recorder and many other instruments. From these results, data-fit formulas were developed for the low-frequency values of the shunt and series length correction of the toneholes in the open and closed states.

These new formulas extend the validity of current tonehole models to toneholes of shorter height and improve their general accuracy. Noteworthy for toneholes of short height, the shunt equivalent length found with the FEM increases with frequency more than is predicted by current theories. The new formulas better match this behaviour. Moreover, the dependence of these series length corrections on the tonehole height  $t$  is found to be much different from that suggested in the literature. This is particularly important for closed toneholes, because the effect of the series length correction cumulates along the instrument.

The shunt equivalent length of closed side holes found with the FEM is shown to be in good agreement with current theories, even though the inner length correction, which becomes significant only for higher frequencies, does not match the values proposed in the literature. This is negligible for the frequencies of interest in musical instrument design.

In [Sec. 2.3.6](#), we found that the shunt equivalent length for a tonehole on a conical waveguide (up to a  $6^\circ$  taper angle) is the same as for a tonehole on a cylindrical waveguide, with a difference smaller than  $4 \times 10^{-5}b$ . The upstream and downstream series length corrections differ slightly, but the impact on the acoustics of woodwind instruments is probably negligible. We concluded that tonehole parameters developed on a cylindrical bore can be used equally for conical instruments.

In [Sec. 2.3.5](#), the effect of a hanging keypad was studied and compared to the predictions of [Eq. 1.3.35](#), which match our FEM results for tall toneholes and values of  $h/a > 0.3$ . For

toneholes of shorter height ( $t/b < 0.5$ ) and when the keypad is closer to the tonehole ( $h/a < 0.3$ ), the length correction due to the presence of a pad is larger by more than 10% of that predicted.

## Chapter 3

# Finite Element Simulations of Woodwind Instrument Air Columns

In this chapter, we use the FEM to calculate the input impedance of complete woodwind-like instrument geometries of increasing complexities and compare these with results obtained using the TMM. Contrary to the TMM, the input impedance calculated with the FEM accounts for any potential internal or external interaction of the evanescent modes excited near each discontinuity. Therefore, a comparison of the resonance frequencies of multi-tonehole systems calculated with both methods will allow us to determine the amount of error to be expected from TMM calculations, which do not account for such interactions. This verification is useful to know if the TMM is sufficiently accurate to be used for the design of woodwind instruments using an optimization method. The FEM provides a valuable computational approach for woodwind instrument modelling, both for the verification of the accuracy of the TMM and for handling complex geometries. The main disadvantage of the FEM compared to the TMM is its long calculation time (hours instead of seconds as discussed in the Introduction).

The simulation of woodwind-like instrument geometries requires accounting for boundary layer losses to obtain accurate results. The phase velocity of the travelling waves in the air column is reduced and their magnitude attenuated. This shifts the resonance frequencies and

attenuates their magnitudes by non-negligible amounts. Most of this effect occurs on the inner wall of the instrument rather than on the tonehole wall. However, in this chapter, the boundary layer losses are added to the tonehole models as a means of verifying to what extent these losses may influence the resonance frequencies of the instrument. As in Chapter 2, the instruments are surrounded by a spherical domain with a non-reflecting, second-order boundary condition.

Thermoviscous boundary layer losses may be approximated with a special boundary condition, such as that presented by Pierce (1989, p. 528), Bossart, Joly, and Bruneau (2003) or Chaigne and Kergomard (2008, p. 211, Eq. 5.138). The expression that we implemented as our boundary condition is:

$$Y_{wall} = -\frac{v_n}{p} = \frac{1}{\rho c} \sqrt{jk} \left[ \sin^2 \theta \sqrt{l_v} + (\gamma - 1) \sqrt{l_t} \right]. \quad (3.0.1)$$

The meanings of the mathematical symbols are:

$v_n$	normal velocity on the boundary,
$k = 2\pi f/c$	wavenumber,
$\theta$	angle of incidence of the wave,
$\mu$	fluid viscosity,
$\rho$	fluid density,
$\gamma$	ratio of specific heats,
$c$	speed of sound in free space,
$Pr$	Prandtl number,
$l_v = \mu/\rho c$	vortical characteristic length,
$l_t = l_v/Pr$	thermal characteristic length.

The angle of incidence may be calculated from  $\cos\theta = \hat{n} \cdot \hat{v}/|\hat{v}|$ , where the normal vector  $\hat{n}$  is unit length and  $\hat{v}$  is the particle velocity vector. The COMSOL/Matlab scripts for the simulations in this chapter are available from the [CAML<sup>1</sup>](#) website, directly by contacting the [author<sup>2</sup>](#) or, for pdf viewers supporting file attachment, directly in this document (see the margin icons). The properties of air at 25°C are used for all the simulation cases.

From the simulation results, the input impedance is evaluated by dividing the complex values of the pressure and normal velocity found on the input plane. Because the solution is computed as a plane wave near the input end (which is defined as at least 3 to 5 times the diameter of the pipe away from the first tonehole), these values are constant on the surface. In order to average any numerical errors, we perform an average on the surface:  $p_{in} = (1/S_{in}) \int_{S_{in}} p dS$  and  $v_{in} = (1/S_{in}) \int_{S_{in}} v dS$ . The normalized input impedance is then  $\bar{Z}_{in} = p_{in}/\rho c v_{in}$ .

The resonance frequencies of the simulated objects are estimated by a linear interpolation of the zeros of the angle of the reflection coefficient  $R = (Z - 1)/(Z + 1)$ . The simulations are performed from 100Hz to 1500Hz in steps of 10Hz.

Two different tonehole models are compared to the FEM results, including that of [Dalmont et al. \(2002\)](#) and the updated model presented in Chapter 2. The transmission matrix of the tonehole is defined by Eq. (1.3.14). For the model of [Dalmont et al. \(2002\)](#), the parameters are:

$$\bar{Z}_s^{(o)} = (j/\delta^2) (kt_i + \tan k(t + t_m + t_r)), \quad (3.0.2)$$

$$\bar{Z}_a^{(o)} = (j/\delta^2) kt_a, \quad (3.0.3)$$

$$\bar{Z}_s^{(c)} = -(j/\delta^2) \cot k(t + t_m), \quad (3.0.4)$$

$$\bar{Z}_a^{(c)} = (j/\delta^2) kt_a, \quad (3.0.5)$$

where  $t_i/b = 0.82 - 1.4\delta^2 + 0.75\delta^{2.7}$ ,  $t_a/b = -0.28\delta^4$ ,  $t_m/b = \delta(1 + 0.207\delta^3)/8$  and  $t_r$  is

<sup>1</sup><http://www.music.mcgill.ca/caml/doku.php?id=projects:fem>

<sup>2</sup>[antoine.lefebvre2@mail.mcgill.ca](mailto:antoine.lefebvre2@mail.mcgill.ca)

calculated with Eq. (1.3.11). The boundary layer losses on the tonehole walls may be included by replacing  $k$  with  $k_c = \omega/c + (1 - j)\alpha$ , where  $\alpha = (1/b)\sqrt{kv/(2\rho c)}(1 + (\gamma - 1)/v)$  and  $v$  is the square root of the Prandtl number.

For the updated tonehole model, Eqs. (2.3.2), (2.3.5) and (2.3.8) are used with a modification to the open shunt impedance to include boundary layer losses, thus:

$$\bar{Z}_s^{(o)} = (j/\delta^2) \tan \{kt_r + k_c(t_i + t + t_m)\}. \quad (3.0.6)$$

In the formulation by Dalmont et al. (2002), the inner length correction does not include boundary layer losses. We found a better match with the simulation results if the inner length correction, but not the radiation length correction, includes boundary layer losses. The open end of our instrument-like systems is modelled with a semi-infinite unflanged pipe radiation impedance given by Eq. (1.3.11).

### 3.1 Validation

The FEM approach was validated for geometries where the TMM is known to be accurate (for 1D wave propagation). These configurations included a cylindrical and a conical waveguide with varying boundary conditions at their ends. We were particularly interested in verifying the accuracy of the boundary layer impedance model and non-reflecting radiation boundary condition.

A 3D FEM simulation of a closed cylindrical pipe of diameter 15 mm and length 300 mm was first computed. To minimize computation time, system symmetries were exploited. The cylinder was split in two along its primary axis and a null normal acceleration boundary condition was imposed on the plane of symmetry. A rigid boundary ( $\hat{v}_n = 0$ ) was created at the pipe end, while the boundary condition along the side walls was that given by Eq. (3.0.1). The COMSOL/Matlab simulation script is `cylinder_closed.m`.



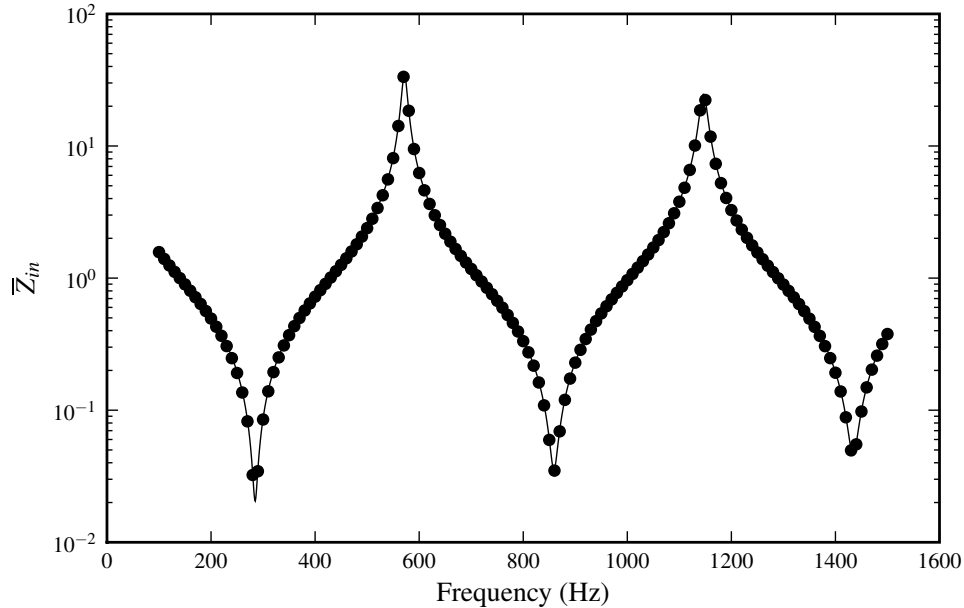


Figure 3.1: Normalized input impedance of a closed cylinder of diameter 15 mm and length 300 mm: FEM results (filled circles) and theoretical solution (solid line).

The results of the FEM simulation (filled circles) are shown in Fig. 3.1 compared to the TMM calculations (solid line). The mesh consists of 2003 cubic elements, giving a total of 12354 degrees of freedom. The first resonance frequencies obtained using the FEM and TMM were 571.74 Hz and 571.69 Hz, respectively, a negligible difference smaller than 0.2 cent. The ratio of the resonance magnitude was about 0.1 dB. Results for the second resonance were even closer, indicating that the boundary condition for wall losses provides accurate results.

The second validation simulation involved replacing the rigid boundary at the pipe output with the impedance boundary condition of Eq. (1.3.11), which is the same expression used for the TMM calculations. The COMSOL/Matlab simulation script is `cylinder_zrad.m`. Discrepancies were again below 0.2 cent.

Next, we simulated the same cylindrical pipe but with the open end radiating into a spherical radiation domain of 50 cm radius and a non-reflecting boundary condition on its outer surface (`cylinder_unflanged.m`). The exterior of the pipe was considered rigid (boundary

layer losses were neglected outside the pipe). We found that the refinement of the mesh along the edge at the opening of the pipe significantly influences the radiation length correction of the pipe. We simulated the same open pipe with an increasing number of elements on this edge and found that the circumference must be approximated with about 100 elements to attain numerical convergence. Once again, discrepancies were below 0.2 cent.

The same procedure was performed for a conical pipe of length 300 mm, with an input diameter of 15.0 mm and an output diameter of 30.7 mm (the half angle is 1.5 degrees): `cone_closed.m`, `cone_zrad.m` and `cone_unflanged.m`. The discrepancies between the resonance frequencies computed using the FEM and TMM were below 0.5 cent for the closed cone and the cone terminated by the radiation impedance. This error is sufficiently small to be neglected. For the cone radiating into a sphere, the first resonance was approximately 1 cent lower in the FEM simulation, indicating that the error introduced by using the radiation model of an unflanged pipe at the end of a conical waveguide in the TMM only causes a negligible difference.

From these validation tests, we conclude that the boundary condition for the thermoviscous losses and the non-reflecting spherical wave boundary condition can be used successfully for the simulation of woodwind instruments and that the maximum error in the calculated resonance frequencies up to 1500 Hz using the TMM is on the order of 1 cent.

## 3.2 Waveguides with a Single Tonehole

The input impedance of a cylindrical and a conical waveguide with a single tonehole was calculated with the FEM and TMM. These geometries allow us to verify the accuracy of the tonehole models while avoiding possible interactions between adjacent holes. In the FEM, the boundary condition approximating the boundary layer losses is defined on all interior surfaces, including the tonehole walls. Boundary layer losses are not normally accounted for along tonehole walls using the TMM. Thus, discrepancies between the FEM and TMM results in this

section are primarily attributable to these losses and, for the conical waveguide, the influence of a main bore taper.

The cylindrical and conical pipes described in the validation section were modified to include a tonehole of height  $t = 2\text{mm}$  and  $\delta = b/a = 0.7$ . For the cylindrical pipe, the tonehole is located at 87.7mm from the open end, while it is located at 141.4mm from the open end of the conical waveguide. The COMSOL/Matlab scripts for the cylindrical pipe are `cylinder_zrad_onehole_open.m` and `cylinder_zrad_onehole_closed.m`; for the conical pipe case, they are `cone_zrad_onehole_open.m` and `cone_zrad_onehole_closed.m`.

The first and second resonance frequencies for the single open or closed tonehole on a cylinder and a cone are listed in Table. 3.1. The FEM simulations are in good agreement with TMM calculations in every cases, the discrepancies being much smaller than 5 cents. The revised TMM model proposed in this thesis and the inclusion of boundary layer losses in the tonehole model slightly improves the results in all cases.



Method	$f_1$ [Hz] (cents)	$f_2$ [Hz] (cents)
Cylinder with one hole closed		
FEM	280.68	842.84
Dalmont w/o losses	280.80 (0.7)	842.90 (0.1)
Dalmont with losses	280.80 (0.7)	842.86 (0.1)
Lefebvre w/o losses	280.72 (0.3)	842.90 (0.1)
Lefebvre with losses	280.71 (0.1)	842.86 (0.1)
Cylinder with one hole open		
FEM	378.80	1123.83
Dalmont w/o losses	379.07 (1.2)	1125.18 (2.1)
Dalmont with losses	378.97 (0.8)	1124.93 (1.7)
Lefebvre w/o losses	379.01 (1.0)	1124.32 (0.7)
Lefebvre with losses	378.82 (0.1)	1123.85 (0.0)
Cone with one hole closed		
FEM	362.32	872.46
Dalmont w/o losses	362.63 (1.5)	872.84 (0.8)
Dalmont with losses	362.62 (1.4)	872.83 (0.7)
Lefebvre w/o losses	362.42 (0.5)	872.49 (0.1)
Lefebvre with losses	362.41 (0.4)	872.47 (0.0)
Cone with one hole open		
FEM	572.85	1019.35
Dalmont w/o losses	573.98 (3.4)	1020.70 (2.3)
Dalmont with losses	573.86 (3.1)	1020.55 (2.0)
Lefebvre w/o losses	573.57 (2.2)	1019.46 (0.2)
Lefebvre with losses	573.30 (1.4)	1019.11 (-0.4)

Table 3.1: Comparison of the resonance frequencies for the cylindrical and conical waveguides with one open or one closed tonehole. The numbers in parentheses represent the intervals in cents relative to the FEM result.

### 3.3 A Cone with Three Toneholes

Method	$f_1$ [Hz] (cents)	$f_2$ [Hz] (cents)	$f_3$ [Hz] (cents)	$f_4$ [Hz] (cents)
Closed toneholes				
FEM	143.23	297.43	460.45	630.03
Dalmont with losses	144.01 (9.3)	298.39 (5.6)	461.02 (2.1)	630.73 (1.9)
Lefebvre with losses	143.45 (2.5)	297.72 (1.7)	460.62 (0.6)	630.00 (-0.1)
Open toneholes				
FEM	172.26	364.93	569.13	774.87
Dalmont with losses	172.62 (3.6)	365.77 (3.9)	570.81 (5.1)	778.62 (8.4)
Lefebvre with losses	172.63 (3.8)	365.73 (3.8)	570.48 (4.1)	777.26 (5.3)

Table 3.2: Comparison of the simulated and calculated resonance frequencies of a conical waveguide with three open or closed toneholes.

A conical waveguide of 966.5 mm length with an input diameter of 12.5 mm and an output diameter of 63.1 mm was simulated. Three toneholes, each of 2 mm height, were located at distances of 760 mm, 818 mm and 879 mm from the input plane with respective diameters of 37.1 mm, 39.3 mm and 41.6 mm. These dimensions are close to those of the three toneholes closest to the bell of an alto saxophone. The COMSOL/Matlab scripts for the simulation of this instrument with all toneholes closed is `cone_with_three_holes_allclosed.m` and with all toneholes open `cone_with_three_holes_allopen.m`. The input impedance of this instrument for all toneholes closed and all toneholes open is shown in Fig. 3.2.

The frequencies of the first four resonances of this system for both closed and open toneholes are presented in Table 3.2. When all toneholes are closed, the resonance frequencies calculated using the TMM with the Lefebvre tonehole model are significantly closer to those found using the FEM. The discrepancies between these results decrease with increasing frequency and are perhaps caused by internal tonehole interactions.

When all toneholes are open, both TMM tonehole models predict resonance frequency values above those found using the FEM, with discrepancies increasing with frequency. There

is no improvement in using the new formula from the previous chapter. Observation of the calculated input impedances in Fig. 3.2, as well as the reflection coefficient magnitudes and equivalent lengths in Fig. 3.3, indicate significant discrepancies between the FEM and TMM results near the tonehole cutoff frequency. The equivalent length is calculated as  $L_o = (\pi - \phi_R)/2k$  (Ayers, 1995), where  $\phi_R$  is the unwrapped phase of the reflection coefficient. The differences are likely more attributable to internal or external tonehole interactions than to the main bore taper. In general, the FEM simulations predict lower resonance frequencies, as well as lower reflection coefficient magnitudes; this result suggests that the tonehole interactions increase the amount of radiated energy. Research on how the TMM may be extended to include this effect would be necessary to further improve the TMM results.

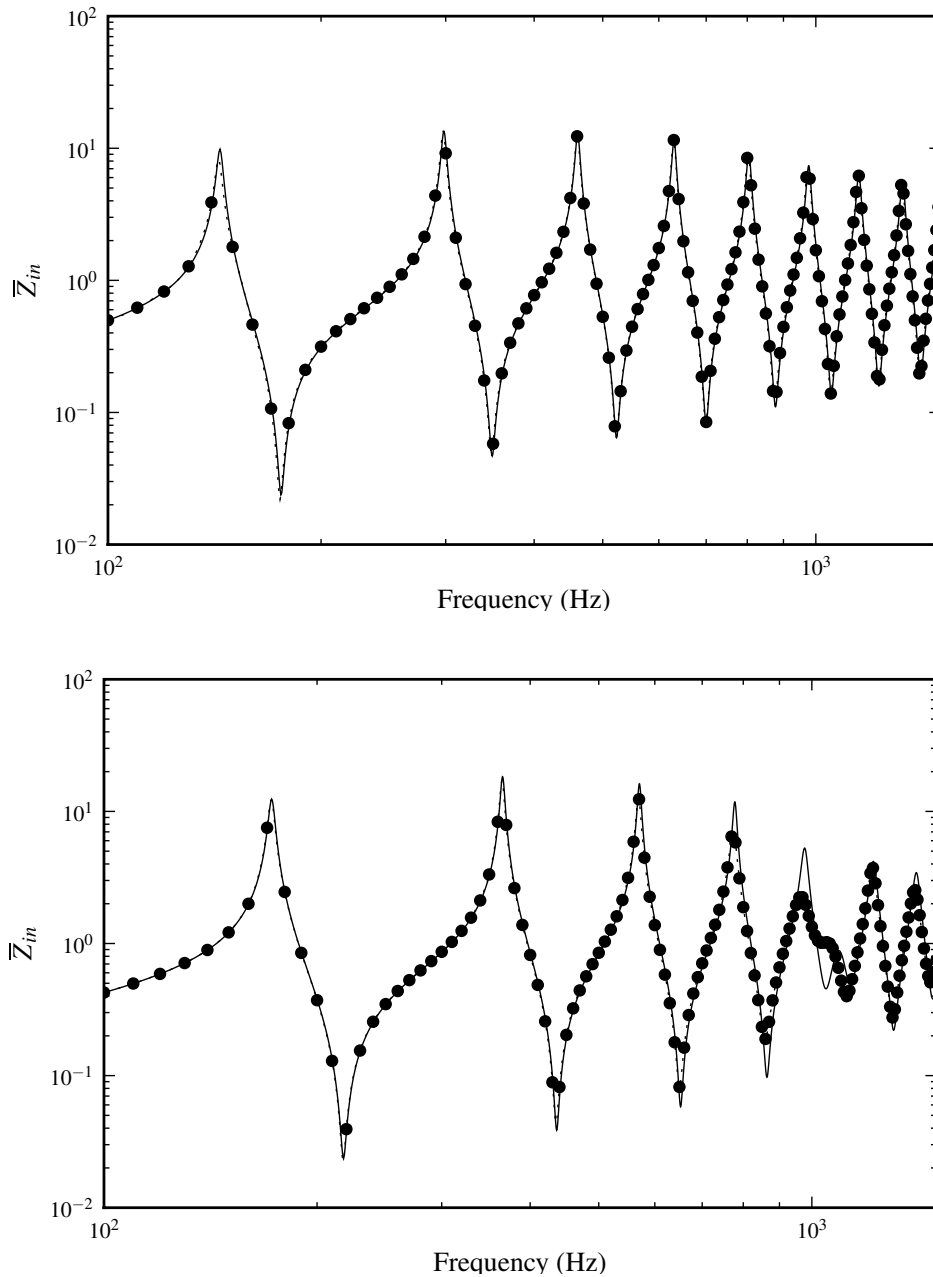


Figure 3.2: Input impedance of a conical waveguide with three toneholes: all closed (top graph) and all open (bottom graph). Comparison between the FEM (filled circles) and the TMM (solid). The dashed line is an interpolation between the FEM data points.

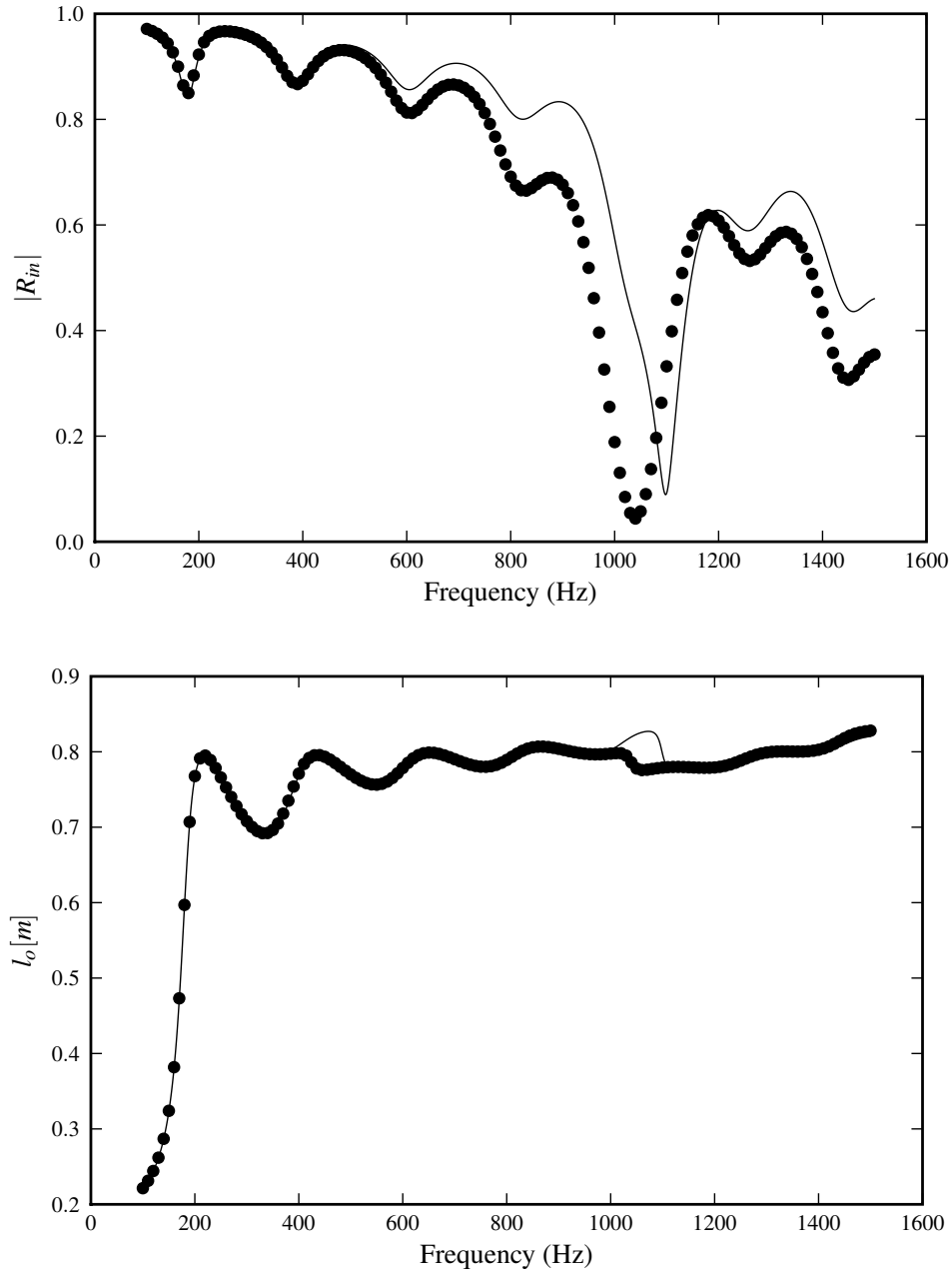


Figure 3.3: Magnitude of the reflection coefficient (top graph) and open cylinder equivalent length (bottom graph) for a conical waveguide with three open toneholes. Comparison between the FEM (filled circles) and the TMM (solid).

### 3.4 A Cylinder with Twelve Toneholes

Method	$f_1$ [Hz] (cents)	$f_2$ [Hz] (cents)	$f_3$ [Hz] (cents)	$f_4$ [Hz] (cents)
Closed toneholes				
FEM	146.83	439.72	737.72	1032.82
Dalmont with losses	146.79 (-0.5)	439.74 (0.1)	737.70 (-0.1)	1032.80 (-0.1)
Lefebvre with losses	146.80 (-0.4)	439.78 (0.2)	737.77 (0.1)	1032.92 (0.2)
Open toneholes				
FEM	294.55	879.06	1448.49	
Dalmont with losses	293.44 (-6.6)	879.82 (1.5)	1452.50 (4.8)	
Lefebvre with losses	293.44 (-6.6)	879.75 (1.3)	1450.66 (2.6)	

Table 3.3: Comparison of the simulated and calculated resonance frequencies of a simple clarinet-like system with twelve open or closed toneholes.

A clarinet-like system was simulated consisting of a cylindrical pipe of 15 mm diameter and 572.2 mm length with 12 toneholes of 6 mm diameter ( $\delta = 0.4$ ) and 6 mm height ( $t/b = 2.0$ ) located at the following distances from the instrument's excitation point (in mm): 265.8, 282.6, 300.3, 319.1, 338.9, 359.9, 382.1, 405.6, 430.4, 456.7, 484.5, 514.0. These toneholes produce a one-octave chromatic scale starting at 146.8 Hz ( $D_3$ ).

This instrument was simulated with all toneholes closed and all toneholes open. The COMSOL/Matlab scripts for the simulation of this instrument are `simpleclarinet_allopen.m` and `simpleclarinet_allclosed.m`. For the open case, the mesh consisted of 24863 cubic elements (125593 DOFs). The impedances calculated with the FEM and TMM are shown in Fig. 3.4. The frequencies of the resonances are compared in Table 3.3.

When all the toneholes are closed, the TMM calculations with both tonehole models produce resonance frequencies that match with great accuracy those found using the FEM. When all the toneholes are open, discrepancies are more significant and are likely due to tonehole interactions. The frequency of the first resonance is 6.6 cents lower in the TMM with both tonehole models; this is a non-negligible and surprising difference because, in every other

cases studied, the FEM predict a lower resonance rather than a higher one. Figures 3.4 and 3.5 indicate a variation between the FEM and TMM results near the tonehole lattice cutoff frequency, which occurs at the minimum of the reflection coefficient magnitude. This again suggests that the interaction between the sound fields of adjacent toneholes can shift the resonance frequencies.

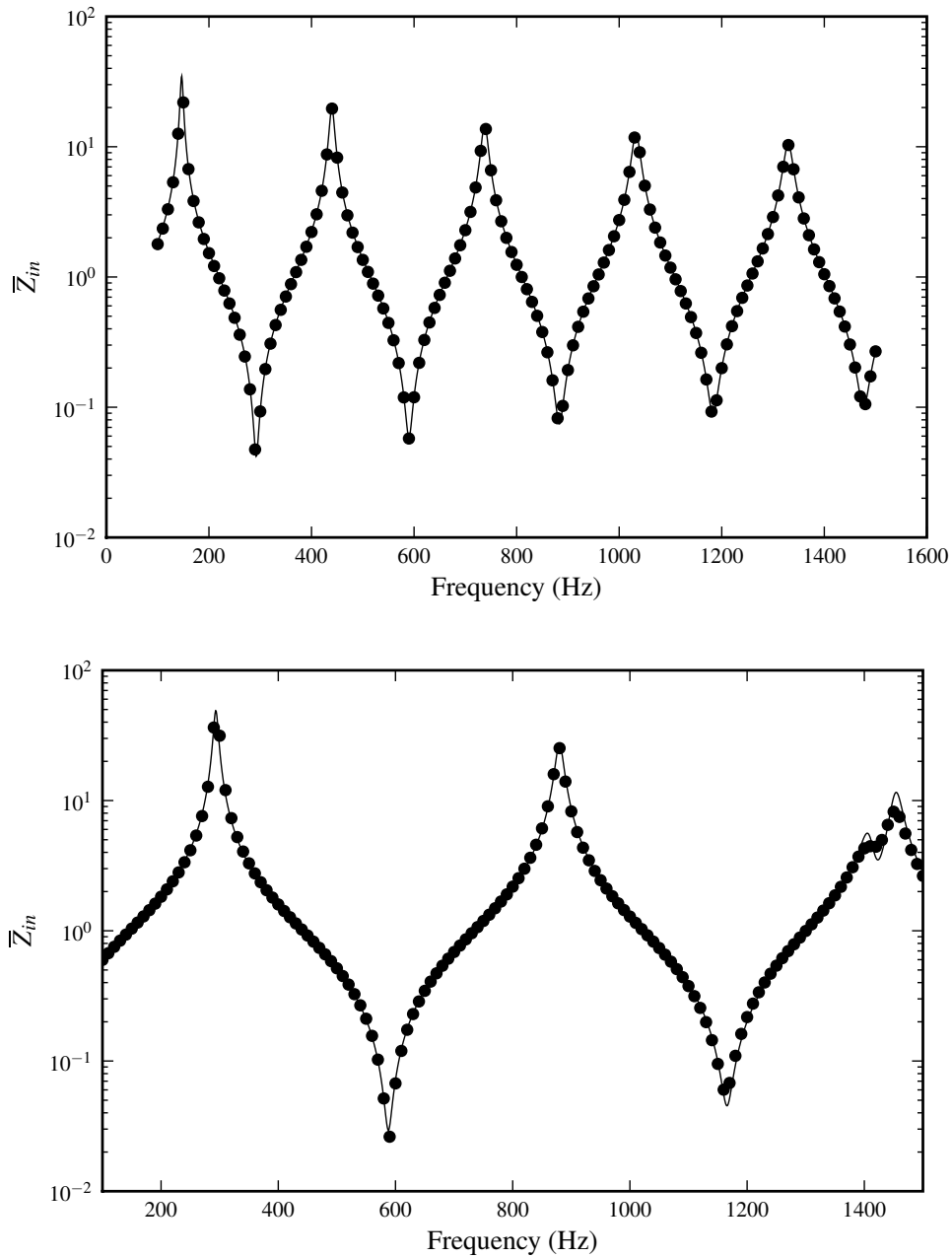


Figure 3.4: Input impedance of a cylindrical waveguide with 12 toneholes: all closed (top graph) and all open (bottom graph). Comparison between FEM simulation of the complete instrument (filled circles) and TMM calculations (solid).

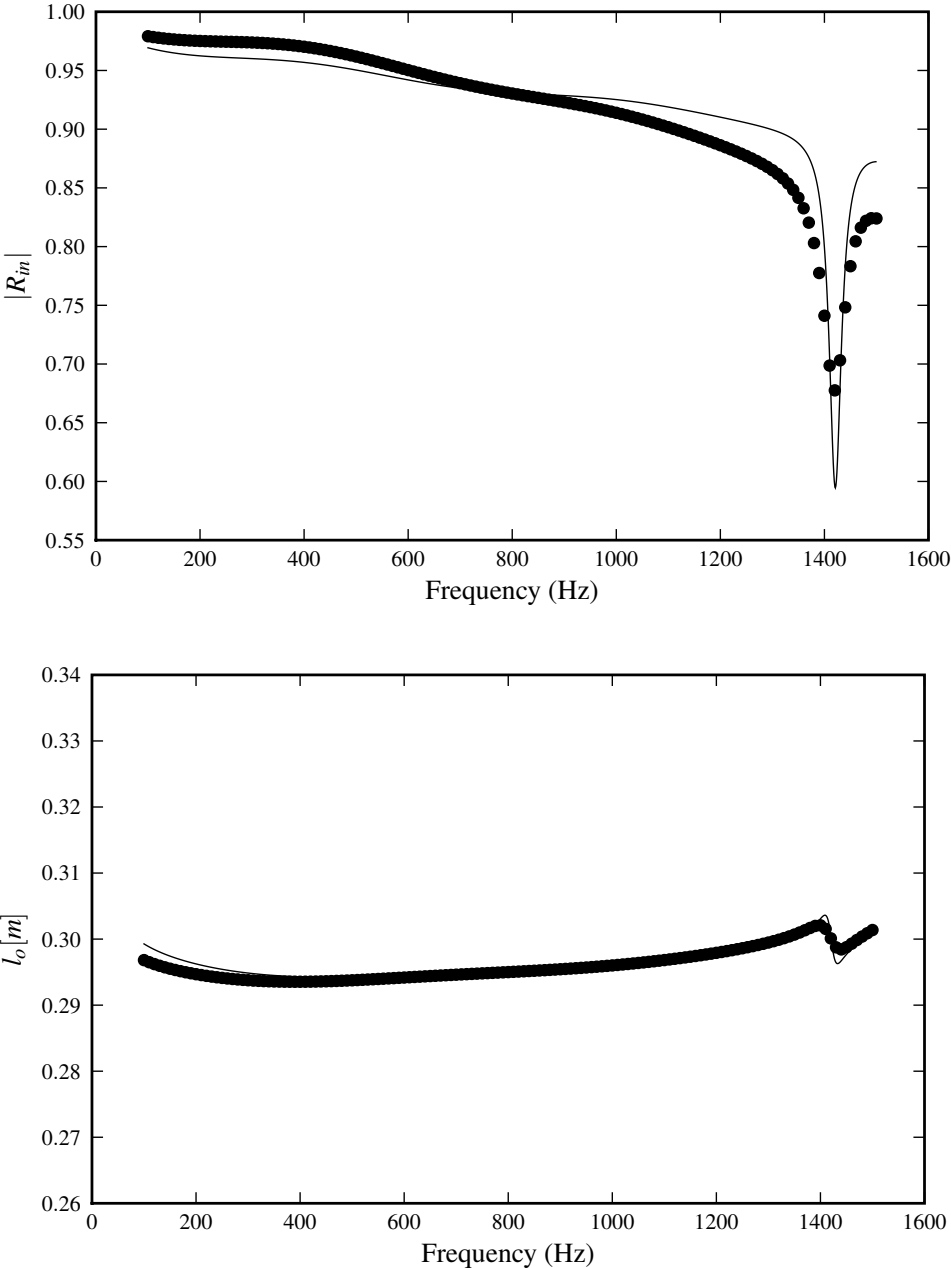


Figure 3.5: Magnitude of the reflection coefficient for a cylindrical waveguide with twelve open toneholes. Comparison between FEM simulation of the complete instrument (filled circles) and TMM calculations (solid).

### 3.5 A Cone with Twelve Toneholes

Method	$f_1$ [Hz] (cents)	$f_2$ [Hz] (cents)	$f_3$ [Hz] (cents)	$f_4$ [Hz] (cents)
Closed toneholes				
FEM	147.19	302.58	461.63	628.60
Dalmont with losses	149.06 (21.9)	304.10 (8.7)	463.98 (8.8)	631.94 (9.2)
Lefebvre with losses	147.85 (7.8)	302.63 (0.3)	461.97 (1.3)	628.76 (0.2)
Open toneholes				
FEM	334.14	733.03	1154.32	
Dalmont with losses	334.31 (0.8)	734.35 (3.1)	1158.30 (6.0)	
Lefebvre with losses	334.28 (0.7)	734.06 (2.4)	1156.56 (3.4)	

Table 3.4: Comparison of the simulated and calculated resonance frequencies of a conical waveguide with twelve open or closed toneholes.

A saxophone-like system was simulated consisting of a conical waveguide of 9 mm input diameter, 61.2 mm output diameter, and 978.9 mm length with 12 toneholes of 2 mm height located respectively at 363.6, 401.9, 441.9, 483.7, 527.4, 573.1, 620.9, 671.0, 723.7, 779.1, 837.5 and 899.1 millimetres from the input end. These toneholes, defined by  $\delta = b/a = 0.7$ , produce a one-octave chromatic scale starting at 146.8 Hz (D3).

The COMSOL/Matlab script for the simulation of this instrument with all toneholes open is `simplesaxophone_allopen.m` and with all toneholes closed `simplesaxophone_allclosed.m`.

The FEM simulation of this instrument was solved for all toneholes closed and all toneholes open. The mesh consisted of 32655 cubic elements (165626 DOFs). The input impedances calculated with the TMM and FEM are plotted in Fig. 3.6 and the resonance frequency values compared in Table 3.4.

For the closed side holes, the TMM results using the Dalmont tonehole model differ significantly from the FEM predictions (22 cents for the first resonance and close to 10 cents for the others). Although the TMM results are closer using the Lefebvre tonehole model, discrepancies remain for the first resonance (8 cents), and support the hypothesis that internal tonehole

interactions lower the low-frequency resonances when the toneholes are closed.

When the toneholes are open, the FEM predicts lower resonances than either of the TMM tonehole models. Again, this seems to be related to tonehole interactions. In this case, the tonehole cutoff frequency is above 1.5 kHz and the first resonance is affected by about only 1 cent, whereas the third resonance is shifted by 4 cents. Contrary to the case for the cylindrical instrument, the first resonance is not significantly affected.

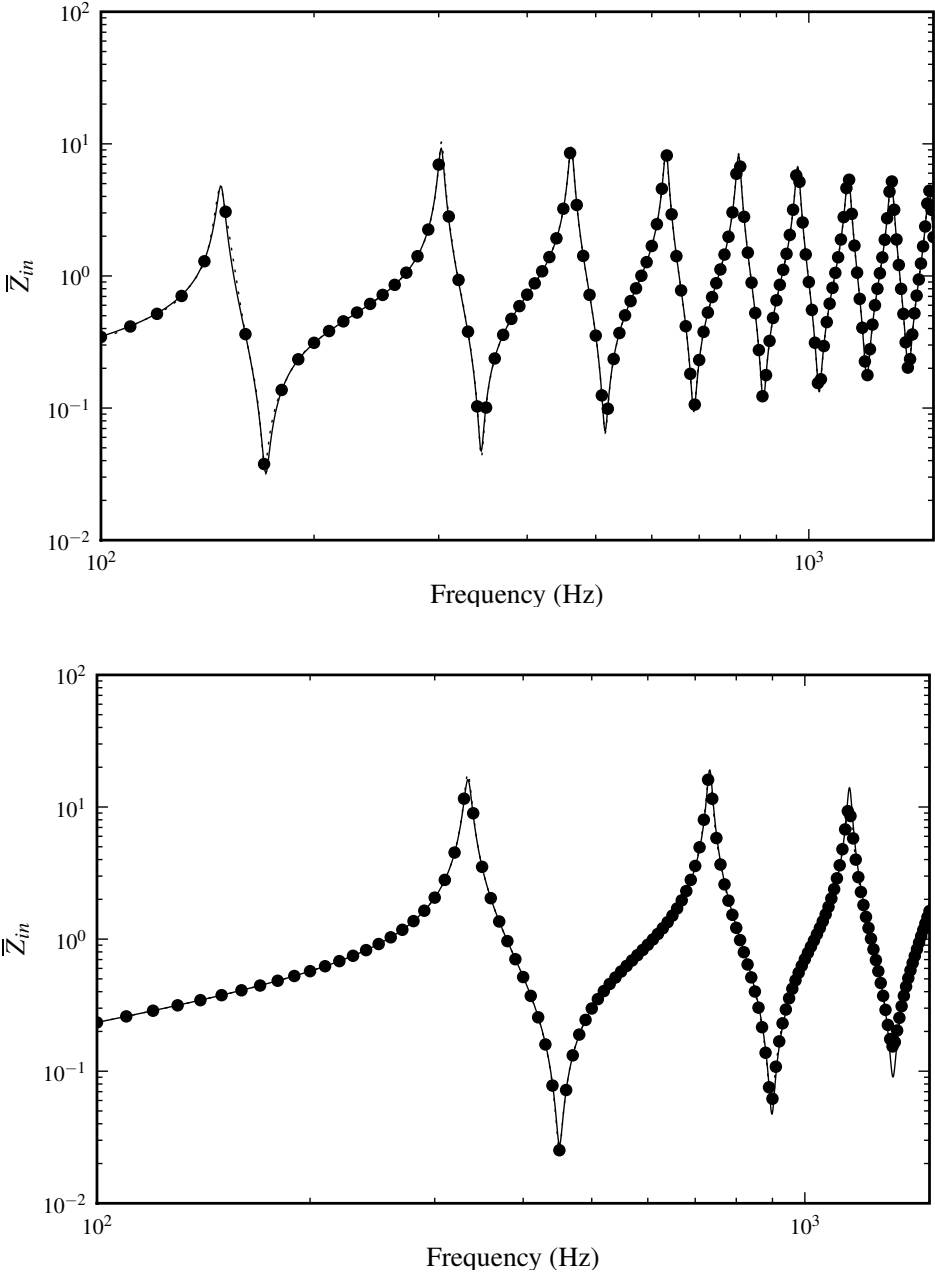


Figure 3.6: Input impedance of a conical waveguide with twelve toneholes: all closed (top graph) and all open (bottom graph). Comparison between FEM simulation (filled circles) and TMM calculations (solid).

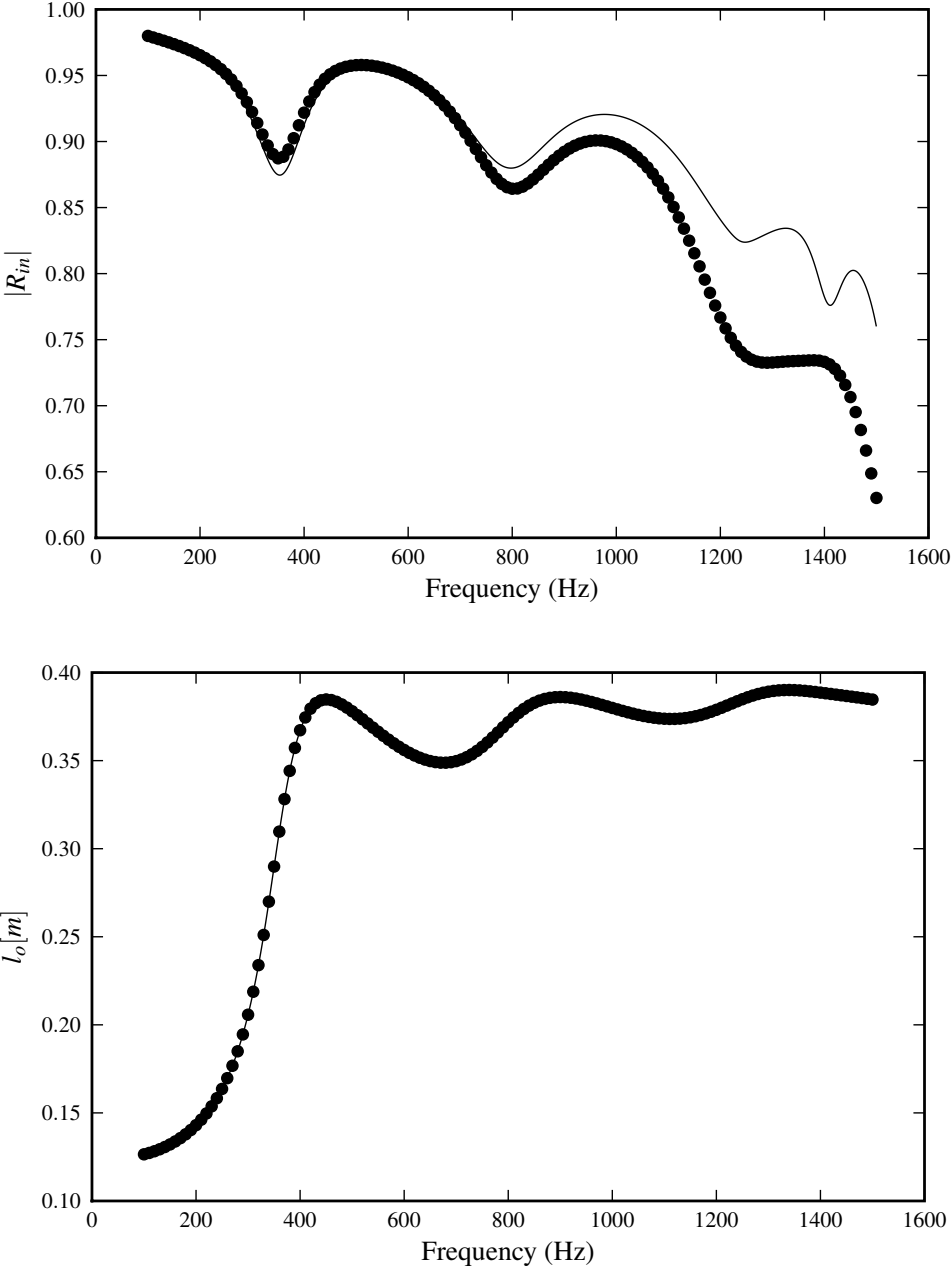


Figure 3.7: Magnitude of the reflection coefficient for a conical waveguide with twelve open toneholes. Comparison between FEM simulation (filled circles) and TMM calculations (solid).

### 3.6 Curvature of the Bore

Method	$f_1$ [Hz] (cents)	$f_2$ [Hz] (cents)	$f_3$ [Hz] (cents)	$f_4$ [Hz] (cents)	$f_5$ [Hz] (cents)
FEM (1)	145.03	304.92	473.41	640.97	804.22
FEM (2)	145.04 (0.1)	304.97 (0.2)	473.58 (0.6)	641.30 (0.9)	804.57 (0.8)
FEM (3)	145.05 (0.2)	305.09 (0.9)	473.98 (2.1)	642.07 (3.0)	805.39 (2.5)
TMM (1)	144.90 (-1.6)	305.24 (1.8)	473.68 (1.0)	640.95 (0.0)	804.19 (-0.1)

Table 3.5: Comparison of the simulated and calculated resonance frequencies for a straight and two curved alto saxophone necks.

Using the FEM and the thermoviscous boundary condition presented in this chapter, the simulation of a curved bore with a varying cross-section and with boundary layer losses is possible. As a case study, we present the results of simulations of a conical waveguide with different geometrical settings: (1) straight, (2) slight curvature and (3) large curvature, as illustrated in Fig. 3.8. There is a cylindrical section at the beginning and at the end of this structure. Each of these three geometries has the same cross-sectional diameter as a function of the distance along the centre line. Therefore, they also have the same volume. Concatenated to these structures was a straight conical waveguide of 760 mm length, input diameter of 23 mm (corresponding to the output diameter of the first segment) and output diameter of 63 mm. An unflanged pipe radiation impedance was applied at the output of the conical section. From the results of the simulations, we compared the first five resonance frequencies of the curved bores to those of the straight bore. We also compared the FEM results of the straight bore with TMM calculations. These results are presented in Table 3.5.

The shift of resonance frequencies with bending is very small for the lowest resonances and gradually increases up to 3 cents for the fourth resonance of the third geometry. The magnitude of the effect in this particular case is negligible. As expected, the object with the most significant curvature has a more pronounced frequency shift. On wind instruments, the curvature of the bore normally comes with an “ovalisation” of the section and possibly a small

reduction of the volume due to the mechanical consequence of bending the pipe. This effect is not discussed here and may have more pronounced consequences on the tuning.

We compared the resonance frequencies for the straight geometry with predictions of the TMM and found surprising differences (see Table 3.5, last line). One hypothesis is that the evanescent modes occurring when the angle of conicity changes (there are three such changes in the current geometry) are the cause of such differences. These differences are negligible.

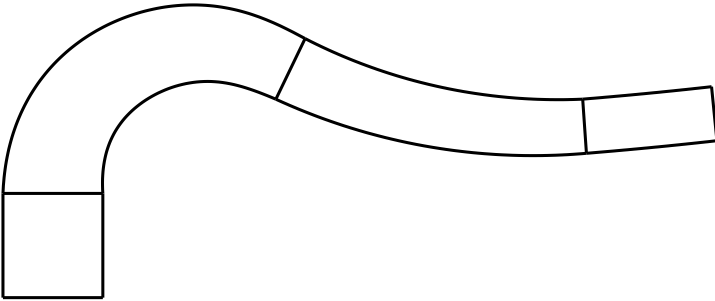
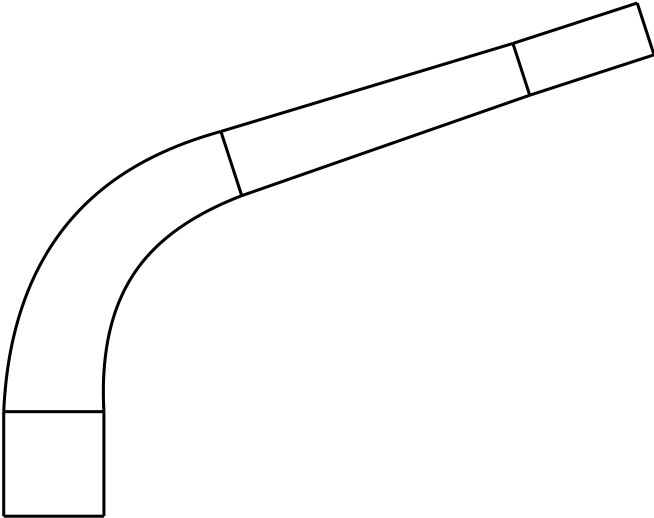
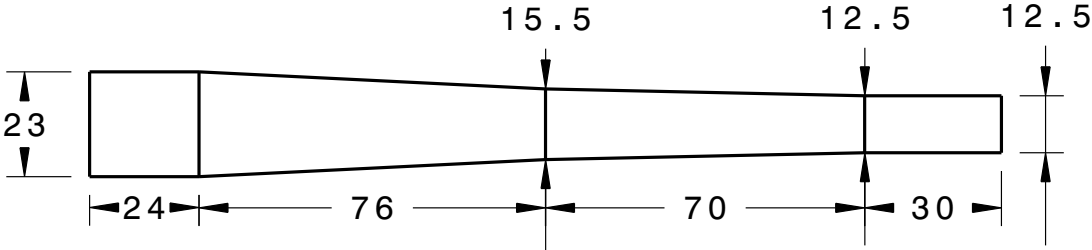


Figure 3.8: Diagram of the three instrument bores simulated for the study of curvature. The dimensions, in mm, are the same for all three instruments.

## 3.7 Radiation from the Bell

The radiation impedance of an alto saxophone bell was obtained using the FEM and compared to predictions of the TMM based on the discretization of the bell into conical segments. Other bell geometries may be obtained with the same method.

The bell of an alto saxophone is formed from a segment of cone followed by a circular arc. The length of the conical segment is 32.25 mm with an input diameter of 73.35 mm and an output diameter of 80.98 mm. The circular arc is tangent to the conical segment. It has a radius of 17.77 mm and its centre is located at 58 mm from the axis of the bell.

In the FEM model, the bell is surrounded by a radiation domain and no boundary layer losses are taken into account. In the TMM, the open end of the bell is modelled as an unflanged open end with a correction factor of 2 to take into account the spherical wave shape (half the area of a sphere is equal to 2 times the area of a circle of the same radius).

The real and imaginary parts of the impedance of this bell are shown in Fig. 3.9 and the open cylinder equivalent length in Fig. 3.10. The results with the TMM approximation are rather different than those of the FEM, confirming that this is not a valid method to model the impedance of the bell. The TMM approximation predicts that the equivalent length is shorter by approximately 10 mm compared to the FEM results.

For purposes of designing a woodwind instrument, the radiation impedance of the bell of the instrument may be pre-calculated using the FEM and used as a radiation condition for the TMM. Alternately, a correction to the plane-wave approximation may be applied following the work of [Nederveen and Dalmont \(2008\)](#).

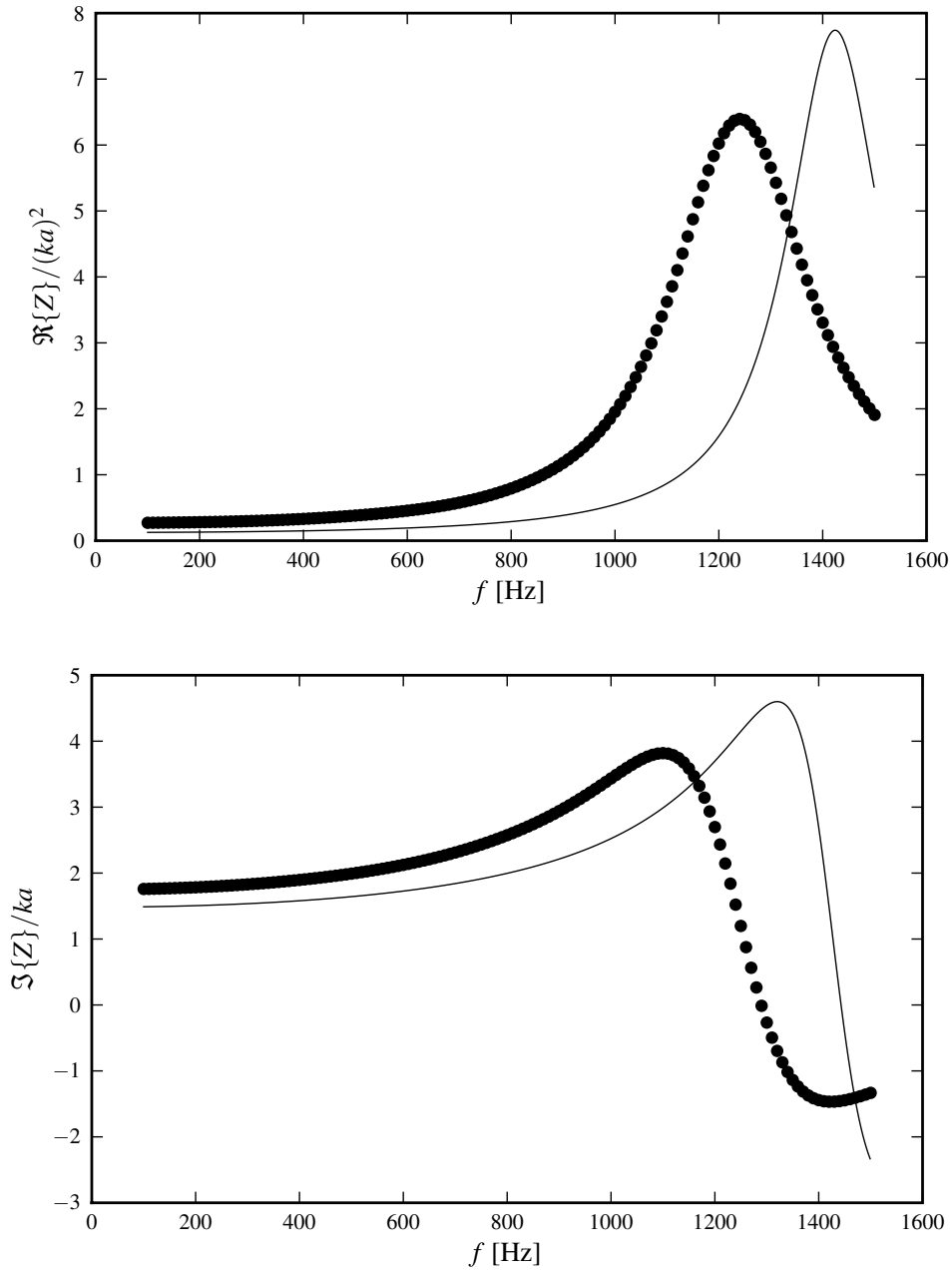


Figure 3.9: Impedance of an alto saxophone bell: real part over  $(ka)^2$  (top) and imaginary part over  $ka$  (bottom). Results of the FEM simulations (filled circles) and results of the TMM approximation (solid line).

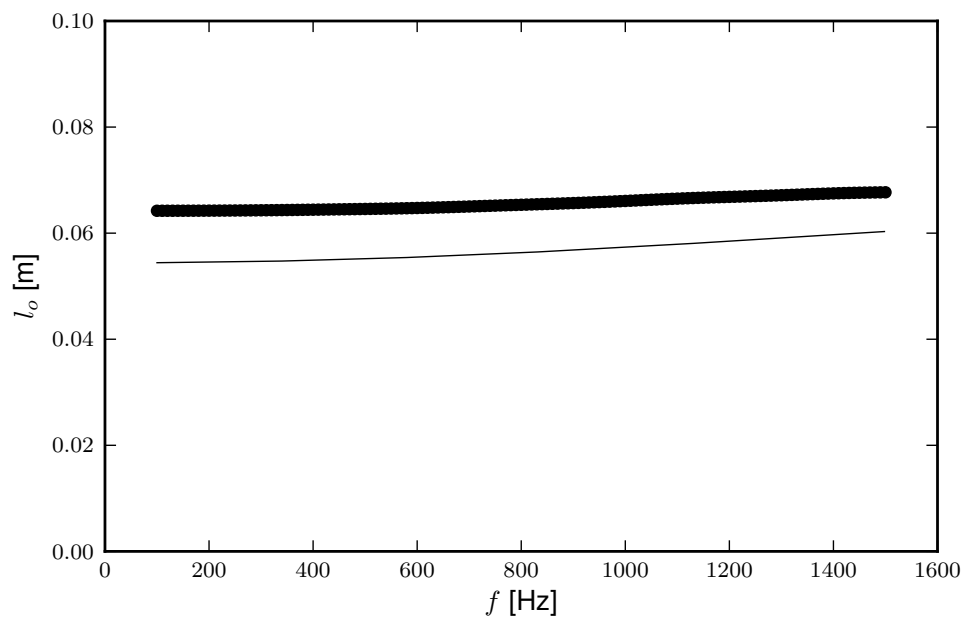


Figure 3.10: Open cylinder equivalent length  $l_o$  of an alto saxophone bell. Results of the FEM simulations (overlapping filled circles) and results of the TMM approximation (solid line).

## 3.8 Summary

The input impedance of simple woodwind-like instruments was evaluated using the Finite Element Method (FEM) and compared to theoretical calculations based on the Transmission-Matrix Method (TMM). This enables a validation of the TMM and an evaluation of the effect of internal and external tonehole interaction, which is neglected in the TMM. Thermoviscous losses were accounted for with an impedance boundary condition based on acoustic boundary layer theory. The systems were surrounded by a spherical radiation domain with a second-order, non-reflecting spherical-wave boundary condition on its outer surface. This method opens the possibility to accurately estimate the resonance frequencies of wind instruments using the FEM, which has never before been possible.

For simple geometries such as closed or open cylindrical and conical waveguides, the FEM results are shown to match theory with great accuracy. When considering waveguides with a single open or closed toneholes, the results of the FEM also match TMM calculations. The inclusion of boundary layer losses in the transmission-matrix model of the tonehole slightly improves the agreement with the FEM calculations but the difference is likely negligible. For geometries with multiple closed or open toneholes, discrepancies between the FEM and the TMM results become more significant and appear to be related to internal or external interactions. For closed side holes, this effect is more important for large diameter toneholes at low frequencies, thus affecting the first few resonances. For the conical waveguide with twelve closed toneholes studied in Sec. 3.5, the resonance frequencies calculated with the TMM better match the FEM when using the new formula for the series length correction presented in the previous chapter but the first resonance remains lower by approximately 8 cents in the FEM simulation. For open side holes, this effect is particularly important near the tonehole cutoff frequency but extends to lower frequencies as well. In the case of a cylinder with twelve open toneholes presented in Sec. 3.4, the first resonance shows an unexplained difference of +6.6 cents in the FEM. In every case, the discrepancies are below 10 cents, and generally less

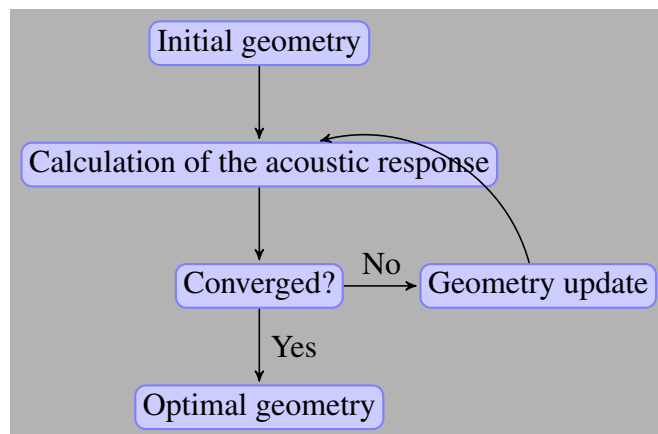
than 5 cents, indicating that the TMM remains a good method for the design of woodwind instruments.

The impact of the curvature of an alto saxophone neck pipe was investigated and the frequencies of the resonances were shifted by a maximum of 3 cents.

The radiation of an alto saxophone bell was obtained from the FEM and compared to TMM calculations. As expected, the differences are important, the equivalent length being approximately 10 mm larger in the FEM compared to the TMM. We conclude that for purposes of designing woodwind instruments, the discretization of a flaring bell in conical segments is not an appropriate method. We recommend pre-calculating the input impedance of the bell using the FEM or another numerical method and using this impedance as the radiation impedance of the instrument being designed.

## Chapter 4

# An Approach to the Computer-Aided Design of Woodwind Instruments



In this chapter, we present our work on solving the problem of calculating the position of the toneholes on woodwind instruments to achieve optimal tuning with various constraints. This method is applied to simple flute-, clarinet- and saxophone-like instruments with six or seven toneholes each. Physical prototypes of these instruments were constructed based on the results of the optimization routine and their playing behaviours are discussed.

The design of a woodwind instrument involves the determination of the positions and dimensions of its toneholes to produce the desired playing frequencies for each requested fingering, given a particular excitation mechanism and bore shape. The toneholes are responsible for the tuning of each individual note, whereas the shape of the bore plays an important role in the harmonicity of the resonances and thus, on the tuning of notes in the upper registers based on higher resonances of a fingering used in the first register. The excitation mechanism must be properly characterized before an attempt is made to design the instrument body.

A method for the design of woodwind instruments was previously presented by [Keefe \(1989\)](#). This author also reports unpublished material attributed to Benade who worked on the iterative calculation of tonehole locations. Benade's method involved calculating the location of each tonehole one by one, starting from the last and using an idealized theory based on an infinite tonehole lattice. When each tonehole had been located once, the procedure was started again, incorporating the effect of the presence of the other toneholes. This was repeated until convergence. This method did not make use of transmission matrix calculations. [Keefe \(1989\)](#) proposed an alternative design algorithm that made use of transmission matrices. The main advantage was an increased accuracy of the results, because they were not based on the idealized theory of an infinite tonehole lattice. This was the basis for the current research. The main problem with Keefe's approach is that he used a simple iterative method, similar to that used by Benade, where the tonehole locations are calculated one by one. This does not always result in convergence, particularly when the number of constraints is important. Also, Keefe reported that only one register can be used at a time and that only the positions of the toneholes are modified by the algorithm and not the diameters. This could result in situations where the toneholes are too close to or too far from one another and where the second register is not well tuned.

We propose to make use of a global optimization approach, a modified L-BFGS-B ([Zhu, Byrd, Lu, & Nocedal, 1994](#); [Lu, Nocedal, Zhu, Byrd, & Byrd, 1995](#)), which generally converges to a solution even for complex sets of constraints. For the research presented in this

chapter, we developed an optimization routine which allows the optimization of the positions, diameters and heights of each tonehole with constraints that include the resonance frequencies of as many fingerings as possible (including cross-fingerings) and for any number of modes. Further, bounds on each of the optimization variables allow control of the ergonomics of the instrument. A future research direction consists in including upper bore perturbations as an optimization variable and, possibly, the harmonicity of the first few resonances and the cutoff frequency of the tonehole lattice as criteria.

In practice, the number of degrees of freedom can be larger than the number of constraints. As an example, for the design of an instrument with 6 toneholes playing 7 notes, optimizing the positions of the toneholes and the length of the instrument is sufficient. Because bounds on the distances between adjacent holes may be used, the inclusion of the diameters may become necessary to obtain a valid solution. The solution to the problem is generally not unique and the instrument designer shall decide which parameters are fixed, which are to be optimized and what are the proper bounds. The method that we propose is an aid to the instrument designer, who must understand the functioning of woodwind instrument to use it properly.

It needs to be taken into account that the requested set of constraints and bounds is often contradictory. As an example, one may limit the diameters of the toneholes and the distances between adjacent toneholes to ensure that the instrument is playable with a normal human hand. In certain circumstances these limits will prevent the algorithm from attaining a small tuning error, which indicates that the requested instrument is not possible. The algorithm converges to the layout with minimal errors within the bounds provided to the algorithm. In complex cases, the resulting instrument still contains tuning errors and it is the responsibility of the instrument maker to decide if these are acceptable and, if not, to change the definition of the problem.

The source code of the L-BFGS-B optimization method is available at <http://www.eecs.northwestern.edu/~nocedal/lbfgsb.html> and is also interfaced to the Python programming language through the package SciPy (Scientific Python). The calculation of tonehole

locations of woodwind instruments using this algorithm requires defining an optimization function that will be provided to the algorithm. The initial values of the parameters, the definition of those parameters and the calculation method for the error norm will all influence the outcome of the algorithm.

Starting with an initial geometry designed using approximate calculations, the toneholes of the instrument are iteratively displaced until the mean square error on the tuning of each fingering has attained a minimum. At each iteration, the playing frequencies for each of the fingerings of the instrument are estimated using the TMM, including a correction for the excitation mechanism as explained in Sec. 1.2.

The resulting instrument will be well tuned if the underlying calculation method gives accurate playing frequencies, if the excitation mechanism was accurately characterized and if the instrument is built according to the calculated dimensions. Very small deviations in the geometry of the bore may cause important tuning deviations, particularly when they occur in the upper part of the instrument. The research presented in the previous chapters of this thesis was intended to verify and update the TMM parameters to ensure the accuracy of the results and the quality of the instruments generated with this optimization method. Based on the results of Chapter 3, we expect the accuracy of the calculation method to be on the order of  $\pm 5$  cents or  $\pm 10$  cents in the worst case. The main source of error seems to come from internal or external tonehole interactions, which are not taken into account in the TMM. Currently, the geometry of the instrument's bore is selected before the optimization is performed and only the length of the instrument, the position of the toneholes and/or their diameters are allowed to change during the optimization process. This geometry may consist of an arbitrary number of cylindrical or conical sections, one of which has to be selected as a variable length section — the lowest note of the instrument depends on the overall length, which will be optimized by changing the length of the selected section. For a conical instrument, the angle of the conical waveguide remains fixed; and if the length is changed by the optimization algorithm, the diameter of the end will scale accordingly. If a bell exists on the instrument, it will also be

scaled proportionally to the diameter at its beginning, which allows the use of a pre-calculated impedance for the bell. If the instrument's bore is curved, the transmission matrix of the curved section may be calculated using the FEM to improve the accuracy of the results. The only drawback of this method is that a tonehole may not be located on this curved section because there is no way to split a pre-calculated transmission matrix to insert the tonehole. In such a case, the curved section has to be considered straight. The resulting playing frequencies may be later verified using the FEM.

The toneholes are inserted on the instrument by splitting the waveguide where they are located. When the toneholes are displaced by the algorithm, the splitting points are changed. If keypads are present on the instrument, their distances are not changed by the optimization algorithm; the distance of the key above the tonehole or the ratio of the distance to the tonehole's diameter remains fixed.

Of course, if the definition of the instrument to be optimized is itself physically impossible (such as a lower frequency for a fingering with more toneholes open), the optimization may fail or the optimized instrument will be out of tune, and the outcome of the algorithm will report a large mean square error. Only realistic configurations can converge to a good instrument, which may require relaxing some of the constraints. A good method consists in starting with simple fingerings and adding more constraints one by one, verifying if a solution exists.

Furthermore, the definition of the optimization variables is important. If they are not chosen carefully, the problem may not converge or may lead to absurd results. As an example, if the tonehole locations are optimized based on their distances from the tip of the mouthpiece, a situation is created in which the optimization algorithm may inadvertently place toneholes out of order or locate one beyond the end of the instrument. This is problematic and will confuse the algorithm. It is more appropriate to define the first variable as the distance of the last hole from the open end; the second variable is the distance from the last hole to the preceding hole, continuing until the first hole. In this manner we can tell the algorithm that the lower bound for these variables is zero and guarantee that the toneholes are always located in the proper

order. This also provides a way to set an upper bound on the distances between two toneholes for the case of instruments with no key systems. Similarly, instead of using the diameter of the toneholes as an optimization variable, we use the ratio  $\delta = b/a$  with both a lower and an upper bound (0 to 1), which prevents a tonehole from becoming larger than the bore.

## 4.1 Selecting the Instrument's Bore Shape

Woodwind instruments air columns are based on cylindrical or conical bores because they produce harmonic partials (Fletcher & Rossing, 1998). A bell may be added to improve the radiation and timbre of low frequency notes (Nederveen, 1969/1998a), and the top part of the instrument's bore may have a different taper angle to improve the pitch of high register notes (Dalmont, Gazengel, Gilbert, & Kergomard, 1995, Sec. 5). The geometries of current woodwind instruments often present other deviations, but no evidence of their usefulness exists (Nederveen, 1969/1998a).

The top part of any woodwind instrument always plays an important role in the tuning of the instrument. As an example, a purely cylindrical concert flute plays flat in the second register because of the properties of the excitation mechanism. To overcome this problem, a tapered head, which raises the pitch of the upper register, is used on modern concert flutes. On the clarinet, the barrel also presents this kind of tapering; and the upper parts of saxophones, oboes and bassoons have similar deviations.

As a verification of this phenomenon, the playing frequencies of two saxophone-like conical instruments, differing in the geometry closer to the mouthpiece (approximately in the region where the neck pipe is normally located), are calculated using the TMM for different playing frequencies. The first instrument is made of a perfectly conical bore and the second presents deviations. Their respective geometries are shown in Fig. 4.1. Both instruments use the same mouthpiece geometry, which is displayed in Fig. A.5, as well as an equivalent volume of  $5.5\text{ cm}^3$  to approximate the excitation mechanism. In the first case, the instrument

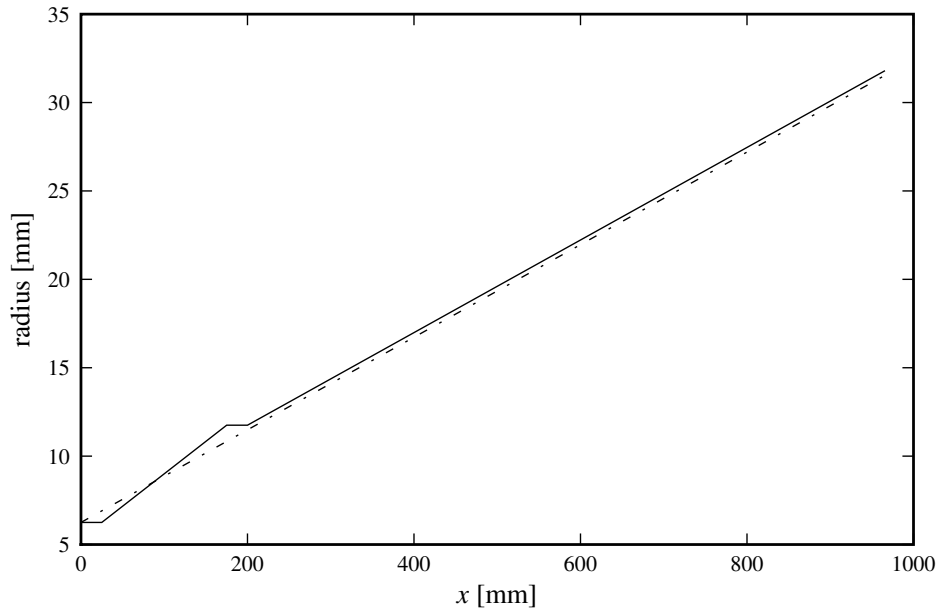


Figure 4.1: Radius as a function of  $x$  for the two saxophone-like conical instruments, differing in the geometry closer to the mouthpiece.

consists of a conical waveguide of 12.2 mm input diameter and 3 different lengths – 965, 600 and 400 mm – and a half angle of 1.5 degrees. For the longest cone, the second register is flat by 22 cents; and for the shortest, it is sharp by 63 cents. In the second case, the instrument consists of 4 sections: a cylinder of 25 mm length and 12.2 mm diameter, a cone of 150 mm length with an inner diameter of 12.2 mm and a outer diameter of 23.5 mm (2.16 degrees half angle), another cylinder of 25 mm length and 23.5 mm diameter and, finally, a cone with different lengths – 765, 400 and 200 mm – and a half-angle of 1.5 degrees. With this instrument, the frequencies of the second register do not deviate by more than 4 cents from the correct frequencies in all three cases.

This example shows two things: (1) a “perfect” cone is not an ideal instrument because it does not yield a correct tuning of the second register; and (2) deviations from a perfect cone in the neck pipe are possible to fix this problem. This will not only improve the tuning of the second register but also the ease of play of the first register, with a better alignment of the

resonances. Similar results may be obtained for other instruments, such as clarinets and flutes, and can support many observations made by musicians of the differences in the behaviour of clarinet barrels, flute heads and saxophone necks. Therefore, it would also be possible to add the geometric parameters of the deviations as an optimization variable. This is a future research direction.

In the examples provided in this chapter, no attempt was made to find the correct upper bore deviations. The objective was to verify the capacity of the algorithm to locate the toneholes for the first register and to build the instrument for verification purposes. The difficulty of building with accuracy an instrument bore with subtle deviations prevented us from going in this direction, but we are confident that if our algorithm is able to calculate the correct location of the toneholes on a cylindrical or conical bore, it will also work on a bore with deviations.

## 4.2 Calculating the Tonehole Positions and Dimensions

In this section, the details of the optimization algorithm are presented using an example of an instrument with 7 finger holes. The vector of the desired playing frequencies

$$\hat{f}_d = \{f_{C4}, f_{D4}, f_{E4}, f_{F4}, f_{G4}, f_{A4}, f_{B4}, f_{C5}\}$$

contains the frequencies in Hertz for each of the fingerings of the instrument. They are the targets for the optimization algorithm. The exact value of each frequency depends on the tuning system. One may use equal tempering or any other playing frequency. The fingerings

are represented by the matrix:

$$\begin{bmatrix} C4 & D4 & E4 & F4 & G4 & A4 & B4 & C5 \\ 0 & 0 & 0 & 0 & 0 & 0 & 0 & 1 \\ 0 & 0 & 0 & 0 & 0 & 0 & 1 & 0 \\ 0 & 0 & 0 & 0 & 0 & 1 & 1 & 1 \\ 0 & 0 & 0 & 0 & 1 & 1 & 1 & 1 \\ 0 & 0 & 0 & 1 & 1 & 1 & 1 & 1 \\ 0 & 0 & 1 & 1 & 1 & 1 & 1 & 1 \\ 0 & 1 & 1 & 1 & 1 & 1 & 1 & 1 \end{bmatrix}, \quad (4.2.1)$$

where each column represents the state of the finger holes, 0 is closed and 1 is open. The left column is the fingering for the lowest note, with all the toneholes closed, for which the desired playing frequency is the first entry in  $\hat{f}_d$ , that is  $f_{C4}$ . The toneholes are opened one by one to go up the scale. Only the last fingering differs; the second tonehole is closed because the cross-fingered C5 is more traditional than that with all toneholes open. The algorithm needs to determine the position of each of the seven toneholes as well as the length of the instrument (diameters are fixed in this example but are usually included, which adds 7 additional variables to optimize). In this case, the vector of optimization variables is  $\hat{x} = \{L, d_{e7}, d_{76}, d_{65}, d_{54}, d_{43}, d_{32}, d_{21}\}$ , where  $L$  is the length of the variable-length section,  $d_{e7}$  represents the distance from the open end to the last tonehole and  $d_{mn}$  the distance between tonehole  $m$  and tonehole  $n$ . The initial geometry of the instrument consists in the vector  $\hat{x}_0$  and each iteration produces a new estimate  $\hat{x}_k$ . At each iteration the vector  $\hat{f}_k = \hat{f}(\hat{x}_k)$  contains the playing frequency of each fingering for an instrument defined by the geometry vector  $\hat{x}_k$ . For a specific geometry vector  $\hat{x}$ , the error norm is calculated as the sum of the squares of the tuning

error of each fingering in cents:

$$e(\hat{x}) = \sum_{i=0}^N [1200 \log_2 (\hat{f}(\hat{x})[i] / \hat{f}_d[i])]^2. \quad (4.2.2)$$

Once the error norm is calculated, the algorithm must determine what changes are to be applied to the geometry vector  $\hat{x}$  in order to reduce this error. This is done by calculating the gradient of the error with respect to each of the optimization variables:

$$g_k = \frac{1}{\varepsilon} \begin{bmatrix} e(\hat{x}_k + \{\varepsilon, 0, 0, 0, 0, 0, 0, 0\}) - e(\hat{x}_k) \\ e(\hat{x}_k + \{0, \varepsilon, 0, 0, 0, 0, 0, 0\}) - e(\hat{x}_k) \\ e(\hat{x}_k + \{0, 0, \varepsilon, 0, 0, 0, 0, 0\}) - e(\hat{x}_k) \\ e(\hat{x}_k + \{0, 0, 0, \varepsilon, 0, 0, 0, 0\}) - e(\hat{x}_k) \\ e(\hat{x}_k + \{0, 0, 0, 0, \varepsilon, 0, 0, 0\}) - e(\hat{x}_k) \\ e(\hat{x}_k + \{0, 0, 0, 0, 0, \varepsilon, 0, 0\}) - e(\hat{x}_k) \\ e(\hat{x}_k + \{0, 0, 0, 0, 0, 0, \varepsilon, 0\}) - e(\hat{x}_k) \\ e(\hat{x}_k + \{0, 0, 0, 0, 0, 0, 0, \varepsilon\}) - e(\hat{x}_k) \end{bmatrix}, \quad (4.2.3)$$

where  $\varepsilon$  is a small number.

This computation of the gradient requires recalculating the error norm for one small displacement of each of the optimization variables. In this case, with 8 fingerings, this requires obtaining 64 resonance frequencies, for each of which the impedance is calculated for many frequencies around the target frequency. This leads to a large number of calculations and explains why it is not practical to use the FEM as the calculation method, whereas the TMM provides sufficiently fast calculations.

For each of the fingerings, the input impedance is calculated for multiple frequencies in a relatively tight range ( $\pm 1$  tone) around the target playing frequency for this fingering. Then, the resonance is determined by finding the zero of the phase of the reflection coefficient using linear interpolation. For this method to work, a zero must exist in the range, which requires that

the instrument must be sufficiently close to a solution, and that the bounds of the optimization method are sufficiently tight. When the range is too wide around each frequency, the algorithm encounters another zero of the phase, which corresponds either to another resonance or to an anti-resonance. This confuses the method and it starts to diverge.

Using the current method with tight bounds and small frequency ranges to search for resonances, we need to provide a good initial instrument. This first instrument is obtained by locating each tonehole individually, thus neglecting the effect of the presence of the other holes. This kind of initial instrument geometry has sufficiently small tuning deviations (generally less than 50 cents) for the algorithm to work.

## 4.3 Examples

This method for the calculation of tonehole location is applied to a few simple cases. First, as a validation, the solution for a six-tonehole flute is compared to the results obtained by [Keefe \(1989\)](#). Then, three instruments are investigated, demonstrating various possibilities of the algorithm, such as the optimization of the tonehole locations and diameters with cross-fingerings, the calculation of the positions for an equally-tempered or a just tuning and the imposition of bounds on the distances between the fingers.

### 4.3.1 Keefe's Flute

This is the case of a simple six-tonehole cylindrical flute. The location of the toneholes is compared to the values obtained by [Keefe \(1989\)](#) as a validation case study. The internal diameter of the instrument is  $2a = 18.9$  mm and the wall thickness, which is equivalent to the tonehole heights, is 3.4 mm. The diameters of each tonehole were fixed to 9.53, 9.53, 7.94, 7.94, 9.53 and 6.35 mm, starting from the top of the instrument. Only the positions were calculated with the optimization algorithm in Keefe's publication. The diameter of the embouchure hole is 12.7 mm and is located at 16 mm from the top of the instrument. The excitation mechanism

Tonehole	Location [mm] (diameter [mm])	
	Keefe	Lefebvre
1	286.5 (9.5)	286.9 (9.5)
2	323.7 (9.5)	324.1 (9.5)
3	359.5 (7.9)	359.5 (7.9)
4	412.5 (7.9)	412.3 (7.9)
5	437.0 (9.5)	437.4 (9.5)
6	476.3 (6.4)	475.8 (6.4)
end	575.6	574.7

Table 4.1: Comparison of the tonehole layout of an optimized flute with Keefe’s flute

is taken into account with the addition of a fixed-length cylindrical segment 42 mm long (this includes the effect of the volume at the left of the embouchure hole). The air temperature was not specified, but properties of air at 25 °C will be used.

In Table 4.1, the positions of the toneholes of Keefe’s flute are compared to the results of the proposed optimization algorithm. The distances are relative to the hypothetical beginning of the instrument based on the excitation mechanism’s equivalent length; that is, to obtain the distances from the centre of the embouchure hole, subtract 42mm. A diagram of the instrument with the configuration of the toneholes for each fingering is shown in Fig. 4.2. There are only small differences between the two flute geometries. They may be due to the tonehole models (we were using the results for the tonehole on a thick pipe from Chapter 3), the radiation models for the open end or the properties of air.

The maximal difference in the positions of the toneholes for the two flutes is 0.5 mm, which represents a frequency shift of no more than 2 cents. This is a negligible difference, and we conclude that the results of the current method are congruent with those of Keefe.

### 4.3.2 PVC Flute

For simplicity of testing the results of the algorithm, another flute is calculated for the geometric properties of a standard 3/4 inch PVC pipe. The internal diameter is  $2a = 17.8$  mm and

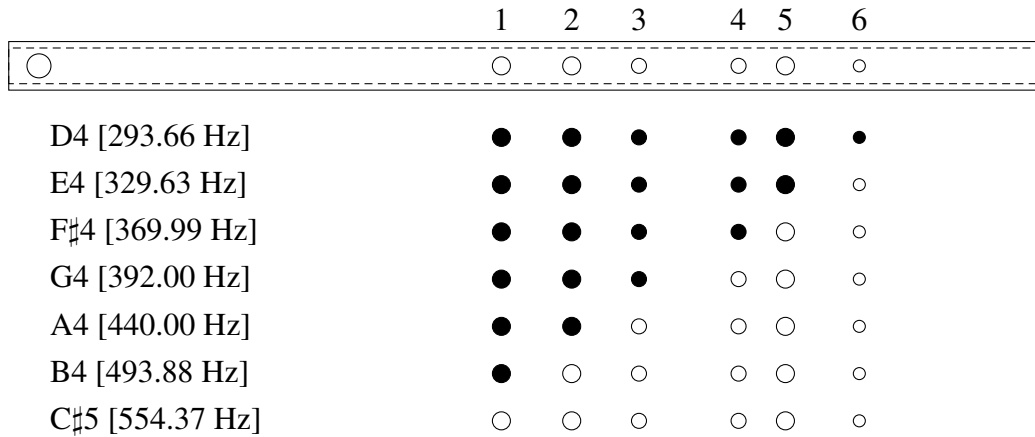


Figure 4.2: Diagram of Keefe's flute.

the wall thickness  $w = 2.25$  mm. The length of pipe between the cork and the embouchure hole is approximately 17 mm, as in a modern concert flute. The tuning will be the same as for Keefe's flute. For the embouchure hole, a wooden sleeve was fabricated to improve the playing characteristics of the instrument, and the height of the embouchure hole becomes 5 mm.

The characterization of the excitation mechanism was done by the author, who is only an amateur flute player. The equivalent length of the excitation mechanism was found to follow  $l_e = 0.0215e^{0.00228f}$  for the first register. The equivalent length is different for the second mode, but no attempt was made to optimize the instrument for both modes.

Two instruments were designed. The first uses large fixed-diameter toneholes and only the position is optimized. For the second flute, cross-fingerings are added for the notes A $\flat$ , B $\flat$  and C. The configuration for these notes follows the fingerings of a Renaissance flute, as recommended by the maker of historical flutes Boaz Berney ([http://berneyflutes.com/material/pdf+img/renaissance\\_fingerings.pdf](http://berneyflutes.com/material/pdf+img/renaissance_fingerings.pdf)). The diameter is free to change to allow for a solution. The distances are relative to the centre of the embouchure hole. The instrument with cross-fingerings converges to a solution with small toneholes. The positions and dimensions of the toneholes are listed in Table 4.2.

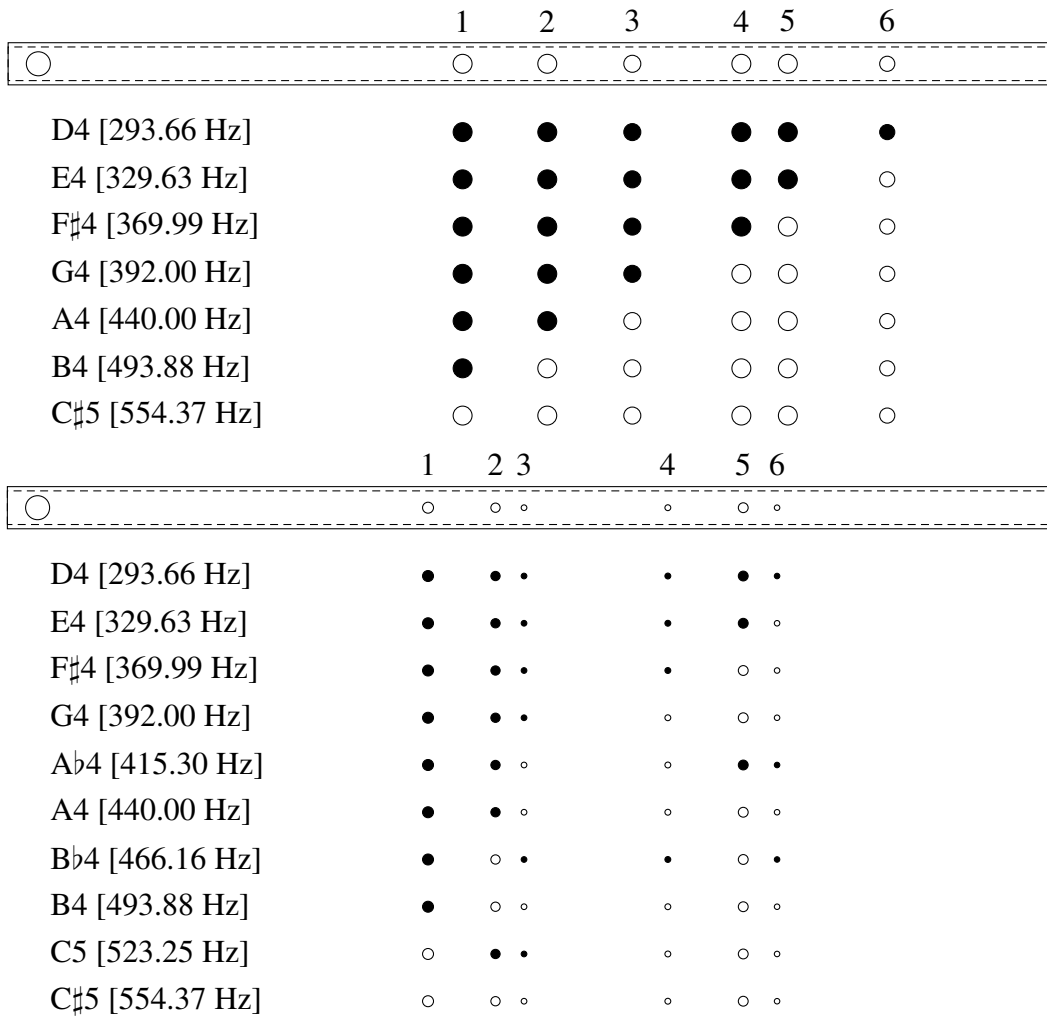


Figure 4.3: Diagram of a large-diameter and a small-diameter tonehole flute.

Tonehole	Location [mm] (diameter [mm])	
	Flute 1 (large holes)	Flute 2 (small holes)
1	223.5 (10.0)	205.6 (5.8)
2	268.3 (10.0)	241.3 (4.9)
3	313.3 (9.0)	256.4 (3.0)
4	371.0 (10.0)	332.5 (3.1)
5	395.6 (10.0)	372.4 (5.2)
6	448.2 (8.0)	390.3 (2.9)
end	534.2	535.9

Table 4.2: Comparison of the tonehole layout for a flute

The flute with large-diameter toneholes was fabricated and played. An obvious problem appears when one tries to play this instrument: the distances between toneholes 2 and 3 (45 mm), as well as between toneholes 5 and 6 (52.6 mm), are so large that the instrument is unplayable. The distance between toneholes 1 and 2 (44.8 mm) is also very large but still playable. The maximal distances between two fingers should probably be kept below 40 mm or even less if possible. Otherwise, the tuning of the instrument corresponds to the target frequencies provided by the algorithm.

While experimenting with this flute, a counterintuitive phenomenon became apparent. The playing frequency of the flute with all toneholes but the first closed is approximately 15 Hz sharper than the playing frequency with all toneholes open. Normally, when toneholes are closed beyond the first open tonehole, the playing frequency becomes lower. The calculated input admittance of the flute for both fingerings, displayed in Fig. 4.4, reveals that this is indeed the behaviour of the flute.

### 4.3.3 Chalumeau

This section describes how a simple six-hole chalumeau was designed and built. The excitation mechanism consisted of a clarinet mouthpiece and reed. Three cylindrical pipes of lengths 148, 296 and 446 mm were played, resulting in the playing frequencies 378, 225 and 160 Hertz,

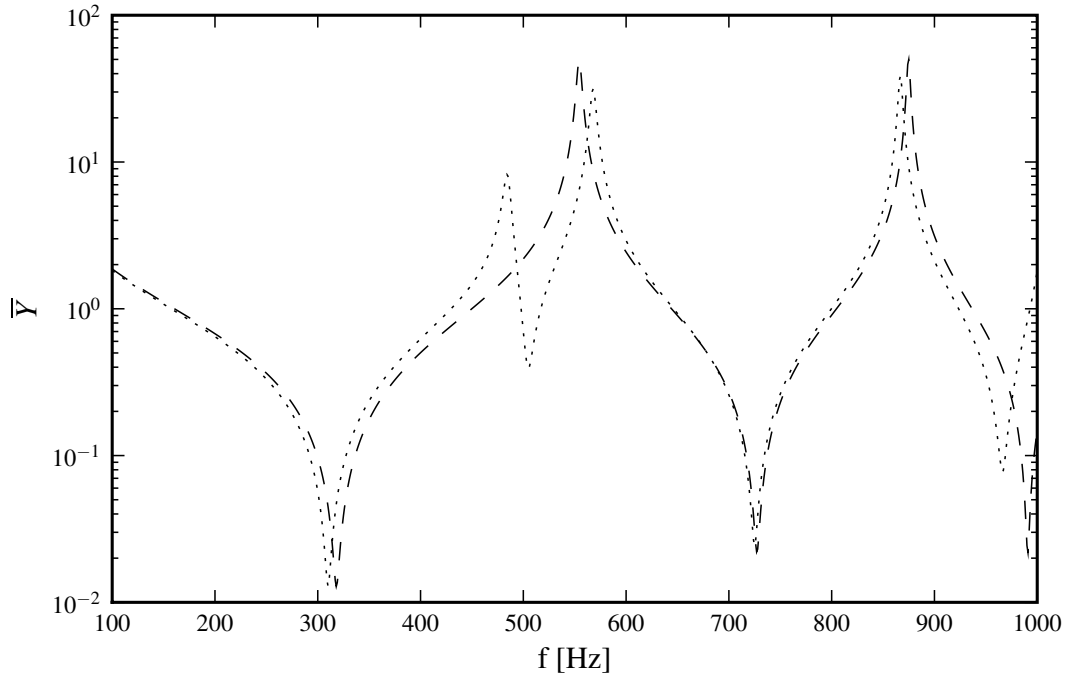


Figure 4.4: Input admittance of the large-toneholes flute for two fingerings:  $[1,1,1,1,1,1]$  (dashed) and  $[1,0,0,0,0,0]$  (dotted).

respectively. From this data, it was found that the mouthpiece assembly could be replaced by a cylindrical pipe of length 80.2 mm to approximate the excitation mechanism. The transmission matrix model of a tonehole in a thick pipe, as presented in a previous chapter, was used for the calculations.

The instrument is made of a thick wooden pipe of internal radius  $2a = 15$  mm and wall thickness  $t = 6.5$  mm. It can play the first 7 notes of a D-major scale by opening one hole after the other. The diameter of the tonehole was selected to be  $2b = 9$  mm, but two of the toneholes were made smaller to diminish the distance and make the instrument easier to play (ergonomy). The results of the optimization for an equal-tempered tuning and a just-tuning are presented in Table 4.3.

The differences in the position of the toneholes for the two tuning systems are correlated

Tonehole	Location [mm] (diameter [mm])	
	Chalumeau	Chalumeau (just)
1	286.6 (9.0)	288.5 (9.0)
2	323.7 (9.0)	327.3 (9.0)
3	349.8 (6.0)	349.2 (6.0)
4	415.4 (9.0)	415.2 (9.0)
5	436.6 (9.0)	440.7 (9.0)
6	474.4 (6.0)	473.1 (6.0)
end	571.6	571.7

Table 4.3: Comparison of the tonehole layout for two chalumeaux (equally tempered vs. just)

with the interval. As an example, for tonehole 5, which serves for degree 3 of the scale (major third relative to the fundamental), the just note is 13.7 cents lower than the equally tempered note and results in a tonehole located farther away from the top by 4.1 mm.

The distances between the toneholes are comfortable for playing the instrument. The tuning corresponds to the desired frequencies, but two of the notes are difficult to play (E and A). For these notes, the sound level is weaker and an attempt to play them louder with more effort fails; the instrument feels “blocked”. This occurs when the first open tonehole is one of the two small 6 mm toneholes. The problem is worse for the lower frequency note (E). When playing the second register of the instrument, this effect does not occur.

This behaviour has been described previously by [Keefe \(1983\)](#) and is attributed to the presence of convective nonlinearities, an effect that is mostly important for low frequency tones because it is proportional to the particle displacement  $d_h$ , which is inversely proportional to the frequency. The acoustic particle velocity  $v_h$  in a tonehole could be obtained from the TMM calculations with an inverse calculation, starting from the input impedance of the instrument by fixing a value of the pressure or velocity at the input and propagating this value up to the first open tonehole. This feature has to be implemented in our TMM software and would enable us to estimate the likelihood of the occurrence of nonlinearities to determine whether or not the tonehole is large enough to work properly in a given wind instrument. No precise

criteria were reported in the literature; more work is required to fully understand this aspect.

#### 4.3.4 A Six-Tonehole Saxophone

The excitation mechanism for this instrument consists of a soprano saxophone mouthpiece and reed. The characterization of an excitation mechanism for conical instruments would require the construction of several cones of different lengths, which is more difficult than for cylindrical pipes. Unfortunately, we only had one such conical waveguide built. We found that a constant equivalent volume of  $4.3 \text{ cm}^3$  coupled to the mouthpiece and conical waveguide gave correct results for the fundamental and first resonance frequencies of the instrument.

This instrument was inspired by The Saxie, a “toy” saxophone (Rycroft, 1999). This instrument was designed to play a D minor scale and some altered notes with cross-fingerings. It is unlikely that the cross-fingerings were made to be played in tune on the existing instruments because this would require very small holes, similar to the case of the flute, which would result in an instrument radiating less energy and being more difficult to play.

In the present optimization study, the instrument consists of a conical bore of 3 degrees taper angle with an input diameter of 9.5 mm. With only six toneholes of 1 mm height, this instrument should be able to play seven standard fingerings. Contrary to The Saxie, a C-Major scale was chosen with the fingerings defined in the following matrix:

$$\begin{bmatrix} C4 & D4 & E4 & F4 & G4 & A4 & B4 \\ 0 & 0 & 0 & 0 & 0 & 0 & 1 \\ 0 & 0 & 0 & 0 & 0 & 1 & 1 \\ 0 & 0 & 0 & 0 & 1 & 1 & 1 \\ 0 & 0 & 0 & 1 & 1 & 1 & 1 \\ 0 & 0 & 1 & 1 & 1 & 1 & 1 \\ 0 & 1 & 1 & 1 & 1 & 1 & 1 \end{bmatrix}. \quad (4.3.1)$$

Tonehole	Location [mm] (diameter [mm])	
	fixed ratio	bounds on distances
1	139.6 ( 7.0)	137.6 ( 6.6)
2	177.0 ( 7.8)	175.0 ( 7.5)
3	222.5 ( 8.9)	211.8 ( 6.3)
4	281.3 (10.2)	275.8 ( 8.7)
5	306.0 (10.7)	307.3 (12.0)
6	370.4 (12.0)	345.3 ( 6.8)
end	471.9	468.5

Table 4.4: Comparison of the tonehole layout for two conical waveguides with six toneholes

One option is to optimize the instrument for the positioning of the toneholes only, with the diameter of each tonehole defined by a fixed ratio  $\delta = b/a$ . The results for this instrument are displayed in Table 4.4. Unfortunately, this instrument is unplayable because some of the toneholes are too large and some of the distances too wide for the instrumentalist’s fingers. To overcome these problems, the diameters may be freely moved and bounds on the distances and diameters added. The distances between two fingers are bounded to lie between 25 and 38 mm, whereas the distances between the two hands does not need such a small bound. The values of  $\delta$  for each hole are bounded to the range 0.25 – 0.8. The resulting geometric parameters for these instruments are also in Table 4.4.

The playing characteristics of this instrument are not very good because the toneholes are too small. The instrument plays only very softly and it responds well only when all the toneholes are closed or when tonehole 5 is the first open tonehole. The thickness of the instrument’s wall is about 2 mm and the toneholes are drilled directly into the wall; therefore, the radius of curvature of the streamline is very small. Because the toneholes are small, the particle velocity becomes large, which seems to cause destructive non-linearities. To work properly, such an instrument would require a chimney with a larger geometric radius of curvature and possibly larger toneholes. A picture of “The Saxie” (Rycroft, 1999) reveals that the toneholes have chimneys instead of being only holes in the body.

The tuning of the six-tonehole saxophone is correct when playing pianissimo. As soon as more pressure is added, the pitch flattens in reaction to the increase of the nonlinear losses in the toneholes.

## 4.4 Summary

The optimization algorithm presented in this section works well and allows for the calculation of the positions and dimensions of the toneholes on a woodwind instrument under various constraints, such as multiple fingerings (including cross-fingerings) and bounds on the distances between adjacent toneholes and on their diameters. The current implementation minimizes tuning errors. It may optimize tonehole positions, diameters and heights with a pre-selected bore shape. The algorithm was verified with the design and fabrication of simple instruments. The applications of this method are numerous: the design of instruments playing in alternative tuning systems, the addition of fingerings for quarter tones to existing instruments, the design of instruments of various sizes, the improvement of the tuning of existing instruments and so forth.

The outcome of this algorithm depends on the model of the excitation mechanism. More work is required with professional musicians to adequately characterize the excitation mechanisms with experimental measurements of the playing frequencies of simple instruments.

In the case of reed instruments, non-linear losses occur in toneholes when they are too small in diameter, short in height, or when they present a small radius of curvature. The instruments become difficult to play under these conditions. A criterion needs to be added to the calculation software to determine the magnitude of these losses and the likelihood that an instrument will become difficult to play. This would help in designing good woodwind instruments with less trial and error.

Future work includes the design of more complex instruments and adding bore perturbations to the optimization variables and more constraints such as the tonehole lattice cutoff

frequency and/or the harmonicity of the resonances.

# Conclusion

This thesis led to the development and application of a number of methods for the computational design of woodwind instruments. First, the Transmission-Matrix Method (TMM) for the calculation of the input impedance of an instrument was implemented. An approach based on the Finite Element Method (FEM) was developed to determine the transmission-matrix parameters of an arbitrary discontinuity inside a waveguide. This was applied to a single unflanged tonehole and a single tonehole on a thick pipe which resulted in the development of revised formula for the transmission-matrix parameters of open and closed toneholes that improve the accuracy of the TMM calculations for toneholes of short height and large diameters. This approach was also applied to investigate the possible variation of tonehole parameters when located on a conical bore. It was found that the shunt impedance is unchanged and the series impedance only slightly affected. Therefore, we concluded that the tonehole transmission-matrix parameters developed on a cylindrical bore are equally valid for use on a conical bore.

Next, the development of a boundary condition for the approximation of the boundary layer losses enabled the simulation of complete woodwind instruments with the FEM. The comparison of the simulations of instruments with many open or closed toneholes with calculations using the TMM reveals small discrepancies that are most likely attributable to internal or external tonehole interactions. This effect is most important in the low frequencies for closed toneholes and near the tonehole lattice cutoff frequency for open toneholes. This interaction increases the amount of radiated energy for open toneholes. This phenomenon is not taken

into account in the TMM and poses a limit to its accuracy ( $\pm 10$  cent in the worse case). Using this boundary condition and the methodology previously developed for the determination of transmission-matrix parameters, one may calculate the transmission-matrix parameters of curved bores of varying cross-sections for use within the TMM. No theoretical solutions exist to account for the effect of curvature and boundary losses in a duct; but by using pre-calculated transmission-matrix parameters for the curved sections of an instrument, one can incorporate the accuracy of the FEM within the TMM.

Finally, we propose an optimization method, which uses the TMM coupled with an excitation mechanism model to estimate the playing frequencies of a hypothetical instrument. This enables us to automate the calculation of the positions and dimensions of the toneholes on a woodwind instrument to minimize tuning errors. The method may optimize an instrument for any number of fingerings, including cross-fingerings and constraints with bounds on the distances between adjacent toneholes and on the toneholes' diameters and heights. The playing frequencies may or may not be chosen to be of equal temperament, allowing for the design of instruments playing in alternative tuning systems. The results of the optimization algorithm are satisfactory and ready to be applied to more complex instruments.

## Future Work

The optimized geometry of woodwind instrument toneholes depends on the excitation mechanism model provided in the algorithm. In this thesis, these models were estimated from simple playing experiments by the author. For the design of professional quality woodwind instruments, the characterization of the excitation mechanism should be done with careful experiments with many professional musicians. This is one of the important future aspects of this research to pursue.

Also, incorporating the tonehole cutoff frequency and/or the harmonicity of the first few

resonance as new criteria for the optimization algorithm would enable optimizing the instrument for timbre evenness and “ease of play” as well as for tuning. This is to be investigated.

Moreover, the findings of Chapter 3 concerning the tonehole interaction should be verified against impedance measurements of fabricated prototypes. In general, the results of FEM simulations and TMM calculations should be compared with experimental measurements. The analysis of this chapter need to be refined to determine in which proportion internal or external interactions are responsible for the discrepancies between the FEM and the TMM.

For purposes of woodwind instrument design, it would be helpful to determine a criterion to evaluate the importance of non-linear losses in toneholes and to help in detecting when toneholes are too small in diameter or when the radius of curvature of the streamline is too small. At this point, only by means of playing experiments can it be verified if the optimized toneholes are going to work properly.

Finally, the methods developed in this thesis need to be applied to specific problems occurring in existing woodwind instruments. This would be an experimental task to pursue in collaboration with professional instrumentalists and instrument makers.



parameters while playing through embouchure control. The resonance frequency of the alto saxophone reed in playing conditions was estimated to be approximately 1 kHz (Boutillon & Gibiat, 1996) but is likely to be higher because notes of higher frequencies are playable, and it is known that the playing frequency may not be higher than the reed resonance frequency. It is also known that the threshold blowing pressure for the saxophone is likely to be approximately 2-3 kPa for all notes (Fuks & Sundberg, 1999). The effect of the excitation mechanism is always to lower the playing frequency of the instrument relative to the resonances of the instrument's air column. Previous investigations tried to add an "equivalent" cylinder at the tip of the instrument to take into account this effect. This method is not adequate, and we propose a more precise model which is frequency dependent.

## A.1 Description

In this section, we present a description of the excitation mechanism with a mathematical analysis from which we will propose a method to incorporate the excitation mechanism in the design process of an instrument. This excitation mechanism is depicted in Fig. A.1, where the variables used in the following analysis are represented. In this diagram, the reed tip is not located at its rest position  $H$  (tip opening) but at the average position  $y_0$  resulting from the static pressure  $p_0$  provided by the player. The tip opening  $H$  may be changed by the instrumentalist by varying the embouchure. The average position  $y_0$  depends on both  $H$  and  $p_0$ . The dynamic position of the reed around  $y_0$  is  $\hat{y}$ . The acoustic flow  $\hat{u}$  entering the reed channel is separated into two parts, the acoustic flow  $\hat{u}_{in}$  entering the instrument's air column and the acoustic flow  $\hat{u}_r$  due to the reed's motion:

$$\hat{u} = \hat{u}_{in} + \hat{u}_r. \quad (\text{A.1.1})$$

Similarly, we can write:

$$-\hat{u} = \hat{u}_u - \hat{u}_r, \quad (\text{A.1.2})$$

where  $\hat{u}_u$  is the acoustic flow leaving the instrumentalist's mouth.

The forces acting on the reed are the pressure on its inner and outer surfaces, that is, the pressure inside the mouthpiece  $p_0 + \hat{p}_u$ , where  $\hat{p}_u$  is the dynamic (acoustic) portion, and inside the mouth  $\hat{p}_{in}$ , as well as forces coming from the interaction with the instrumentalist's lip, which are not known and are not considered in our analysis. Consequently, the parameters of the reed will include the effect of the interaction with the lip and are likely to be different for players with contrasting playing styles (embouchures).

The acoustic flow  $\hat{u}$  entering the reed channel is a non-linear function of the pressure difference  $\Delta p = p_0 + \hat{p}_u - \hat{p}_{in}$ , which can be linearized and represented by the generator admittance  $Y_g$  to yield:

$$\hat{u} = u_0 + Y_g \Delta p. \tag{A.1.3}$$

The acoustic flow induced by the reed motion can also be characterized by the reed admittance  $Y_r$ :

$$\hat{u}_r = Y_r \Delta p. \tag{A.1.4}$$

Defining the input impedance of the air column as  $Z_{in}$  and of the vocal track as  $Z_u$ , we obtain the system of Fig. A.2.

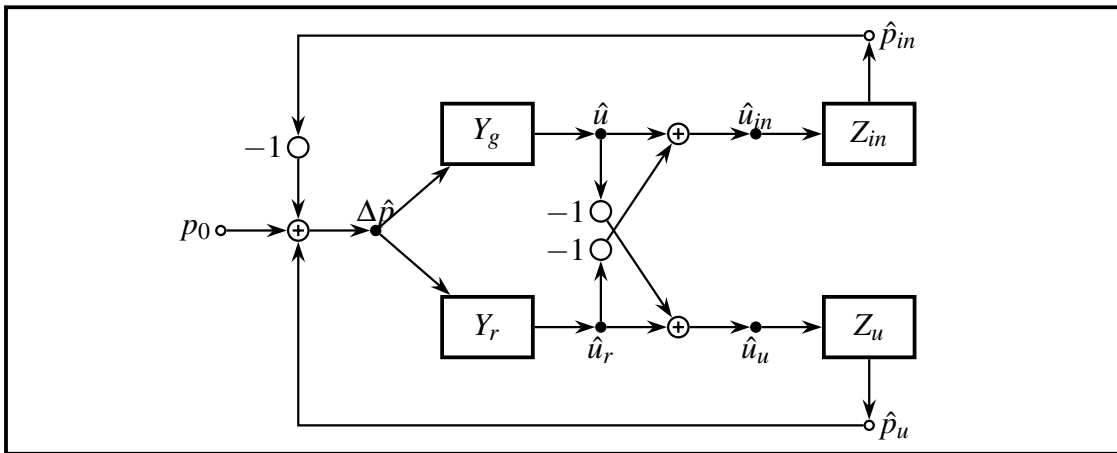


Figure A.2: Block diagram of the single reed excitation mechanism system.

The transfer function between the pressure at the input of the air column and the static pressure in the mouth is:

$$\frac{\hat{p}_{in}}{p_0} = \frac{(Y_g - Y_r)Z_{in}}{1 + (Y_g - Y_r)(Z_{in} + Z_u)}, \quad (\text{A.1.5})$$

for which the limit of stability occurs when:

$$Y_g - Y_r + \frac{Y_{in}}{Y_{in}/Y_u + 1} = 0. \quad (\text{A.1.6})$$

If we neglect the influence of the vocal track, which is a valid hypothesis when playing in the normal register of the instrument, the expression can be simplified to:

$$Y_g - Y_r + Y_{in} = 0. \quad (\text{A.1.7})$$

## A.2 Reed Admittance

We modelled the reed as a linear mass-spring-damper system, using the same notation as in Eq. (1) from [Dalmont et al. \(1995\)](#):

$$\frac{d^2y}{dt^2} + g_r \frac{dy}{dt} + \omega_r^2(y - H) = \frac{-\Delta p}{\mu_r}, \quad (\text{A.2.1})$$

where  $y$  is the displacement of the reed relative to its equilibrium position  $y_0$  (positive when going away from the mouthpiece's lay),  $g_r$  is the reed damping factor,  $\omega_r = 2\pi f_r$  is the angular eigenfrequency (resonance frequency in absence of damping),  $\mu_r$  is an equivalent mass per unit area and  $\Delta p = p_0 + \hat{p}_u - \hat{p}_{in}$ , where  $p_0$  is the static pressure in the mouth,  $\hat{p}_u$  is the upstream dynamic pressure (in the instrumentalist's mouth) and  $\hat{p}_{in}$  is the pressure inside the mouthpiece, near the reed's tip. In the frequency domain, replacing  $y = y_0 + \hat{y}e^{j\omega t}$  and  $\Delta p = p_0 + (\hat{p}_u - \hat{p}_{in})e^{j\omega t} = p_0 + \hat{p}_\Delta e^{j\omega t}$  in Eq. [A.2.1](#), we obtain:

$$\mu_r(\omega_r^2 - \omega^2 + j\omega g_r)\hat{y}e^{j\omega t} + \mu_r\omega_r^2(y_0 - H) = -p_0 - \hat{p}_\Delta e^{j\omega t}. \quad (\text{A.2.2})$$

The following equation is obtained by equating constant terms:

$$y_0 = H - \frac{P_0}{\mu_r \omega_r^2}, \quad (\text{A.2.3})$$

and we obtain the transfer function of the reed displacement relative to  $\hat{p}_\Delta$  by equating terms in  $e^{j\omega t}$ :

$$\frac{\hat{y}}{\hat{p}_\Delta} = \frac{-1}{\mu_r(\omega_r^2 - \omega^2 + j\omega g_r)} = -D(\omega), \quad (\text{A.2.4})$$

where

$$D(\omega) = \frac{\omega_r^2 - \omega^2 - j\omega g_r}{\mu_r \left[ (\omega_r^2 - \omega^2)^2 + \omega^2 g_r^2 \right]}. \quad (\text{A.2.5})$$

The acoustic flow induced by the reed is:

$$\hat{u}_r = j\omega S_r \hat{y}, \quad (\text{A.2.6})$$

where  $S_r$  is the reed's effective area. An estimation of its value will be discussed later.

Finally, using Eq. (A.2.6) and Eq. (A.2.4), we obtain the reed admittance:

$$Y_r = \frac{\hat{u}_r}{\hat{p}_\Delta} = -j\omega S_r D(\omega) = -j\omega C(\omega). \quad (\text{A.2.7})$$

It is interesting to investigate the equivalent volume  $V_e$  due to reed-induced acoustic flow, calculated as:

$$V_e(\omega) = \rho c^2 C(\omega). \quad (\text{A.2.8})$$

The low frequency approximation  $C(\omega \rightarrow 0) = C_0 = \frac{S_r}{\mu_r \omega_r^2}$  is commonly used in the literature as a frequency independent length correction.

Consideration of Fig. A.3 suggests that the approximation of constant length correction may not be correct, and that the value of the damping factor greatly influences the length

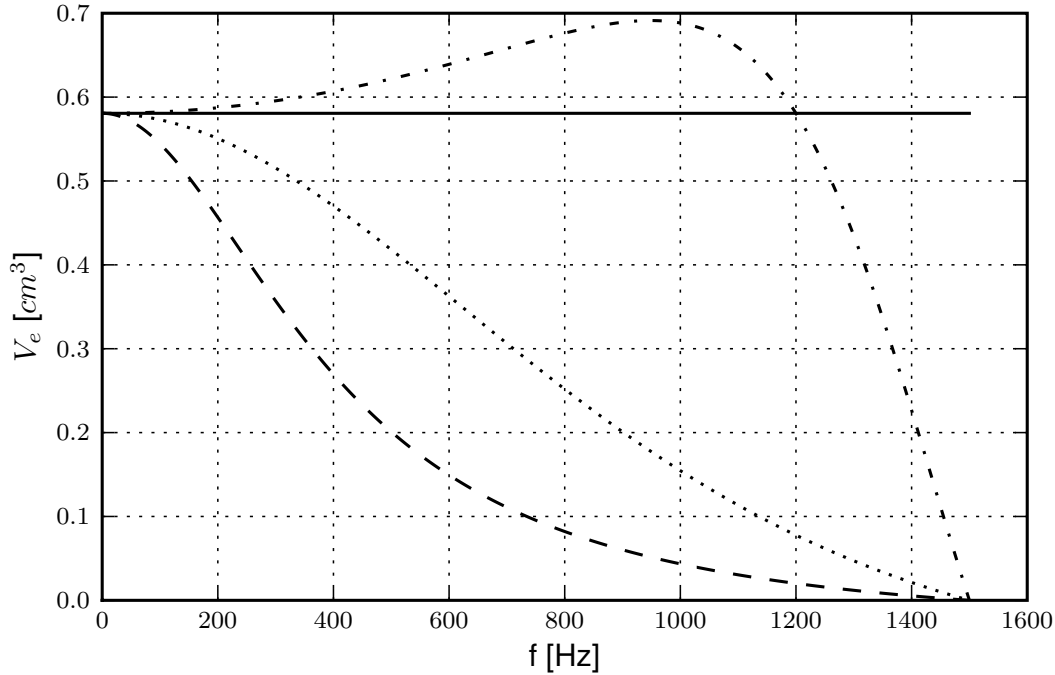


Figure A.3: Equivalent volume  $V_e$  due to reed admittance  $Y_r$  as a function of frequency for three reeds. Common parameters are  $u_r = 0.075 \text{ kg/m}^2$ ,  $f_r = 1000 \text{ Hz}$ ,  $S_r = 7.5 \times 10^{-5} \text{ m}^2$ . The damping factor  $g_r$  is: (dashed)  $4 \times \omega_r$ , (dotted)  $2 \times \omega_r$  and (dash-dot)  $0.7 \times \omega_r$ . The solid line represents the low frequency approximation  $\rho c^2 C_0$ .

correction due to reed-induced acoustic flow. We must also consider that the simple spring-mass-damper representation of the reed may be inadequate.

### A.3 Generator Admittance

The acoustic flow entering the reed channel responds to a non-linear function of the pressure difference between the player's mouth and the mouthpiece. It also depends on the reed-valve opening, controlled by the dynamics of the reed motion. Such a system has been studied by [Backus \(1963\)](#), but we are presenting a slightly simplified equation here by neglecting the

mass of air in the reed slit and assuming the Bernoulli equation to be valid (compare Eq. (25) from Backus):

$$\Delta p = \frac{\rho u^2}{2w^2 y^2}, \quad (\text{A.3.1})$$

where  $w$  is the width of the reed channel. Assuming sinusoidal excitation, we replace  $u = u_0 + \hat{u}e^{j\omega t}$ ,  $y = y_0 + \hat{y}e^{j\omega t}$  and  $\Delta p = p_0 + \hat{p}_\Delta e^{j\omega t}$  in Eq. (A.3.1), which yields:

$$p_0 + \hat{p}_\Delta e^{j\omega t} = \frac{\rho}{2w^2} \frac{(u_0 + \hat{u}e^{j\omega t})^2}{(y_0 + \hat{y}e^{j\omega t})^2}. \quad (\text{A.3.2})$$

Collecting constant terms, we obtain:

$$p_0 y_0^2 = \frac{\rho u_0^2}{2w^2}, \quad (\text{A.3.3})$$

and terminate in  $e^{j\omega t}$ :

$$2p_0 y_0 \hat{y} + y_0^2 \hat{p}_\Delta = \frac{\rho u_0}{w^2} \hat{u}. \quad (\text{A.3.4})$$

Using Eq. (A.3.3) and Eq. (A.2.3) to eliminate  $u_0$  and  $y_0$  from Eq. (A.3.4) as well as the reed transfer function from Eq. (A.2.4) to replace  $\hat{y}$ , we obtain the generator admittance:

$$Y_g = \frac{\hat{u}}{\hat{p}_\Delta} = w \frac{H - p_0 [1/\mu_r \omega_r^2 + 2D(\omega)]}{\sqrt{2p_0 \rho}}. \quad (\text{A.3.5})$$

This equation is important because it shows the relation between the acoustic flow in the reed channel and the dynamic reed. The consequence is that there is an imaginary part to the generator admittance and, therefore, a length correction. The reed damping term  $g_r$  in Eq. (A.2.5) is responsible for this effect. The low frequency approximation of the generator admittance is:

$$Y_g(\omega \rightarrow 0) = w \frac{H - p_0 [1/\mu_r \omega_r^2 - 2j\omega g_r / \mu_r \omega_r^4]}{\sqrt{2p_0 \rho}}, \quad (\text{A.3.6})$$

where we can observe that the imaginary part of this admittance, like the reed admittance, is proportional to  $\omega$  in the low frequency limit; that is, there exists a length correction associated

with the generator admittance in the low frequency limit.

The low frequency approximation of the generator equivalent volume is:

$$V_e = -\rho c^2 \frac{\Im(Y_g)}{\omega} = w c^2 \sqrt{2 p_0 \rho} [g_r / \mu_r \omega_r^4]. \quad (\text{A.3.7})$$

This equivalent volume is proportional to the reed damping factor, an effect that can be observed in Fig. A.4. This low frequency approximation also reveals that the equivalent volume is inversely proportional to the fourth power of the reed's resonance frequency; therefore, we expect that this is an important mechanism for controlling the playing frequency using lip pressure variations.

Notice also that the equivalent volume is proportional to the square root of  $p_0$ , the static pressure in the player's mouth. This implies that the playing frequency decreases when the instrumentalist plays louder. It is likely that this effect is counterbalanced by a tighter embouchure, which raises the reed's resonance frequency and has the opposite effect.

## A.4 The Reed's Effective Area

The acoustic flow induced by the reed's motion is:

$$u_r = S_r \dot{y}_{tip} = w \int_0^l \frac{dy(x)}{dt} dx, \quad (\text{A.4.1})$$

where  $w$  is the width of the reed and  $l$  is the length of reed that is free to move. If we suppose that the reed moves rigidly as if it were rotating around its contact point with the lay (at  $x = 0$ ), then:

$$\frac{dy(x)}{dt} = \dot{y}_{tip} \frac{x}{l}, \quad (\text{A.4.2})$$

which yields  $S_r = wl/2$ . This value is thus a maximal boundary on the effective area of the reed. If we suppose instead that the reed's motion is not rigid but follows the lay's shape,

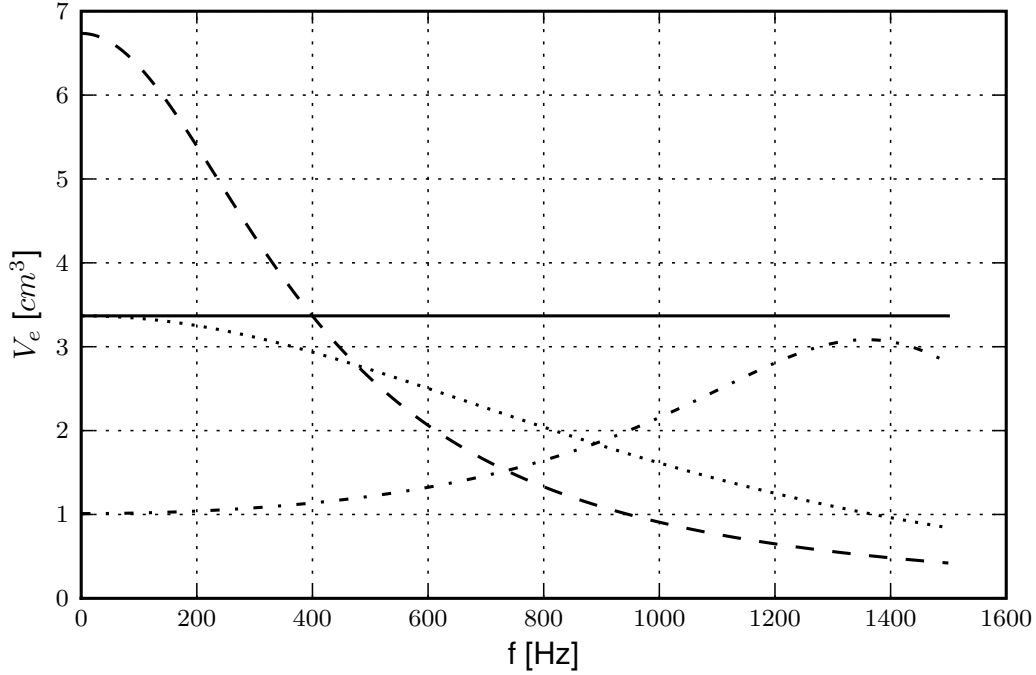


Figure A.4: Equivalent volume  $V_e$  due to the generator admittance  $Y_g$  as a function of frequency for three reeds. Common parameters are  $u_r = 0.075 \text{ kg/m}^2$ ,  $f_r = 1000 \text{ Hz}$ ,  $S_r = 7.5 \times 10^{-5} \text{ m}^2$ . The damping factor  $g_r$  is: (dashed)  $4 \times \omega_r$ , (dotted)  $2 \times \omega_r$  and (dash-dot)  $0.7 \times \omega_r$ . The solid line represent the low frequency approximation given by Eq. (A.3.7) for the second reed.

we obtain a smaller value. We may suppose a parabolic shape such that  $y(x) = ax^2$ , so that  $\frac{dy(x)}{dt} = ax^2$  with  $\dot{y}_{tip} = al^2$ , which finally yields:

$$\frac{dy(x)}{dt} = \dot{y}_{tip}(x/l)^2. \quad (\text{A.4.3})$$

Performing the integration in Eq. (A.4.1), we obtain the value  $Sr = wl/3$ , which is a more realistic value.

## A.5 Estimation of the Playing Frequencies

For the design of a single-reed woodwind instrument, it is important to estimate the equivalent volume of the excitation mechanism and its frequency dependence. Unfortunately, the parameters of the reed model are not known with precision. In this section, we provide simple experimental results along with calculations of the playing frequencies based on the simple model we have presented in order to estimate the equivalent volume.

From Eq. (A.1.7), Eq. (A.2.7) and Eq. (A.3.5), we can calculate the theoretical playing frequency and threshold blowing pressure for a given air column's input impedance  $Z_{in} = 1/Y_{in}$  and a reed model characterized by the parameters  $\mu_r$ ,  $g_r$ ,  $\omega_r$  as well as  $H$ ,  $w$  and  $S_r$ . We need only to solve simultaneously the real and imaginary parts:

$$\Re(Y_g - Y_r + Y_{in}) = 0,$$

$$\Im(Y_g - Y_r + Y_{in}) = 0.$$

We are going to compare theoretical calculations with experimental values of the playing frequencies for a simple conical air column with input diameter  $d_i = 12.5$  mm, output diameter  $d_o = 63.1$  mm and length  $L = 965.2$  mm coupled to a standard mouthpiece model Meyer #8. The measured input impedance of such a cone corresponds with great precision to theoretical calculations (Lefebvre & Scavone, 2008). The volume of the missing part of the cone is  $V_{missing} = 9.75$  cm<sup>3</sup>. The geometry of the mouthpiece is depicted in Fig. A.5, where the dashed vertical line shows the location where the cone is joined to the mouthpiece. The total volume of the mouthpiece is  $V_m = 8.1$  cm<sup>3</sup>.

With the air column defined by the mouthpiece coupled to the conical waveguide, we were able to find, through a process of trial and error, a set of excitation mechanism parameters that predicts relatively accurately the measured playing frequencies. The results are

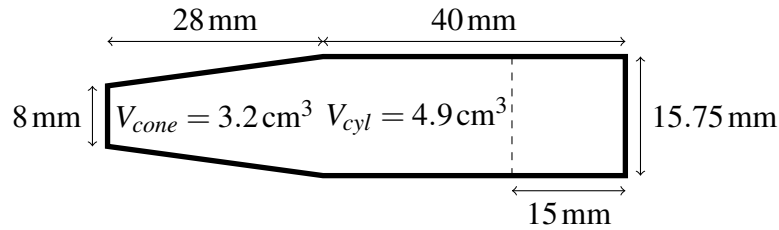


Figure A.5: Diagram of the mouthpiece geometry.

shown in Table A.1 and the parameters are indicated in the caption. For the fundamental resonance, the sum of the mouthpiece volume ( $8.1 \text{ cm}^3$ ) and the equivalent volume due to the excitation mechanism ( $3.9 \text{ cm}^3$ ) is larger than the volume of the missing part of the conical bore ( $12 \text{ cm}^3 > 9.75 \text{ cm}^3$ ). For higher frequencies, the equivalent volume due to the excitation mechanism increases even more; it is more than double for the eighth resonance. The relatively good ( $\sim 10$  cents) correspondence between the measured and predicted playing frequencies suggests that the excitation mechanism model is representative of the reality.

Even though the parameters of the excitation mechanism are not well known and difficult to measure, the playing frequencies of an instrument can be predicted with relative accuracy using the one degree of freedom mass-spring-damper model. The most important observation from these results is that the equivalent volume due to the excitation mechanism is a growing function of frequency for a fixed embouchure setting. This contrasts with the commonly used approach, which consists of using a constant equivalent volume. Instead of painstakingly estimating the values of the various parameters to obtain the correct equivalent volume as a function of frequency, it is possible to experimentally determine the equivalent volume of the excitation mechanism as a function of frequency, from which a data-fit formula may be obtained. Since this characterization will produce different results for different mouthpiece assemblies and instrumentalists, it is important that it be done with an instrumentalist and a mouthpiece assembly representative of the targeted market (students, professionals, classical, jazz etc.).

As an example, the data obtained from the cone, presented in Table A.1, is displayed in

Theoretical				Experimental	Interval
$f_r$ [Hz]	$f_p$ [Hz]	$V_e$ [cm <sup>3</sup> ]	$p_{th}$ [kPa]	$f_m$ [Hz]	$1200 \log_2(f_m/f_p)$
139.8	138.6	3.86	2.6	138.6	-0.3
286.6	279.3	3.86	2.3	280.2	+5.7
439.6	424.4	4.04	2.2	424.6	+0.7
598.4	577.0	4.40	2.2	573.5	-10.6
761.8	735.1	4.99	2.3	730	-12.2
928.4	895.5	5.91	2.5	890	-10.7
1097.3	1054.7	7.36	3.1	1055	+0.5
1267.6	1208.4	9.88	4.8	1212	+5.1

Table A.1: Estimation of the playing frequencies for the successive harmonics of a conical bore with mouthpiece and excitation mechanism ( $\mu_r = 0.0475 \text{ kg/m}^2$ ,  $f_r = 1500 \text{ Hz}$ ,  $g_r = 0.6\omega_r$ ). Resonance frequencies of the air column at the tip of the mouthpiece ( $f_r$ ), playing frequencies estimated from the mouthpiece model coupled to the air column ( $f_p$ ), equivalent volume of the excitation mechanism ( $V_e$ ) at the playing frequency, threshold blowing pressure at the playing frequency ( $p_{th}$ ), experimental measurement of the playing frequency of the instrument ( $f_m$ ), interval between the experimental and theoretical playing frequencies (last column).

Fig. A.6 along with the data fit formula  $V_e = 3.85 + 7.24 \times 10^{-7} f^2 + 2.33 \times 10^{-12} f^4$ .

It is interesting to compare these predictions of playing frequencies with other methods presented in the literature. It was customary to replace the real mouthpiece and excitation mechanism effect with an equivalent cylindrical mouthpiece, or to add a cylindrical section at the tip of the mouthpiece. This method would shift the impedance curves so that the playing frequency could be estimated by the resonance frequencies of the equivalent system composed of the instrument and the “equivalent” cylinder. We have tested these two techniques to compare with our previous results. In the first case, we calculated that a cylinder of length  $L = 93.7 \text{ mm}$  (and diameter  $D = 15.75 \text{ mm}$ ) would produce the correct playing frequency for the fundamental ( $f_p = 138.6 \text{ Hz}$ ). In the second case, we used the same mouthpiece geometry depicted in Fig. A.5 with an additional cylinder of length  $55.5 \text{ mm}$  and diameter  $8 \text{ mm}$ . The predicted playing frequencies and calculated errors are presented in Table A.2. Even though the second model provides better results than the first, they are not as good as those based on

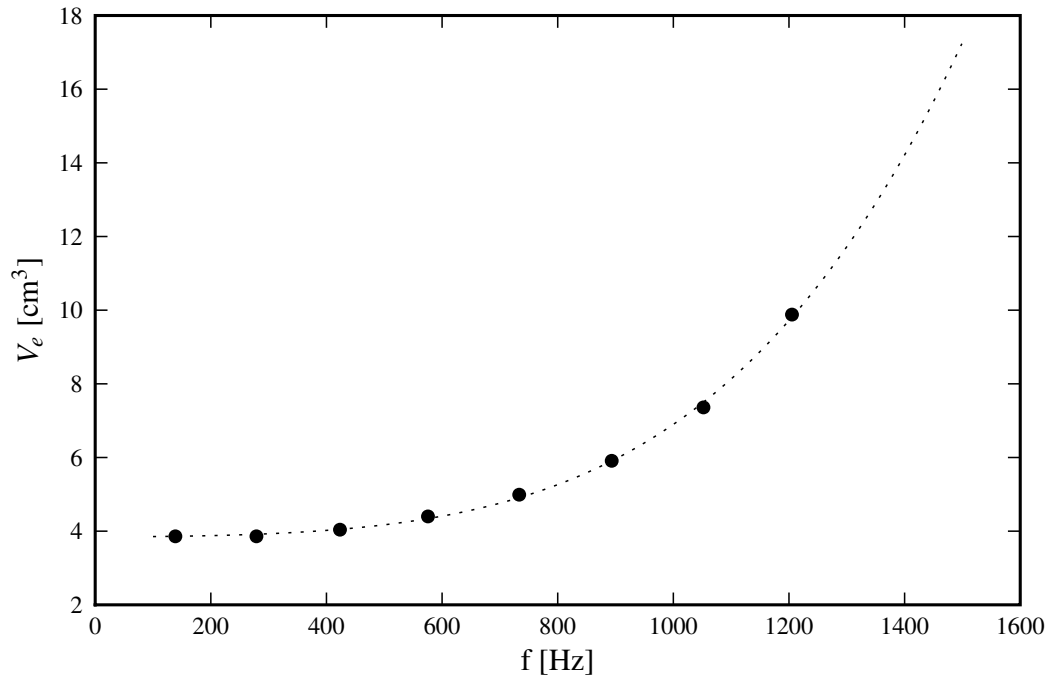


Figure A.6: Total equivalent volume  $V_e$  as a function of frequency. Data-fit formula (dashed), data points (filled circles).

the excitation mechanism model.

$f_m$	Cylindrical mouthpiece		Mouthpiece + cylinder	
	$f_p$	$1200 \log_2(f_m/f_p)$	$f_p$	$1200 \log_2(f_m/f_p)$
138.6	138.6	0.0	138.6	0.0
280.2	269.0	+70.5	280.8	-3.5
424.6	406.3	+76.2	427.9	-13.4
573.5	559.9	+41.6	582.1	-25.8
730	722.7	+17.4	741.8	-27.7
890	889.3	+1.4	904.1	-27.2
1055	1057.2	-3.5	1066.1	-18.1
1212	1224.8	-18.2	1223.4	-16.2

Table A.2: Estimation of the playing frequencies for the successive harmonics of a conical bore with cylindrical mouthpiece models: (1) the mouthpiece is a cylinder and (2) the mouthpiece geometry described in Fig. A.5 is elongated with a cylinder.

# References

- Ayers, R. D. (1995). Two complex effective lengths for musical wind instruments. *J. Acoust. Soc. Am.*, 98(1), 81–87.
- Backus, J. (1963). Small-Vibration theory of the clarinet. *J. Acoust. Soc. Am.*, 35(3), 305–313.
- Barjau, A., & Gibiat, V. (1997). Study of woodwind-like systems through nonlinear differential equations. Part II. Real geometry. *J. Acoust. Soc. Am.*, 102, 3032–3037.
- Bayliss, A., Gunzburger, M., & Turkel, E. (1982). Boundary conditions for the numerical solution of elliptic equations in exterior regions. *SIAM Journal on Applied Mathematics*, 42(2), 430–451.
- Benade, A. H. (1960). On the mathematical theory of woodwind finger holes. *J. Acoust. Soc. Am.*, 32, 1591–1608.
- Benade, A. H. (1990). *Fundamentals of musical acoustics* (second ed.). New York: Dover Publications.
- Blaikley, D. J. (1879). On quality of tone in wind instruments. *Proceedings of the Musical Association*, 6, 79–90.
- Bossart, R., Joly, N., & Bruneau, M. (2003). Hybrid numerical and analytical solutions for acoustic boundary problems in thermo-viscous fluids. *J. Sound Vibrat.*, 263(1), 69–84.

- Boutillon, X., & Gibiat, V. (1996). Evaluation of the acoustical stiffness of saxophone reeds under playing conditions by using the reactive power approach. *J. Acoust. Soc. Am.*, *100*(2).
- Brindley, G. S. (1973). Speed of sound in bent tubes and the design of wind instruments. *Nature*, *246*, 479–480.
- Bruneau, A. M., Bruneau, M., Herzog, P., & Kergomard, J. (1987). Boundary layer attenuation of higher order modes in waveguides. *J. Acoust. Soc. Am.*, *119*, 15–27.
- Caussé, R., Kergomard, J., & Lurton, X. (1984). Input impedance of brass musical instruments – Comparaison between experimental and numerical models. *J. Acoust. Soc. Am.*, *75*, 241–254.
- Chaigne, A., & Kergomard, J. (2008). *Acoustique des instruments de musique*. Paris, France: Édition Belin.
- Coltman, J. W. (1971). Effect of material on flute tone quality. *J. Acoust. Soc. Am.*, *49*, 520–523.
- Dalmont, J., Gazengel, B., Gilbert, J., & Kergomard, J. (1995). Some aspects of tuning and clean intonation in reed instruments. *Appl. Acoust.*, *46*, 19–60.
- Dalmont, J., & Nederveen, C. (2001). Radiation impedance of tubes with different flanges: numerical and experimental investigations. *J. Sound Vibrat.*, *244*, 505–534.
- Dalmont, J., Nederveen, C., Dubos, V., Ollivier, S., Meserette, V., & Sligte, E. te. (2002). Experimental determination of the equivalent circuit of an open side hole: Linear and non linear behaviour. *Acustica*, *88*, 567–575.
- Dubos, V., Kergomard, J., Khettabi, A., Dalmont, J., Keefe, D., & Nederveen, C. (1999a). Theory of sound propagation in a duct with a branched tube using modal decomposition. *Acustica*, *85*, 153–169.

- Dubos, V., Kergomard, J., Khettabi, A., Dalmont, J., Keefe, D., & Nederveen, C. (1999b). Theory of sound propagation in a duct with a branched tube using modal decomposition. *Acustica*, 85, 153–169.
- Eisner, E. (1967). Complete solutions of the “Webster” horn equation. *J. Acoust. Soc. Am.*, 41, 1126–1146.
- Facchinetti, M. L., Boutillon, X., & Constantinescu, A. (2003). Numerical and experimental modal analysis of the reed and pipe of a clarinet. *J. Acoust. Soc. Am.*, 113, 2874–2883.
- Félix, S., Nederveen, C., Dalmont, J., & Gilbert, J. (2008). Effect of bending portions of the air column on the acoustical properties of a wind instrument. *J. Acoust. Soc. Am.*, 123, 3447.
- Fletcher, N. (1978). Mode locking in nonlinearly excited inharmonic musical oscillators. *J. Acoust. Soc. Am.*, 64, 1566–1569.
- Fletcher, N. (1979). Excitation mechanisms in woodwind and brass instruments. *Acustica*, 43(1), 63–72.
- Fletcher, N., & Rossing, T. (1998). *The physics of musical instruments* (2nd ed.). New York: Springer-Verlag.
- Fritz, C., Farner, S., & Kergomard, J. (2004). Some aspects of the harmonic balance method applied to the clarinet. *Appl. Acoust.*, 65, 1155–1180.
- Fuks, L., & Sundberg, J. (1999). Blowing pressures in bassoon, clarinet, oboe and saxophone. *Acustica*, 85, 267–277.
- Gazengel, B. (1994). *Caractérisation objective de la qualité de justesse, de timbre et d'émission des instruments à vent à anche simple*. Ph.D. thesis, Université du Maine.

- Gilbert, J. (1991). *Étude des instruments de musique à anche simple: extension de la méthode d'équilibrage harmonique, rôle de l'inharmonicité des résonances, mesure des grandeurs d'entrée*. Ph.D. thesis, Université du Maine.
- Givoli, D., & Neta, B. (2003). High-order non-reflecting boundary scheme for time-dependent waves. *Journal of Computational Physics*, 186(1), 24–46.
- Hartmann, W. M. (1996). Pitch, periodicity, and auditory organization. *J. Acoust. Soc. Am.*, 100(6), 3491–3502.
- Kantartzis, N. V., Katsibas, T. K., Antonopoulos, C. S., & Tsiboukis, T. D. (2004). A 3d multimodal fdtd algorithm for electromagnetic and acoustic propagation in curved waveguides and bent ducts of varying cross. *COMPEL*, 23, 613–624.
- Kausel, W., & Mayer, A. (2008). More experimental evidence favouring the hypothesis of significant wall vibration influence on radiated horn sound. *J. Acoust. Soc. Am.*, 123, 3120.
- Keefe, D. (1981). *Woodwind tone hole acoustics and the spectrum transformation function*. Ph.D. thesis, Case Western Reserve University.
- Keefe, D. (1982a). Experiments on the single woodwind tonehole. *J. Acoust. Soc. Am.*, 72(3), 688–699.
- Keefe, D. (1982b). Theory of the single woodwind tonehole. *J. Acoust. Soc. Am.*, 72(3), 676–687.
- Keefe, D. (1983). Acoustic streaming, dimensional analysis of nonlinearities, and tone hole mutual interactions in woodwinds. *J. Acoust. Soc. Am.*, 73, 1804–1820.
- Keefe, D. (1984). Acoustical wave propagation in cylindrical ducts: Transmission line parameter approximations for isothermal and nonisothermal boundary conditions. *J. Acoust. Soc. Am.*, 75(1), 58–62.

- Keefe, D. (1989). Woodwind design algorithms to achieve desired tuning. *J. Catgut Acoust. Soc.*, *1*, 14–22.
- Keefe, D. (1990). Woodwind air column models. *J. Acoust. Soc. Am.*, *88*, 35–51.
- Keefe, D., & Benade, A. (1983). Wave propagation in strongly curved ducts. *J. Acoust. Soc. Am.*, *74*, 320–332.
- Kim, J.-T., & Ih, J.-G. (1999). Transfer matrix of curved duct bends and sound attenuation in curved expansion chambers. *Appl. Acoust.*, *56*, 297–309.
- Kirchhoff, G. (1868). On the influence of heat conduction in a gas on sound propagation. *Ann. Phys. Chem.*, *134*, 177–193.
- Kulik, Y. (2007). Transfer matrix of conical waveguides with any geometric parameters for increased precision in computer modeling. *J. Acoust. Soc. Am.*, *122*, EL179–EL184.
- Lefebvre, A. (2006). *La mesure de l'impédance acoustique du saxophone alto*. Master thesis, École Polytechnique de Montréal, Montréal, Canada.
- Lefebvre, A., & Scavone, G. (2008). Input impedance measurements of conical acoustic systems using the two-microphone technique. *J. Acoust. Soc. Am.*, *123*, 3015.
- Lefebvre, A., Scavone, G. P., Abel, J., & Buckiewicz-Smith, A. (2007). A comparison of impedance measurements using one and two microphones. *Proceeding of the ISMA*.
- Levine, H., & Schwinger, J. (1948). On the radiation of sound from an unflanged circular pipe. *Phys. Rev.*, *73*, 383–406.
- Lindsay, R. B. (1966). The story of acoustics. *J. Acoust. Soc. Am.*, *39*, 629–644.
- Lu, P., Nocedal, J., Zhu, C., Byrd, R. H., & Byrd, R. H. (1995). A limited memory algorithm for bound constrained optimization. *SIAM Journal on Scientific Computing*, *16*, 1190–1208.

- Mapes-Riordan, D. (1993). Horn modeling with conical and cylindrical transmission-line elements. *J. Audio Eng. Soc.*, *41*, 471–482.
- McIntyre, M. E., Schumacher, R. T., & Woodhouse, J. (1983). On the oscillations of musical instruments. *J. Acoust. Soc. Am.*, *74*(5), 1325–1345.
- Nederveen, C. (1998a). *Acoustical aspects of woodwind instruments* (Revised ed.). DeKalb, Illinois: Northern Illinois University Press. (Original work published 1969)
- Nederveen, C. (1998b). Influence of a toroidal bend on wind instrument tuning. *J. Acoust. Soc. Am.*, *104*, 1616–1626.
- Nederveen, C., & Dalmont, J. (2008). Corrections to the Plane-Wave approximation in rapidly flaring horns. *Acustica*, *94*(3), 461–473.
- Nederveen, C., Jansen, J., & Hassel, R. R. van. (1998). Corrections for woodwind tone-hole calculations. *Acustica*, *84*, 957–966.
- Nief, G., Gautier, F., Dalmont, J., & Gilbert, J. (2008). Influence of wall vibrations on the behavior of a simplified wind instrument. *J. Acoust. Soc. Am.*, *124*, 1320–1331.
- Noreland, D. (2002). A numerical method for acoustic waves in horns. *Acustica*, *88*, 576–586.
- Norris, A. N., & Sheng, I. C. (1989). Acoustic radiation from a circular pipe with an infinite flange. *J. Sound Vibrat.*, *135*, 85–93.
- Pagneux, V., Amir, N., & Kergomard, J. (1996). A study of wave propagation in varying cross-section waveguides by modal decomposition. Part I. Theory and validation. *J. Acoust. Soc. Am.*, *100*, 2034–2048.
- Pierce, A. D. (1989). *Acoustics, an introduction to its physical principles and applications*. Woodbury, New York: Acoustical Society of America.

- Plitnik, G. R., & Strong, W. J. (1979). Numerical method for calculating input impedances of the oboe. *J. Acoust. Soc. Am.*, *65*, 816–825.
- Pyle, J. (1997). How brass instruments are built: Art, craft, perhaps even science. *J. Acoust. Soc. Am.*, *101*, 3056. (<http://www.acoustics.org/press/133rd/2amu4.html>)
- Rayleigh, J. (1945). *The theory of sound* (Vol. 2). New York: Dover Publications. (Original work published 1896)
- Rycroft, D. (1999). A six-finger hole saxophone: The saxie. *The Galpin Society Journal*, *52*, 195–201.
- Scavone, G. P. (1997). *An acoustic analysis of single-reed woodwind instruments, with an emphasis on design and performance issues and digital waveguide modeling techniques*. Ph.D. thesis, Stanford University.
- Scavone, G. P., Lefebvre, A., & Silva, A. R. da. (2008). Measurement of vocal-tract influence during saxophone performance. *J. Acoust. Soc. Am.*, *123*, 2391–2400.
- Silva, A. da, Scavone, G., & Lefebvre, A. (2009). Sound reflection at the open end of axisymmetric ducts issuing a subsonic mean flow: A numerical study. *J. Sound Vibrat.*, *327*, 507–528.
- Silva, A. da, Scavone, G. P., & Walstijn, M. van. (2007). Numerical simulations of fluid-structure interactions in single-reed mouthpieces. *J. Acoust. Soc. Am.*, *122*, 1798–1809.
- Silva, A. R. da. (2008). *Numerical studies of aeroacoustic aspects of wind instruments*. Ph.D. thesis, McGill University.
- Tijdeman, H. (1975). On the propagation of sound waves in cylindrical tubes. *J. Sound Vibrat.*, *39*, 1–33.

- Tsynkov, S. V. (1998). Numerical solution of problems on unbounded domains. a review. *Applied Numerical Mathematics*, 27, 465–532.
- Vergez, C., Almeida, A., Caussé, R., & Rodet, X. (2003). Toward a simple physical model of double-reed musical instruments: Influence of aero-dynamical losses in the embouchure on the coupling between the reed and the bore of the resonator. *Acustica*, 89, 964–973.
- Walstijn, M. van, & Campbell, M. (2003). Discrete-time modeling of woodwind instrument bores using wave variables. *J. Acoust. Soc. Am.*, 113, 575–585.
- Webster, A. G. (1919). Acoustical impedance, and the theory of horns and of the phonograph. *Proc. Nat. Acad. Sci. U.S.A.*, 5, 275–282.
- Worman, W. (1971). *Self-sustained nonlinear oscillations of medium amplitude in clarinet-like systems*. Ph.D. thesis, Case Western Reserve University.
- Zhu, C., Byrd, R. H., Lu, P., & Nocedal, J. (1994). L-BFGS-B: FORTRAN subroutines for large-scale bound constrained optimization. *ACM Trans. Math. Software*, 23, 550—560.
- Zorumski, W. E. (1973). Generalized radiation impedances and reflection coefficients of circular and annular ducts. *J. Acoust. Soc. Am.*, 54, 1667–1673.